TAMPEREEN TEKNILLINEN YLIOPISTO
TAMPERE UNIVERSITY OF TECHNOLOGY
Julkaisu 723 • Publication 723

Pekka Ronkanen

Current Measurement in Control and Monitoring of Piezoelectric Actuators

Tampere 2008

Tampereen teknillinen yliopisto. Julkaisu 723
Tampere University of Technology. Publication 723

Pekka Ronkanen

Current Measurement in Control and Monitoring of Piezoelectric Actuators

Thesis for the degree of Doctor of Technology to be presented with due permission for public examination and criticism in Tietotalo Building, Auditorium TB109, at Tampere University of Technology, on the 28th of March 2008, at 12 noon.

Tampereen teknillinen yliopisto - Tampere University of Technology
Tampere 2008

ISBN 978-952-15-1938-3 (printed)
ISBN 978-952-15-1947-5 (PDF)
ISSN 1459-2045

Tampereen Yliopistopaino Oy, 2008

Abstract

This thesis discusses the usability of current measurement in controlling and monitoring piezoelectric actuators. Current measurement contains information about the actuator and its environment. This work presents methods for utilizing the information in several control applications used in microrobotics, such as displacement control and external force estimation. The importance of current measurement is also discussed in context with piezoactuator -related problems, such as self-heating.

After an introduction to the topic, an electromechanical model of a piezoelectric actuator is presented. The model summarizes the different effects and inputs that affect the output of piezoelectric actuators. The model is later utilized as basis for the development of more specialized models for several control applications.

This thesis presents several control schemes which utilize current measurement in displacement control. The control methods utilize inverse actuator models to estimate the current required for the actuator to move as desired. The experiment results are very good: hysteresis is less than 2% and drift about 1% of the motion range.

Force estimation without the use of force sensors is accomplished with an actuator model that approximates the present external force by combining information about the current, voltage and displacement. The measured displacement can be simultaneously utilized in feedback control, thus enabling precise microrobotic operations. The accuracy of the estimated force is within 10% of the force range, with an average inaccuracy of about 3%.

Current measurement can be used to estimate the self-heating of periodically actuated piezoactuators. Peak-to-peak current increases concurrently with increasing temperature. Experiments show that the current increase is 0.5% per one degree increase in actuator temperature. In addition, a compensation method is presented for the displacement changes induced by self-heating. The displacement error of the heated actuator is reduced to an average of one third when the proposed compensation is used.

This thesis discusses current measurement as a part of a self-diagnostic system. Current measurement has potential in diagnosing faults and monitoring the condition of piezoelectric actuators.

The experimental results achieved with several control applications indicate that the proposed electromechanical actuator model is feasible. Moreover, the results reveal that current measurement provides valuable information that can be utilized in displacement control, and force and self-heating estimation, among others. Consequently, the information obtained by current measurement can often be used to replace a sensor, thus decreasing the complexity of the system.

Acknowledgements

I would like to start by acknowledging the vital financial support of the Graduate School of Electronics, Telecommunications and Automation (GETA); the Finnish Funding Agency for Technology and Innovation (TEKES); the Finnish Cultural Foundation; the Finnish Foundation for Technology Promotion; and the Department of Automation Science and Engineering (formerly the Institute of Automation and Control). I would also like to thank GETA's Ms Marja Leppäharju for creating such a pleasant atmosphere in the graduate school.

My deepest gratitude goes to my supervisors, Prof. Heikki Koivo and Prof. Pasi Kallio. Together they provided an excellent foundation for me to work and learn in. They offered me perspective, experience, expertise, dynamics, freedom, innovation, humour, reliability, wisdom, and the resources and networks of two Universities.

I would like to thank Dr. Tech. Matti Vilkko for modelling co-operation and the productive discussions we shared. Likewise I would like to thank Prof. Zhou Quan for granting me the opportunity to work with the environmental chamber.

I truly appreciate the work of Prof. André Preumont and Prof. Antoine Ferreira, who reviewed this thesis and provided significant contributions towards the improvement of the quality of this thesis.

I applaud the Institute for being such an enjoyable place to work in. In particular I would like to express my appreciation to the Institute's secretaries, but my regard also extends to all the colleagues and professors I have had the pleasure of knowing. In addition to providing an enjoyable environment to work in, the Institute has also organized enjoyable recreational activities, such as summer barbeques and Christmas parties.

The atmosphere in the Micro- and NanoSystems Research (MST) Group has been outstanding, and for this I am forever indebted to all the group members, past and present. The atmosphere is greatly due to Johana, but I would also like to extend a great big thank

you to Marek, Katrin, Mikko and Joose, to name just a few. I cherish the wonderful memories of our time together, in and out of the office.

A very special thank you to all my friends and loved ones, and to the people, who helped me widen my perspectives and relax amongst my hobbies, such as aeromodelling, sailing and badminton.

Last, but not least, a heartfelt thank you to my loving family, and to Satu for being the sunshine of my life.

Tampere, February 2008

Pekka Ronkanen

Table of Contents

List of Publications

Parts of this thesis have been previously published. The following publications are included:

I P. Ronkanen, P. Kallio, and H.N. Koivo, "Current control of piezoelectric actuators with power loss compensation," *IEEE/RSJ International Conference on Intelligent Robots and Systems (IROS)*, Lausanne, Switzerland, pp. 1948-1953, October 2002.

II P. Ronkanen, P. Kallio, M. Vilkko, and H.N. Koivo. "Displacement control of piezoelectric actuators using current and voltage," Submitted to *IEEE/ASME Transactions on Mechatronics.*

III P. Ronkanen, P. Kallio, Q. Zhou, and H.N. Koivo, "Current control of piezoelectric actuators with environmental compensation," *Micro.Tec 2003, 2nd VDE World Microtechnologies Congress*, Munich, Germany, pp. 323-328, October 2003.

IV P. Ronkanen, P. Kallio, and H.N. Koivo, "Simultaneous actuation and force estimation using piezoelectric actuators," *IEEE International Conference on Mechatronics and Automation (ICMA)*, Harbin, China, pp. 3261-3265, August 2007.

V P. Ronkanen, P. Kallio, M. Vilkko, and H.N. Koivo, "Self-heating of piezoelectric actuators: Measurement and compensation," *IEEE International Symposium on Micro-Nanomechatronics and Human Science (MHS)*, Nagoya, Japan, pp. 313 - 318, November 2004.

The Author's Contribution:

Author has designed the methods, planned and conducted the experiments, analysed the results, and is the main author of all Papers.

Notations and Abbreviations

Notations

ε_{ik}^{T}	permittivity
a	constant describing relation between velocity and current
b	temperature dependant factor
C	capacitance
c_1	constant in Power Loss Model
c_2	constant in Power Loss Model
d	displacement
d_a	actual displacement
d_d	desired displacement
D_i	electric displacement
d_{kij}	piezoelectric constants
E_k	electric field
f	frequency
F_e	estimated external force
F_{ext}	external force
F_{spring}	force generated by a spring
G	conductance of an actuator
i_a	actual current
i_c	charging current
i_d	desired current
i_l	leakage current
i_m	motion model current
I_{pp}	peak to peak current
i_s	static model current
I_{sp}	set point peak to peak current

k	constant to define a shape of weight function
k_s	spring constant
k_1	constant describing actuator compliance
K_1	controller parameter 1
k_2	constant describing effect of constant voltage on displacement
K_2	controller parameter 2
K_3	controller parameter 3
P_{in}	input power
P_{out}	output power
Q	charge
r	constant to normalize velocity over the selected velocity range
R	resistance
s	Laplace variable
S_{ij}	strain
s^E_{ijkl}	compliance matrix
t	time
T	temperature
T_{kl}	stress
v	velocity
V	voltage
wf_m	weight function for motion model
wf_s	weight function for static model
x	elongation of a spring
X	impedance representing the cause of power losses

Abbreviations

A	amplitude
AC	alternating current
AD	analogue-digital
Cr	controller
DA	digital-analog
DC	direct current
IEEE	Institute of Electrical and Electronics Engineers
LVDT	linear variable differential transformer
MST group	Micro- and Nanosystems Research Group at TUT
Op1	voltage driving option
Op2	current driving option
PC	personal computer
PI	proportional and integral
PID	proportional, integral and derivative
PZT	plumbum (lead) zirconate titanate

RH	relative humidity
SSE	sum of the squared errors
tansig	hyperbolic tangent sigmoid transfer function
TUT	Tampere University of Technology

1. Introduction

Piezoelectric actuators are one of the most important actuators in microrobotics. Their favourable properties include high resolution and speed. The active actuator material enables simple actuator structures that can be easily miniaturized. Piezoactuators suffer from high hysteresis and drift, and their output is influenced by temperature and load, among other factors. These deficits cause additional effort to be put on the control issues of these actuators. As will be introduced in the following section, these actuators also work as sensors. Typically, however, this function has not been utilized in control applications. The approach in this work is more to utilize the information that the actuator can provide. In practice, this means focusing not only on the actuator input voltage but also including input current into consideration in the control schemes.

The goal of this work is to study how an actuator's current measurement can be utilized in control applications. The control applications on which this work concentrates are the displacement control and force and self-heating estimation. To achieve the goal, an actuator model consisting of all the inputs that affect the output of the actuator is created. This actuator model is then utilized in individual control applications to verify the model.

This chapter provides background on the topic; piezoelectricity in Section 1.1 and different actuators in Section 1.2. Section 1.3 presents displacement control methods, Section 1.4 introduces force control, and Section 1.5 discusses the self-heating of piezoelectric actuators. Section 1.6 presents the organisation of the thesis, and Section 1.7 the contribution of the thesis.

1.1 Piezoelectricity

Pierre and Jacques Curie discovered the piezoelectric effect in 1880. Pierre Curie had previously studied the relations of pyroelectricity and crystal symmetry, and this must have been the driving force to seek electrification from pressure. The brothers also had an understanding of the direction in which pressure should be applied and applicable crystal classes. Hankel proposed the name 'piezoelectricity' where the prefix 'piezo-' is derived from the Greek word for 'press'. In the following year, Lippmann predicted the existence of the inverse piezoelectric effect from thermodynamic considerations, and the Curies verified this before the end of 1881 [31].

Piezoelectric actuators are based on the inverse piezoelectric effect. Direct piezoelectric effect occurs when pressure is applied to a piezoelectric material, resulting in a voltage between the crystal surfaces. In inverse piezoelectric effect, voltage is applied to an asymmetrical crystal lattice, causing the material to deform in a certain direction [18].

The piezoelectric effect requires crystal asymmetry, which causes an electric dipole to the crystal. The electric dipole can be affected by applying stress on the material, which then causes a change in the dipole moment (direct piezoelectric effect) or by straining the dipole by applying electric field over the crystal faces (inverse piezoelectric effect). Even though individual crystals have electric dipoles, no net effect occurs in the material on a macroscopic scale before the material is poled, because the neighboring dipoles cancel each other. This is due to the random orientation of the dipoles. During the poling process, ceramics are heated above the so-called Curie temperature, where the central ion causing the asymmetricity moves to the centre so that the crystal becomes symmetric. The material is then cooled under an electric field causing asymmetricity to occur in the same direction. After this, the material has a certain net dipole over the whole piece in the desired direction.

Hysteresis and Drift

After poling, the net dipole exists over the whole piece, the material has still many regions with different dipole directions, called ferroelectric domains, while the regions between different domains are called domain walls. When the material is subjected to an increasing electric field, polarization of domains with unfavourable dipole direction starts to switch to the closest possible direction parallel to the direction of the applied field. This leads to moving and switching of domain walls. Since domain wall switching spreads as the field increases, larger regions participate in generating material strain in larger fields. This leads to a larger relative movement, or in other words, $\Delta d/\Delta V$ increases at higher voltages, which can be seen in Figure 1.1 in the shift between point A and B. As the field starts to decrease, a smaller or even opposite field is required to switch the domain walls back. This can be seen in Figure 1.1 from point B to point C. As a consequence of the domain wall switching, hysteresis occurs. Note that with higher electric fields than presented in the figure, all the domains are aligned and the material response is more linear. This region, however, is not typically utilized in actuators. Using high electric fields can cause undesired results, such as 180° polarization switching with an electric field opposite to poling direction and dielectric breakdown. Furthermore, the relative movement is smaller at the high field region. The switching is not only affected by the electric field, but also the time. A smaller field over a longer time period causes switching of the polarization and resulting as strain. This can be seen as a drift on a macroscopic level [15].

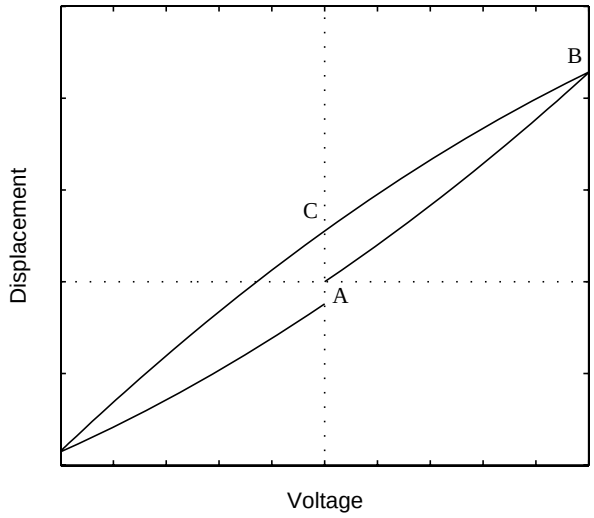

Figure 1.1. Typical hysteresis of piezoelectric actuators.

Sensors and Power Harvesting

Applications, where direct piezoelectric effect is utilized, are different sensor [69] and power harvesting [65] applications. Note, however, that some sensors, such as different resonators [5], are based on mechanical motion, and thus, utilize inverse piezoelectric effect.

1.2 Piezoelectric Actuators

This section presents different piezoelectric actuator principles. They include stacks, benders, and various motors [56]. A stack contains a pile of piezoceramic layers and electrodes, thus increasing the maximum displacement. The properties of a stack resemble most on the actual material: high force (proportional to area, in MPa range) and speed (kHz), very good resolution (nm), and small displacement (0.1-0.2%). Benders have mechanical motion amplification, where two piezoceramic layers are attached with opposing polarisation. Thus, the first layer expands while the other shrinks under voltage excitation. This causes the structure to bend, and the overall motion on the actuator tip is greater than the strain of the ceramics. The result, aside from greater motion, is smaller force and lower resonance frequency.

To overcome the small motion range, various piezoelectric motors have been developed. The general idea in the motors is to add small microscopic motions into a larger motion. They include ultrasonic motors [54], impact [28] and “stick and slip” [8] drives, and inchworm motors [24].

1.3 Displacement Control

Piezoelectric actuators are widely used in applications requiring high resolution and accuracy. Their favourable dynamic properties extend the application areas into high-speed areas such as vibration control. However, large hysteresis, drift, self-heating, and load effects decrease the open-loop positioning accuracy. If a high accuracy is required, these non-linearities have to be compensated for. The compensation is usually accomplished by means of four control principles: *feedforward voltage control*, where non-linear models are typically used [12], [14], [25]; *feedback voltage control*, where various displacement sensors are used [10], [27], [35], [38], [41], [44]; *feedforward charge control*, where the operating current is controlled [55], and *feedback charge control*, where charge is measured and controlled [13], [23], [58]. These different control principles are presented in Figure 1.2 and are introduced in the following sections.

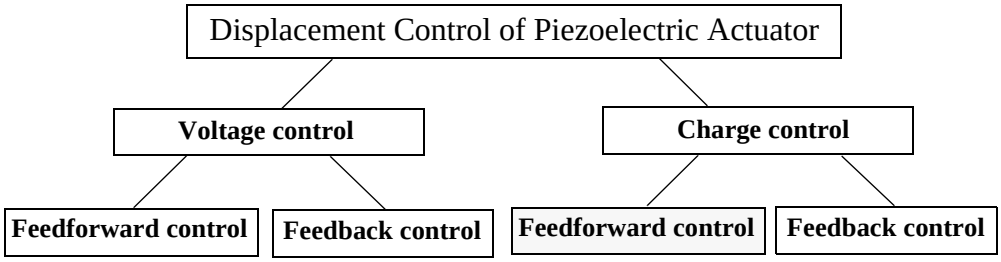

Figure 1.2. Displacement control principles. The focus of this work is feedforward charge control.

Piezoelectric actuators are commonly controlled by using voltage as an input signal. The greatest difference between the voltage and charge control approaches can be seen in hysteresis and drift; the displacement with respect to voltage contains hysteresis, while the displacement with respect to charge is quite linear (with an assumption that the electric field is small enough that it does not result 180° domain wall switching). The reason for this is that the hysteresis between the electric field and the strain results from the hysteresis between electric field and polarization, whereas the relationship between polarization and strain is nonhysteretic [15]. Polarization (charge/area), on the other hand, is proportional to charge. In practice, however, some hysteresis still exists in charge control approaches, although reduced to at least one fifth of the original [13], [23], [58]. The disadvantages include the need for additional electric circuits and, thus, the increased complexity of the control hardware.

1.3.1 Feedforward Voltage Control

Feedforward voltage control scheme contains an actuator model [12], [14], [19], [25], [40]. The model can be either a direct or an inverse model. Their usage differs by model type, Figure 1.3. The direct actuator model is used to obtain feedback for the controller, while the inverse actuator model estimates the input for the desired output to be obtained. The benefit of the feedforward voltage control is the low hardware complexity of the

system, since sensors or complicated driving circuits are not required. A drawback is a highly complicated actuator model, if all non-linearities would be included, such as hysteresis, drift, load, and temperature effects. Hysteresis is typically modelled using Preisach model and its many variations [19], [29], [66].

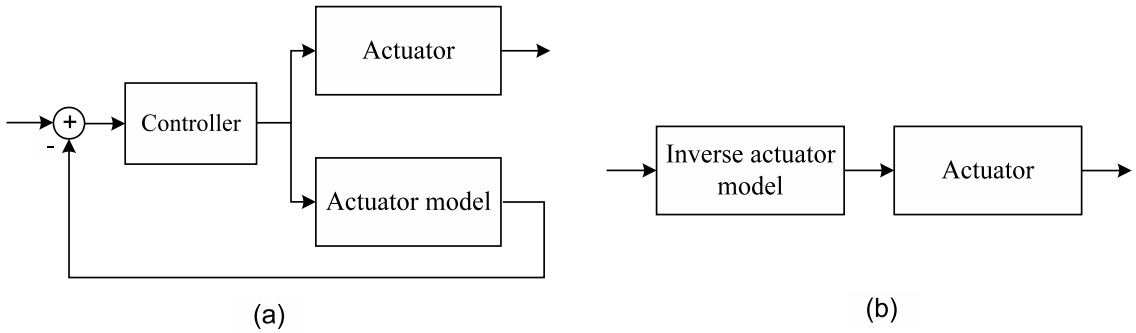

Figure 1.3. Model-based control principles (a) with actuator model and (b) with inverse actuator model.

1.3.2 Feedback Voltage Control

Feedback voltage control utilizes various sensors to measure the output of the actuator. Typically a PI- or PID-controller is used. Various sensors have been used to measure the response of piezoactuators, including linear variable differential transformer (LVDT) [10], capacitive sensor [41], Hall sensor [35], laser sensor [27], strain gauges [44], and piezoceramics [38].

1.3.3 Feedforward Charge Control

Charge control circuits can be divided into two groups: feedback and feedforward circuits. Current drives utilize feedforward control. A charge can be obtained by integrating a known current over a period of time. Constant current has been used over a variable period of time in [55] to obtain a certain displacement of a piezoelectric actuator but without taking into account any power losses. A couple of current amplifiers have been published: an amplifier that can be modified to be used either as a current or charge amplifier is presented in [21] and a commercial current driver is presented in [16].

1.3.4 Feedback Charge Control

In feedback charge control, the charge is measured and used for feedback control. The charge measurement can be accomplished by two methods: The first, and more common method, utilizes a capacitor in series with a piezoelectric actuator, as presented in [7], [13], [21], [58] and [76]. This is quite a simple solution, but the voltage over the serial capacitor is not directly proportional to the charge of the actuator. This setup is known as Sawyer-Tower circuit [63]. In another method, the voltage of subsidiary electrodes is measured and used in the feedback [23]. The electrodes are additional layers of the actuator, to which a charge proportional to the internal charge is induced.

A charge control model combining actuator, mechanics and charge control is presented in [2]. This model is intended for model based controller design.

Most of the charge control applications have been created utilizing Sawyer-Tower circuit and its modifications, and both inverting [76] and non-inverting [7] amplifier approaches exist. To overcome possible stability problems at low frequency, often a resistor is added parallel to the capacitor [7], [22], [76]. Thus, the control acts as a voltage control at low frequency losing its hysteresis reduction capability. Some small modification to the Sawyer-Tower approach exists, such as utilization of a current mirror to obtain the same charge to the actuator as to a reference capacitor [22] and a switching charge amplifier to regain the charge from the actuator and later to re-use it [47].

Self-sensing is one area very close to charge control, since there the focus is often to measure the charge and use it for e.g. force estimation or vibration suppression. Some vibration suppress approaches could perhaps be considered belonging to charge control group, since charge is measured and utilized in motion control. However, since the disturbances, such as force acting on the actuator, originate from an outside source, unlike the intrinsic hysteresis that this section focuses, these methods will be discussed more in the following section. A review of vibration suppression methods is presented in [53] presenting many different electrical circuits to measure charge.

1.4 Force Control

Micromanipulation techniques are widely used in research of several fields. Common to the majority of the cases is the required operator. For the micromanipulation techniques to be exploited in high volumes in areas such as industrial and biological applications, the role of the operator should be reduced to a minimum. This can be achieved by increasing the automation level [34].

Previously, the research has focused on the development of microrobots, -manipulators and tools. This has led to a situation where the performance of the devices and tools would support fully automated systems, but the knowledge about the target itself is inadequate. Therefore, the research trend has recently shifted towards techniques that gather more knowledge about the objects to be manipulated and about the operating environment. These techniques include machine vision and various sensor developments such as force sensors. These are not competitive techniques but rather complimentary.

Contact sensing is one of the most important actions; for example, in pick and place, for an operational point of view. The most generic method to sense this event is the application of force sensors. Many other methods are based on certain target properties such as conductivity. Further, in biological applications such as in manipulation tasks related to cell cultivation and microdissection of tissues, force and contact sensing are

required to enable full automation as well as to gather information on the mechanical properties of the target.

There are various methods to measure forces; many of the most suitable methods for micromanipulation are listed in review articles such as [17] and [46]. These methods include strain gauges; use of piezoresistive, piezoelectric and piezomagnetic effects; capacitive sensors; and optical sensors [17], [46]. Perhaps the most convenient of these methods are the ones based on the piezoelectric effect, since they enable simultaneous sensing and actuation, simplifying the mechanisms and enabling further miniaturizing of the system as compared to a setup with a separate actuator and force sensor. Rest of the section presents different approaches to measure forces and vibrations using piezoelectric actuators. First, couple of methods are introduced that do not utilize charge. After this, approaches utilizing charge are presented with some examples. The division there is based on the applications, which include vibration suppression and external force estimation.

Simultaneous sensing and actuation using piezoelectric materials is not as rare as one could imagine; the mass quartz balance is perhaps the best example of this. The mass quartz balance is vibrating, and a shift in the resonance amplitude is measured that is proportional to the measured mass. Other examples can be found, where piezoceramics is actuated by AC voltage for sensing purposes, such as [73] and [42]. This sensing method gives good results when masses or other mechanical properties of objects are needed to be measured. This method cannot be utilized for a more general use in microrobotics, since it requires a certain motion to be generated for the measurement. In microrobotics, the motion trajectories cannot be specified in advance, and they can have some static positions as well.

A force control approach is proposed in [1], where a sliding-mode-based force control method is presented; it is based on a non-linear electromechanical model of the actuator and a displacement measurement using strain gauges. Force is estimated using the actuator input voltage, the output displacement, and the non-linear actuator model. The difference between the model output and the real displacement is used to approximate the external force. The obtained results are relatively good, but as this paper points out, any inaccuracy in the model will cause errors in the force estimation.

Utilizing charge to estimate and suppress external disturbances, such as force or structural vibration, is referred as self sensing [53]. First, vibration suppression is introduced. This can be divided into two groups: (i) plain vibration suppression, where no other movements is desired [48], [70]; and (ii) vibration suppression with other movements [33], [64]. Often a capacitance bridge, similar to the Wheatstone bridge, is used when other movements are desired [33], [64]. Also here, resistors are added parallel to capacitors to overcome the dc-drift. Thus, the bridge measures only voltage at lower frequencies. The bridge is sensitive to capacitance variation that occurs in the actuator and

attempts to reduce this problem are such as additional capacitors to the bridge [64] and using similar actuator as a counter capacitor [33].

The approaches to measure actual external force can also be divided into two similar groups as before: (i) without other movement [39] and (ii) with other movements [19], [68], [72]. An example of application, where no other motion is required, is a tactile sensor. An array of these was constructed using piezoelectric polymer (polyvinylidene fluoride - PVDF) matrix and metal-oxide-semiconductor field-effect-transistor (MOSFET) amplifier arrangement. One polymer surface was grounded, while the other was directly connected to the MOSFET gate. Due the stability issues, the polymers were pre-charged with bias voltage before the measurement. The response was quite linear over the measurement range with some hysteresis present [39].

To enable force control of a gripper consisting of a piezoelectric bender, a self sensing approach was created by using serial capacitance with a parallel resistor [68]. The obtained force was quite close to the desired force, however, numerical values of the accuracy was missing. For a micromanipulation tasks, the drawback of this setup is the lack of displacement control.

A system to measure torque acting on a piezoelectric motor was introduced in [72]. The torque leads to a phase difference between the input voltage and the resulting charge. This phase difference is analysed and used to determine the motor torque. Typical error of 5% was reported while the error increased with higher torques.

An elegant force estimation scheme is presented in [19]. There an adaptive filter is used to approximate the actuator capacitance, thus enabling separation of the charge induced by external force and the charge caused by control voltage without capacitance bridge. However, the method how actuator charge is actually measured remains unclear. The estimation method shows quite good linearity and accuracy [20] and is utilized in force control of a microgripper.

1.5 Self-Heating

Driving piezoelectric actuators with fast periodic control signals causes intrinsic heat generation in the piezoelectric elements. The increased temperature causes inaccuracy in the operation of the piezoelectric actuators due to heat expansion and variation of the characteristics of the element as a function of the temperature; and it can even cause destruction of the element itself.

When a piezoelectric actuator is under a varying electric field, the actuator heats until a steady-state is reached. In the steady-state, the heat generation and radiation are at the same level [43], [67], [71], [75].

Issues influencing self-heating include the frequency and amplitude of the driving voltage, the size-or, more specifically, the volume-area ratio of the actuator, the actuator material itself, and the used frequency with respect to resonance frequency.

It is suggested that dielectric losses are the main reason for self-heating [6], [43], [71], [74], [75]. The heat generation appears to be proportional to the driving frequency and to the square of the amplitude of the driving voltage [43], [75]. Since the actuator produces heat in the entire volume and dissipates it through the surface area, it seems quite obvious that the heat generation is proportional to the volume/area of the actuator [71]. The mechanical quality factor (reciprocal of internal friction) of the piezoelectric material affects the amount of self heating, and besides this, the Curie temperature limits the allowable highest temperatures. These vary between different materials and for high power and temperature applications, the material should be carefully chosen [77].

Heat generation increases rapidly when frequency approaches resonance frequency, this is caused by the increase of mechanical losses [45]. Although losses increase, the maximum efficiency can be expected at the resonance frequency [11]. However, slightly higher mechanical quality factor values than at the resonance frequency can be found at electrical antiresonance, where the actuator impedance increases rapidly [71]. Antiresonance frequencies locate in the proximity of resonance frequencies [61].

Some piezoelectric materials exhibit other effects very closely related to piezoelectricity such as pyroelectric effect. The typical actuator material PZT is one of them. As the name pyroelectric refers, "pyro-" derived from Greek words meaning "fire", it occurs as the change of polarization charges with temperature. Pyroelectricity can be divided into primary and secondary pyroelectric polarization. The first of which is observed with a clamped crystal, while the latter refers to a chain of events; change of temperature causes thermal expansion which leads to polarization through piezoelectric effect [9]. The effect of temperature on the polarization switching rate was observed in [52]. Therefore, it would indicate that the pyroelectricity is related to enhancement of the polarization switching with the increased temperature.

Therefore, it does not come as a surprise that temperature influences the output of piezoelectric actuators [79]. The outside temperature is rather simple to measure, but intrinsic heat generation requires a sensor attached to the actuator. In some applications, this might be difficult to accomplish.

Besides pyroelectricity, change in conductance with a temperature change influences the actuator current. At temperatures below the Curie temperature, influence of pyroelectricity appears to be larger than the effect of increased conductance [37].

1.6 Organization of the Thesis

This thesis is organised as follows: Chapter 1 introduces the topic. Chapter 2 presents the used methods and devices. After these, an electromechanical model of piezoelectric actuators is created in Chapter 3. This is then utilized in different control applications, including displacement control in Chapter 4 and external force estimation in Chapter 5. Utilization of current measurement in self-heating is discussed in Chapter 6. Chapter 7 introduces other possible control applications for current measurement. Chapter 8 concludes the thesis.

1.7 Contributions of the Thesis

The contributions of the thesis are the following.

1. Show the value of current measurement in control and monitoring of piezoactuators, having the capability to replace one sensor in many cases.

2. A new electromechanical model for piezoelectric actuators is developed, combining different inputs and phenomena that affect the output of the actuator.

3. Two novel displacement control methods are developed utilizing the current measurement, including temperature compensation for one of the methods.

4. A novel external force estimation method is presented that does not use force sensors. The method enables simultaneous position feedback control.

5. A new method is presented for the estimation of a self-heating state by current measurement.

6. A novel compensation method to decrease the effects of self-heating on displacement is developed.

7. New ideas to utilize current measurement in fault diagnostics and in condition monitoring are proposed.

2. Methods

This chapter introduces methods utilized in the experiments described in Chapters 4 to 6. These include modelling methods, control methods, control software and devices, tools, and actuators. Section 2.1 presents the modelling methods used such as grey-box and neural networks. Section 2.2 introduces feedforward and feedback control methods, Section 2.3 presents the used software, and Section 2.4 describes the devices, tools, and actuators.

2.1 Modelling Methods

This section presents briefly the modelling methods used in the following chapters and in the papers that are part of the thesis. These include grey-box and neural network models.

2.1.1 Grey-Box

Grey-box models are utilized in models when part of the physical phenomenon is quite well understood. Thus, this known phenomenon is introduced into the model when - more complicated and less understood relations are modelled with experimental models such as with neural networks. A good example of the physical phenomenon utilized in actuator models is the Ohm's Law. When the actuator is held stationary, the required control current can be modelled with Ohm's Law to estimate the leakage current occurring in the actuator. This is utilized in several models in Chapter 4 and in Papers I-III.

2.1.2 Neural Networks

Neural networks are utilized in several actuator models in Chapters 4 and 5, and in Papers II and IV. Multilayer perceptron networks have the capacity to model non-linear phenomena and powerful software tools to create, train, and simulate these models are available. The used network is the feedforward type, and the training function is Levenberg-Marquardt backpropagation [50]. All networks used are two-layer networks; the number of neurons at the first layer is two in Chapter 4, Paper II, and 10 in Chapter 5, Paper IV.

2.2 Control Methods

This section introduces control methods used in the experiments presented in Chapters 4 to 6 and in all Papers. The developed control methods are the feedforward type of control but require feedback control in some supporting functions such as in current driver or in position control.

2.2.1 Feedforward Control

This section presents the model-based feedforward control method utilized in the experiments. Figure 2.1 presents a block diagram of the feedforward control principle utilizing an inverse process model. The inverse process model has a setpoint as an input and generates an input for the actual process to obtain the desired output value. This approach is utilized in the displacement control in Chapter 4 and in self-heating temperature compensation in Section 6.3.; the difference is that some other process information is also provided for the model input, including actuator voltage in Chapter 4 and current in Section 6.3.

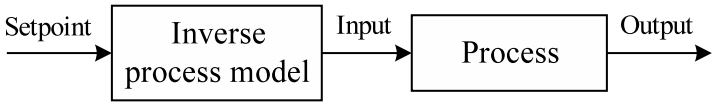

Figure 2.1. Feedforward control principle utilizing inverse process model.

The force and self-heating temperature estimation methods presented in Chapter 5 and in Section 6.1 have a structure as presented in Figure 2.2. The estimates can be utilized further in a model-based control. In Chapter 5, the process information is actuator current and voltage, and position. In Section 6.1, the process information is actuator current.

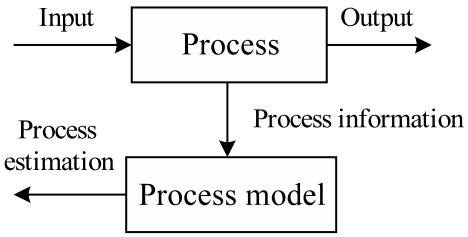

Figure 2.2. Block diagram of process estimation methods.

2.2.2 Feedback Control

This section presents a feedback control method utilized in the experiments. Although the actual target of this work is to develop new feedforward control methods, the feedback controller is required to enable certain functions such as a current drive in displacement

control in Chapter 4 and a simultaneous displacement control in force estimation in Chapter 5. The control principle is presented in Figure 2.3.

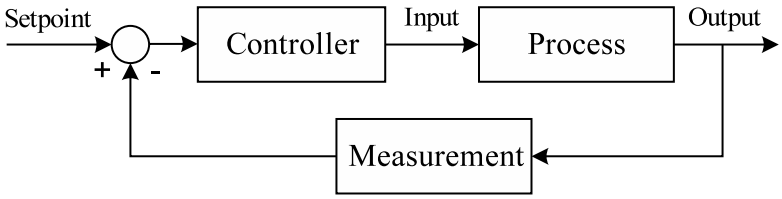

Figure 2.3. Feedback control principle.

2.3 Software

This section introduces software used in the experiments presented in Chapter 4 to 6. These include DOS software, a real-time Linux software, and an XPc target from Matlab.

2.3.1 DOS Software

DOS software is used in the experiments presented in Section 4.3.1, in Section 4.3.3, and in Papers I and III. It is control software with a built-in PID controller running at 250 Hz. The software reads the desired control value from the file, and has two measurement channels and one output channel. All the signals are recorded into a file. The software was developed by the Micro- and Nanosystems Research Group (MST group) at Tampere University of Technology (TUT).

2.3.2 RT-Linux software

Real-time Linux software GMC-RT is used in the experiments presented in Chapter 6 and in Paper V. It is a measurement and control software with an adjustable number of measurement channels and outputs. Either a PID controller or other simple controller can be used. The control frequency can be about 5 to 10 kHz at maximum. The software was developed at the MST group at TUT by Tuukka Ritala [62].

2.3.3 XPc-target

XPc-target is an additional toolbox for Matlab. It consists of a real-time operating system for the target PC running the created controller, and a library of data-acquisition blocks for Simulink. XPc-target enables usage of complex control schemes with a relatively high frequencies up to 50 kHz. XPc-target is used in experiments presented in Section 4.3.2, in Chapter 5, and in Papers II and IV.

2.4 Hardware

This section presents the devices, tools, and actuators used in the experiments described in Chapters 4 to 6. These include a piezo amplifier, current meters, data-acquisition boards, displacement meters, piezo actuators, an environmental chamber, thermistors, and methods to create the external forces.

2.4.1 Piezo Amplifier

The piezo amplifier used in all the experiments is a Piezo Systems EPA 102. It has a voltage range of ± 200 V and a maximum current of 200 mA [60].

2.4.2 Current Meters

The current meter used in most experiments is a 160B Digital Multimeter by Keithley Instruments (USA). Current control principles require a very sensitive current meter. The maximum resolution of this device is 10 pA, and it has an analog voltage output proportional to the current measurement.

Since the 160B has a cutoff frequency of 40 Hz, the current measurement in higher frequency self-heating experiments, as described in Chapter 6 and in Paper V, are done with a 10 Ω resistor.

2.4.3 Data-Acquisition

Data-acquisition is performed in the experiments presented in Section 4.3.2, in Chapter 5, and in Papers II and IV with a National Instruments AD-board having two analog outputs (PCI-6052E). In the rest of the experiments, data-acquisition is performed using an AD-board model PCI-6036E of National Instruments.

2.4.4 Position Sensors

Displacement in the experiments presented in Section 4.3.1 and in Paper I is measured using a laser position sensor M5L/2 from Mel Mikroelektronik with a measurement range of ±1 mm. Displacement in the rest of the experiments is measured using a laser position sensor M5L/0,5 with a measurement range of ±250 µm from the same company [51].

2.4.5 Signal Generator

The signal generator used in the self-heating experiments presented in Chapter 6 and in Paper V is 33120A from Agilent [3].

2.4.6 Piezo Actuators

The piezo actuator used in the experiments presented in Section 4.3.1, in Section 4.3.3, and in Papers I and III is a piezoelectric bender NB 40x10x0.6-21 by Tokin (Japan). A similar actuator is used in the experiments presented in Section 4.3.2 and in Chapter 5, and in Papers II and IV, where the used actuator is a bimorph bender NB38*4*0.6, also from Tokin. In the self-heating experiments presented in Chapter 6 and in Paper V, three piezo stacks with different sizes are used; 3*3*18 mm from Marco (Germany) with resonance frequency of 70 kHz [49], 5*5*18 mm from Noliac (Denmark), and 10*10*10 mm also from Noliac. The actual resonance frequencies of the latter two actuators is unknown, but are at minimum of 22 kHz and 11 kHz respectively. The probable resonance

frequencies are, however, closer to 100 kHz [57]. The material of all the three stacks is a soft-doped PZT.

2.4.7 Environmental Chamber

An environmental chamber used in the experiments presented in Section 4.3.3 and in Paper III was developed in the MST-group at TUT and is introduced in detail in [78]. The temperature can be controlled between -10 to 40^{o}C and relative humidity (RH) between 5 to 80%.

2.4.8 Thermistors

Thermistors used in the self-heating experiments presented in Chapter 6 and in Paper V to measure the actuator temperature are surface-mount NTC thermistors by Bc Components Vishay, Part No. 2322 615 13472. Thermistors are glued onto the actuators with thermally conductive glue.

2.4.9 External Force

The external force used in the experiments described in Chapter 5 and in Paper IV is produced in two ways: (i) by attaching lead weights to the actuator and (ii) using a plastic cantilever that acts as a spring-type load. Lead weights produce constant force on the actuator, while the force generated by the cantilever is displacement dependent, as is described by Hooke's law:

$$F_{spring} = -k_s \cdot x, \tag{2.1}$$

where F_{spring} is the force generated by the spring, k_s the spring constant, and x is the distance by which the spring is elongated from its equilibrium position.

Figure 2.4 presents the measurement setup. In the figure, a plastic cantilever pushes the piezoelectric bender downwards. The cross-sectional dimensions of the plastic cantilever are 7.5 mm x 1.0 mm, and the bending length is 23 mm.

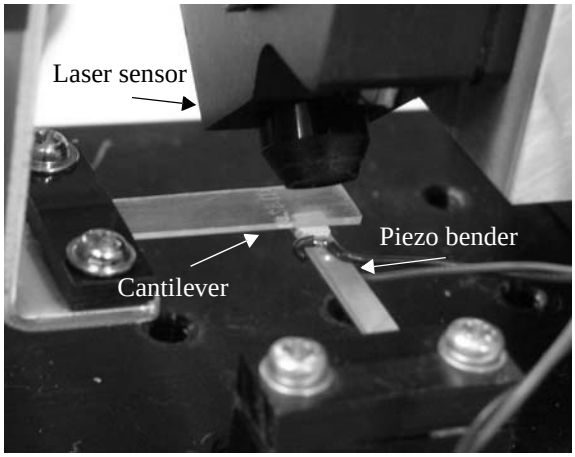

Figure 2.4. Measurement setup of force estimation system presented in Chapter 5.

3. Electromechanical Modelling of Piezoelectric Actuators

This chapter presents a general model of piezoelectric actuators. The model summarizes different effects and inputs that affect the output of piezoelectric actuators. Relations between different inputs and outputs will be presented, including voltage, current, external force, displacement, and temperature. For the complexity of the effects and their connection mechanisms, the model will be presented at a general level. The model will be used in the following chapters as a basis for more specific models and control methods.

Section 3.1 presents the relation among voltage, displacement, and external force. Effects of temperature and humidity are discussed in Section 3.2. Section 3.3 introduces the self-heating effect. Relation between input voltage and current is presented in Section 3.4. All these are then combined as a single actuator model proposed in Section 3.5.

3.1 Relation between Voltage, Displacement, and Force

This section discusses the relation between voltage, displacement, and force. Constitute equations of piezoelectricity describe the relation among the electric field (proportional to voltage), strain (relation to displacement), and stress (force/area) as presented in IEEE standards of piezoelectricity [30]:

$$S_{ij} = s^{E}_{ijkl} T_{kl} + d_{kij} E_k \tag{3.1}$$

$$D_i = d_{ikl} T_{kl} + \varepsilon^{T}_{ik} E_k \tag{3.2}$$

where S is strain (6×1 vector), s is compliance matrix (6×6 matrix), T is stress (6×1 vector), d presents piezoelectric constants (d_{kij} 3×6 matrix, d_{ikl} 6×3 matrix), E is electric field (3×1 vector), D is electric displacement (3×1 vector), and ε is permittivity (3×3 matrix). The Cartesian tensor notation is used in the constitute equations.

To illustrate the effect of the external force, Equation (3.1) is converted to a simplified relation between force and displacement under a constant electric field

$$d = -k_1 F_{ext} + k_2, \tag{3.3}$$

where k_1 and k_2 are constants, d displacement, and F_{ext} external force. The direction of force F_{ext} is opposite to displacement d. This equation describes the force-displacement line presented in Figure 3.1. By increasing the voltage, the line can be shifted, as illustrated in Figure 3.1.

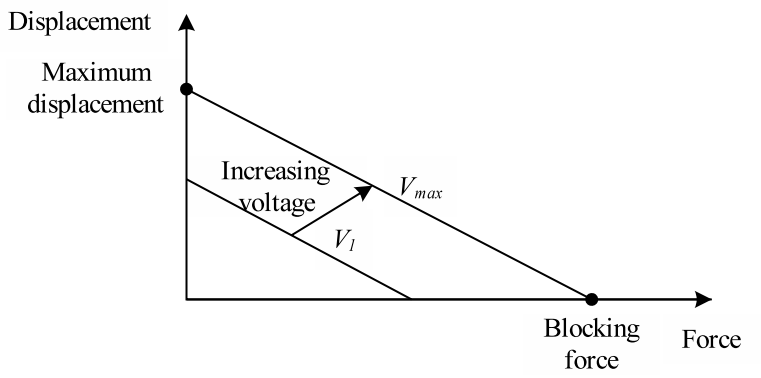

Figure 3.1. Force-displacement line under constant electric field.

The presented relation among voltage, displacement, and external force is a simplified linear representation of the actual phenomenon. In real actuators, the relation is compliated by non-linearities such as hysteresis and drift as discussed in Section 1.1.

3.2 Temperature and Humidity Effects

This section discusses the effects of temperature and humidity. These effects on piezoelectric actuators are quite insufficiently studied; manufacturers have made some studies regarding how the temperature affects the maximum displacement [4], the piezoelectric effect, and the thermal expansion of the ceramics [59]. The effects of temperature and humidity on the maximum displacement of a piezo bender were reported in [79]. The displacement varied with both temperature and humidity. Since protection against humidity is quite simple, and studies in Paper II showing the effect of humidity is not significant; it will be left out of consideration in the general actuator model. Thus, only the effect of temperature is included in the model. One coupling mechanism for the temperature effect is the pyroelectric effect that seems to enhance the polarization switching, as discussed in Section 1.5, resulting to a higher strain with a same voltage.

3.3 Self-Heating

Driving piezoelectric actuators with fast periodic control signals causes intrinsic heat generation in the piezoelectric elements. The increased temperature causes inaccuracy in the operation of the piezoelectric actuators due to heat expansion and variation of the characteristics of the element as a function of the temperature. Heat generation can cause even the destruction of the element itself.

Self-heating will be included in the actuator flow chart presented in Figure 3.2 since it is affecting the actuator temperature. Self-heating will be presented on an energy level to illustrate how different losses such as dielectric, piezoelectric coupling, and mechanical losses generate heat. Self-heating, however, is not included in the actuator model, due to its indirect influencing mechanism through the actuator temperature.

3.4 Relation between Voltage and Current

Piezoelectric actuators are commonly controlled by using voltage as an input signal. Since the primary electrical property of piezoelectric actuators is capacitance, it also describes the relationship between charge Q and voltage V:

$$C = \frac{Q}{V} \tag{3.4}$$

The capacitance is a function of the permittivity of the piezoceramics and the actuator dimensions; areas of electrodes and their distances from each other. If capacitance C was constant, using voltage or charge as an input signal would give the same result. However, mainly due to changes in permittivity caused by polarization switching [15], discussed in Section 1.1, the deformation of the material results in a change in the capacitance. Thus, a charge as a control signal gives results different from those that a voltage gives. Therefore, the changes in the capacitance are interesting from a control point of view.

Both (i) the distance and the area and (ii) permittivity affecting through polarization change as the piezoceramics deforms and, thus, the capacitance varies according to the displacement of the actuator. Therefore, the capacitance can be written as a function of the displacement, and we mark it as $C(d)$. The goal is not to create an analytical model of the capacitance; therefore, actuator dimensions and permittivity are left out of the capacitance function. Only the change of capacitance is of interest and it can be considered as a function of the actuator displacement.

Charge Q can obtained by integrating a known charging current i_c over a period of time, as presented in Equation (3.5).

$$Q = \int_0^t i_c(t)dt \tag{3.5}$$

The assumption behind this equation is an ideal actuator; no loss current i_l occurs. Since the ceramics has a certain finite resistance, the occurring leakage current is influenced by voltage $V(t)$ according to Ohm's Law. Temperature $T(t)$ has an effect on the leakage current by changing the material conductance [37], as for most of the materials. Furthermore, changes in displacement $\Delta d(t)$ cause piezoelectric coupling and mechanical

losses, such as elastic losses [71]. By including the loss current $i_l(V(t),T(t),d(t))$ into Equation (3.5), the result is

$$Q = \int_0^t (i_c(t) - i_l(V(t), T(t), d(t)))dt. \tag{3.6}$$

By combining Equations (3.4) and (3.6), we obtain

$$V = \frac{\int_0^t (i_c(t) - i_l(V(t), T(t), d(t)))dt}{C(d)} \tag{3.7}$$

Thus, the primary issues that cause changes on the relation between voltage and current include voltage, temperature, and displacement.

3.5 General Model of Piezoelectric Actuators

This section presents a general model of piezoelectric actuators. The previous sections have discussed the different effects and connections of displacement, force, temperature, self-heating, voltage, and current. This section combines these properties into a single model. The detailed relations among these different properties are too complex for an analytical equation, but a function combining the effects is presented.

The different aspects discussed in the previous sections are implemented as a block diagram in Figure 3.2. Both voltage and current driving options are included in the chart. These are marked as Op1 for voltage and Op2 for current. In the following, the chart is discussed. For clarity, when referring to parts in the chart, first letter of the name is capitalized.

This section discusses the Piezoactuator part in the chart. Inverse piezoelectric effect presented in Equation (3.1) (Section 3.1) is represented in the chart by Voltage $V(t)$ and External Force $F_{ext}(t)$ inputs and Displacement $d(t)$ as output. As the linear equation describes, the chart presents that Displacement $d(t)$ is affected by Voltage $V(t)$ and External Force $F_{ext}(t)$. The material constants are left out of the chart for simplicity, since the real phenomena are not linear, although simplified in Equation (3.1). A Force potential is added after the ceramics to illustrate the output of the ceramics with Voltage input. This describes Force potential that can either strain the material or act as an opposing force to External Force. The connection between the Displacement $d(t)$ and the Piezoceramics describe two issues: (i) Direct piezoelectric effect occurs when External Force strains the material and, thus, Piezoceramics generates a charge, which results in Current or Voltage, depending on the driving method. Besides the direct piezoelectric effect, the connection

between Displacement and the Piezoceramics describes also (ii) the change in the actuator electrical properties due to the change in Displacement, as presented in Section 3.4.

Temperature changes the actuator properties, as presented in Section 3.2. This is illustrated by a connection between Temperature and the Piezoceramics in the chart. Temperature is affected by Self-Heating as presented in the chart. The amount of Self-Heating is influenced by power losses occurring in the actuator, which is the difference between Input and Output Power. Power losses include dielectric, piezoelectric coupling, and mechanical losses. Mechanical losses contain elastic losses [71]. Input Power is presented in Equation (3.8) and Output Power in Equation (3.9). The power issues and losses are discussed from an actuator point of view and are different when considered from a sensor point of view.

$$P_{in} = V(t) \cdot i(t) \tag{3.8}$$

$$P_{out} = \frac{F_{ext}(t) \cdot d(t)}{t} \tag{3.9}$$

The relation between Voltage and Current discussed in Section 3.4 is presented in the chart: Either Voltage (Op1) or Current (Op2) is fed to actuator, and the resulting Current (Op1) or Voltage (Op2) depends not only on the actuator physical properties but also on Temperature and on the actuator state (Displacement), as discussed in the previous section.

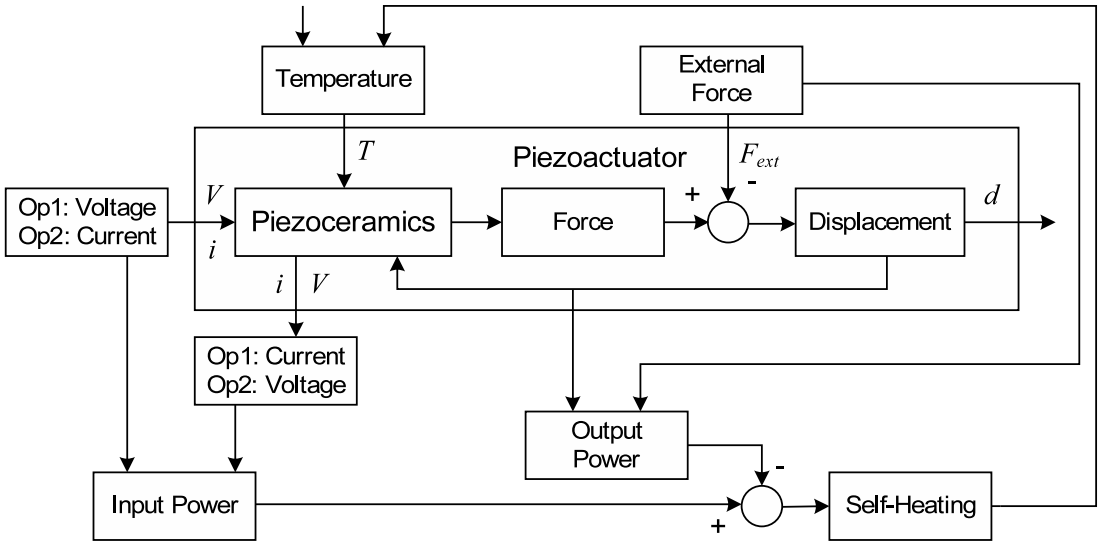

Figure 3.2. Flow chart of the piezoactuators.

In mathematical form, the current $i(t)$ can be given as

$$i(t) = f(V(t), T(t), F_{ext}(t), d(t)) \tag{3.10}$$

This states that current $i(t)$ is a function of input voltage $V(t)$, actuator temperature $T(t)$, external force $F_{ext}(t)$, and displacement $d(t)$. Similarly, voltage $V(t)$ in the second option (Op2.) can be presented with the following equation

$$V(t) = g(i(t), T(t), F_{ext}(t), d(t)) \tag{3.11}$$

The following chapters utilize these equations in more-specific control applications, where actuator models are presented. They are based on the relations given in these equations. These control applications include sensorless displacement control without external force (Chapter 4) and external force estimation (Chapter 5) under constant temperature.

4. Displacement Control

This chapter discusses the application of current measurement on the displacement control, Papers I-III. The focus of the thesis is on this chapter, since the displacement control is one of the most important control issues in the application of piezoelectric actuators. This chapter shows how valuable the current measurement is in displacement control. This is done by introducing several control schemes where the current measurement improves the positioning accuracy in comparison to open-loop control. The reason for the improved positioning results is the inside information of the piezoactuator state that the current measurement provides.

The rest of the chapter is organised as follows: Section 4.1 introduces developed control methods utilizing current measurement. Section 4.3 presents control results of these control methods. Discussion is provided in Section 4.4, and conclusions are drawn at the end in Section 4.5.

4.1 Control Methods

This section presents displacement control methods based on utilization of current control. The methods are based on Equation (3.10), with an assumption that the external force is constant. Chapter 5 discusses a case where this assumption is not valid. With this assumption, the equation simplifies to

$$i(t) = f(V(t), T(t), d(t)), \tag{4.1}$$

where $i(t)$ is the current, $V(t)$ the voltage, $T(t)$ temperature, and $d(t)$ displacement.

Based on this equation, two feedforward control methods were developed. Both of these methods assume constant temperature. In some applications, temperature varies significantly; therefore, an additional temperature compensation extension is developed for one of the methods. These two methods estimate current needed to be fed to the actuator to obtain the desired motion trajectory. The methods differ by model structure. The first model makes an imaginary division of the total current flowing in to or out from the actuator into two subcurrents: (i) to a current causing charging and discharging of the actuator (i_c), and (ii) to a current that does not contribute charging of the actuator but is counted as power losses (i_l). This model is called as Power Loss Model and will be

introduced in Section 4.1.1. The second model is a grey-box model of the actuator. This model estimates the current needed to be fed to the actuator to obtain the desired motion trajectory. One of the two model components is based on physical properties of the actuator; hence, the "grey-box" model. This model is called Actuator Current Model and will be discussed in Section 4.1.2. Later, a temperature compensation was added to the Power Loss Model. This model is called Temperature Compensation of Power Loss Model and will be presented in Section 4.1.3.

4.1.1 Power Loss Model

This section presents a feedforward control method that utilizes Power Loss Model. The method is described in full detail in Paper I. Figure 4.1 presents the block diagram of the control method utilizing the Power Loss Model.

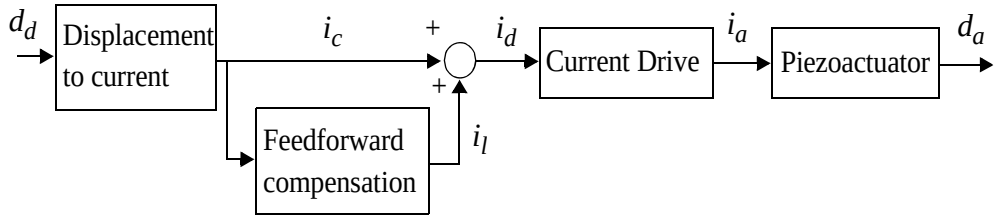

Figure 4.1. Block diagram of the control method utilizing the Power Loss Model.

The desired actuator current i_d is divided into two imaginary subcurrents: (i) to a current causing charging and discharging of the actuator (i_c), and (ii) to a current that does not contribute to charging of the actuator but is counted as power losses (i_l):

$$i_d(t) = i_c(t) + i_l(t), \tag{4.2}$$

The background assumption in charge control is that the charge is proportional to the displacement. The charge can be obtained by integrating the charging current. The relationship between the displacement and the charging current is as follows:

$$d(t) = a \cdot \int_0^t i_c(t)dt, \tag{4.3}$$

where $d(t)$ is the displacement and a a constant.

Solving for current i_c from (4.3) indicates that it can be used in control corresponding to velocity:

$$i_c(t) = \frac{1}{a} \cdot \frac{d}{dt}d(t) = \frac{v(t)}{a}, \tag{4.4}$$

where $v(t)$ is the velocity of the actuator.

The power loss includes dielectric, mechanical, and piezoelectric losses [71]. As a control point of view, the mechanical output power is also considered as power loss. With the assumption that the temperature and load are constant, the above mentioned losses are influenced by electric field and actuator velocity. Thus, the power loss current i_l can be presented as follows:

$$i_l(t) = \frac{V(t)}{X} \tag{4.5}$$

where X presents impedance and is influenced by the actuator velocity $v(t)$.

Velocity, on the other hand, is proportional to charging current i_c, as described in Equation (4.4). Thus, the charging current will be utilized here for convenience. A series of experiments was conducted with different charging currents to obtain the corresponding impedance values. The resulted impedance values showed rapid decrease when the charging current started to increase from zero. With higher charging currents, the impedance values continued to decrease, but at a slower rate. To obtain a model for the impedance X, several model structures were tried, all asymptotically approaching zero. From these, the best result was obtained with the following

$$X(i_c) = \frac{R}{\sqrt{(c_1 \cdot i_c(t))^2 + 1}}, \tag{4.6}$$

where R is the constant resistance of the ceramics and c_1 is a constant.

The full description of the experiments and the comparison between different models can be found in Paper I. This impedance model describes a linear relationship between current and voltage in a no-motion case. Such an electrical model for piezoelectric actuators at zero frequency can be found in [26], for example.

In the experiments, voltage $V(t)$ is estimated by integrating charge current over time:

$$V(t) = \frac{1}{C}\int_0^t i_c(t)dt, \tag{4.7}$$

where C is the actuator capacitance and for the voltage estimation is approximated to be constant. The voltage could also be obtained by measuring. However, with the used measurement setup, this was not possible; therefore, voltage was estimated by integration. The actuator resistance R, capacitance C, and the constants a and c_1 were experimentally defined.

4.1.2 Actuator Current Model

This section presents a feedforward control method utilizing an actuator model to estimate the needed current for the desired motion velocity. The approach is to construct a model having two inputs, actuator velocity and voltage, which are known to have an effect on the required current, as described in the previous section and in Chapter 3, and one output, the required current. On contrary to the Power Loss Model, charging of the actuator and power losses are not considered separately and, thus, cannot be distinguish from each other. An exception to this, however, exists in one of the two submodels of the Actuator Current Model. Paper II presents the method in full detail. Figure 4.2 presents the block diagram of the control method.

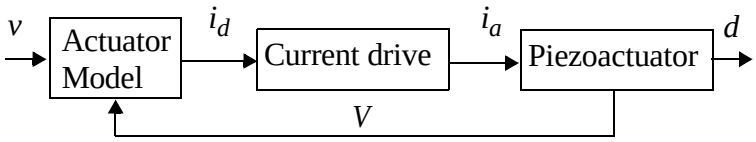

Figure 4.2. Block diagram of the feedforward control method based on the actuator model.

The control method is similar to the model presented in the previous section. However, the Power Loss Model is laborious to create. Another drawback is the long-term stability, since voltage information used in context with the impedance model was estimated and not actually measured. The goal is to simplify the actuator model so that it could be specified for each actuator with a minimum effort. This means that the required number of experiments and the consumed time should be minimized for the model parameter estimation. Another goal is to keep the structure of the control method simple enough that the control algorithms could be implemented using only simple arithmetic operations.

A model architecture with two components was selected. The reason for this is the sensitivity of the control performance to driving current values when the actuator is desired to hold its position. Thus, as one part is modelling the actuator motion, and the other part is modelling the actuator in a static operation mode, an extra attention can be given to the accuracy of static operations. Aside from the motion and static models, a mode selector is included for switching between the two models. Figure 4.3 presents the structure of the actuator model architecture.

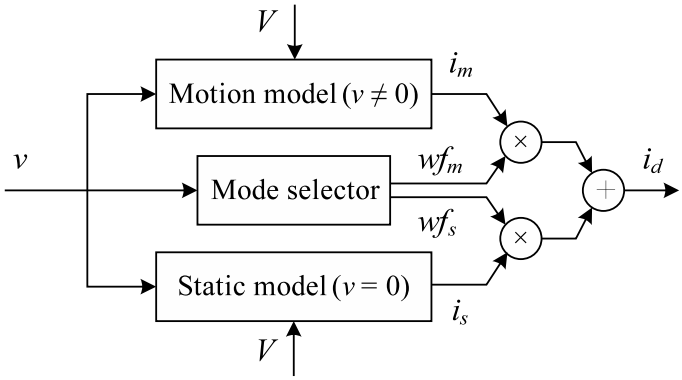

Figure 4.3. Structure of Actuator Current Model.

Motion Model

This section discusses the motion part of Actuator Current Model. As presented in Chapter 3, the dependency between the actuator velocity, the input current, and the input voltage is non-linear. Therefore, non-linear mapping is required. The goal was to create as simple model as still feasible. This would result in faster training and implementation of the model and would require fewer computations in actual control. It was discovered that as simple as a 2*1 neural network can model the actuator quite accurately. Figure 4.4 presents the model structure. The non-linear function is hyperbolic tangent sigmoid transfer function tansig. Both non-linear and linear transfer functions include bias values.

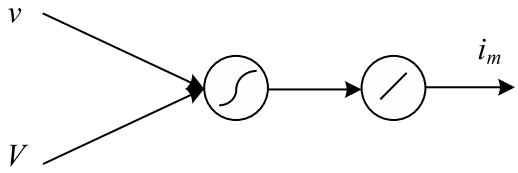

Figure 4.4. Neural network structure of motion model.

Training data can been obtained by driving random current to the actuator while the actuator velocity and voltage is recorded, Figure 4.5.

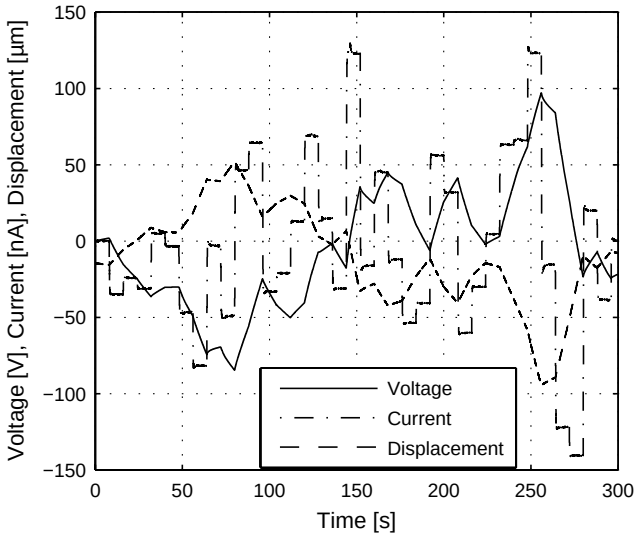

Figure 4.5. Training data for motion model, continues line presents voltage, dash-dot line current and dashed line displacement.

Static Model

This section presents the static part of Actuator Current Model. It is included to enhance the model performance when the actuator is needed to hold its location or when the desired motion velocity is very small. Here, a simplified version of the Power Loss Model presented in the previous section will be utilized, only dielectric losses are considered. Thus, the power loss current i_l will be linearly dependent on the voltage, as presented in Equation (4.8). In the no-motion case, it works similarly as in the Power Loss Model but differs when some motion is desired. The model is intended to work in a no-motion case or when only very slow motions are desired.

$$i_l(t) = G\,V(t), \tag{4.8}$$

where G is a constant describing the conductance of the actuator. In addition to the electrical conductance of the actuator, other effects such as drift in electrical capacitance due to mechanical drift may influence this and can be included in practical cases.

Similar charging current $i_c(t)$ - actuator motion velocity $v(t)$ relation is used as in power loss model in previous section.

$$i_c(t) = \frac{v(t)}{a}, \tag{4.9}$$

where a is constant describing the relation between the velocity and the current.

Figure 4.6 presents the block diagram of the static model.

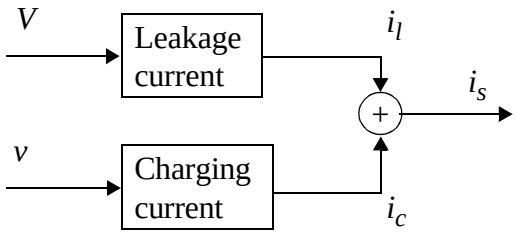

Figure 4.6. Block diagram of the static model.

Mode Selector

This section presents the mode selector used to switch between the two models: the motion model and the static model.

To avoid a jump in the actuator model output due to the difference in outputs of the two submodels, the mode selector should perform a smooth transition between the two models. A simple way to enable this is to create weight functions for the two models, defining how much each model should be taken into account. This approach is derived from fuzzy logic methodology. To avoid "if" and "then" clauses in the controller, the weight functions should be continuous over the used velocity range. The following equation presents the weight function used for the static model:

$$wf_s = \frac{1}{k(rv)^2 + 1}, \tag{4.10}$$

where k defines the shape of the weight factor, r normalizes the velocity according to the selected velocity range, and v is the velocity. Figure 4.7 presents the weight function wf_s with different values of k. The weight function for the motion model becomes

$$wf_m = 1 - wf_s. \tag{4.11}$$

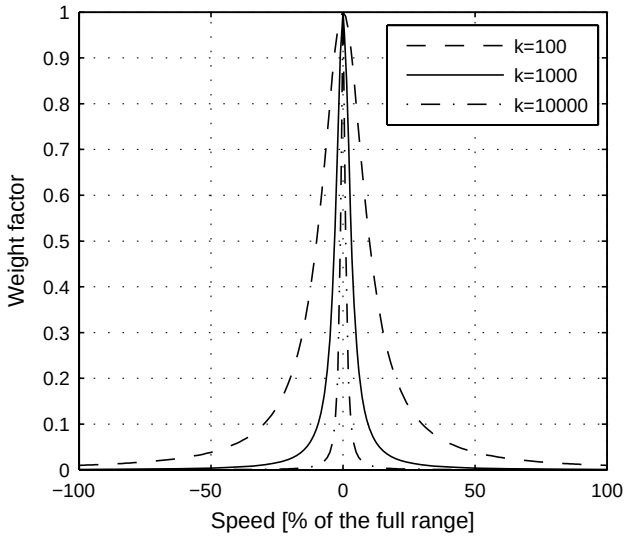

Figure 4.7. The weight function wf_s with different values of *k*.

4.1.3 Temperature Compensation of Power Loss Model

This section introduces an environmental compensation method for feedforward control utilizing the Power Loss Model. Full details of the method are presented in Paper III. The temperature range to be covered is between 10°C and 40°C. Figure 4.8 presents the block diagram of the feedforward control method utilizing Power Loss Model with Environmental Compensation.

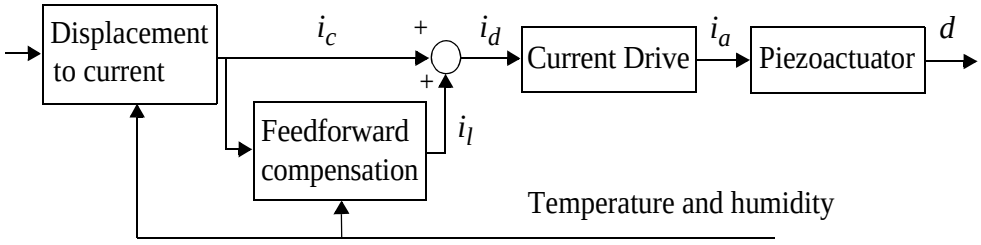

Figure 4.8. Block diagram of the feedforward control method utilizing Power Loss Model with Environmental Compensation.

It was discovered that the constant *a* in Equation (4.4) is not temperature or humidity dependent. On the other hand, the relation between current and electric field depends on the temperature due to the pyroelectric effect and changes in conductivity [37]. Thus, the impedance $X(i_c)$ in Equation (4.5) is temperature dependant $X(i_c,T)$, but, according to experiments, not affected by humidity until very high humidity levels are reached, at which point the behaviour of the actuator changes drastically. A small modification has been made to the impedance equation in order to improve the model performance at higher current values in comparison to Equation (4.6) by adding parameters *b* and c_2. Equation (4.12) presents the modified impedance with temperature dependent factors.

$$X(i_c, T) = \left(\frac{1 - b(T)}{\sqrt{(c_1 \cdot i_c(t))^2 + 1}} + (1 + c_2 \cdot |i_c(t)|) \cdot b(T) \right) R(T), \quad (4.12)$$

where $b(T)$, and constants c_1 and c_2 are factors describing how the impedance varies with the charging current. Factors $b(T)$ and c_2 describe the relation at higher currents and c_1 at lower currents. $R(T)$ is the resistance. Temperature dependence of $R(T)$ and $X(T)$ is determined experimentally, the results are presented in Paper III in detail. The effect of temperature on the impedance is shown in Figure 4.9, where the impedance measurements at different temperatures are depicted. The figure also shows that the relation between the impedance and the temperature is quite linear.

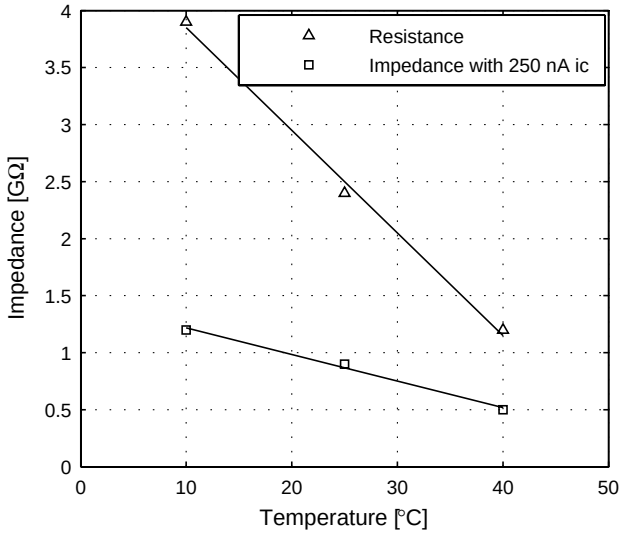

Figure 4.9. Impedance as a function of temperature. Triangle points present resistance $R(T)$ with respect to temperature. Square points present impedance with 250 nA charging current i_c.

The actuator resistance $R(T)$ is dependent of the temperature as follows:

$$R(T) = -0.09 \frac{G\Omega}{^\circ C} \cdot T + 4.7 G\Omega. \quad (4.13)$$

Temperature dependency of other factors is experimentally determined. c_1 and c_2 can be assumed to be constants if $b(T)$ is assumed to be temperature dependent. The effect of temperature on the factor $b(T)$ is presented in Figure 4.10, and the linear approximation in Equation (4.14).

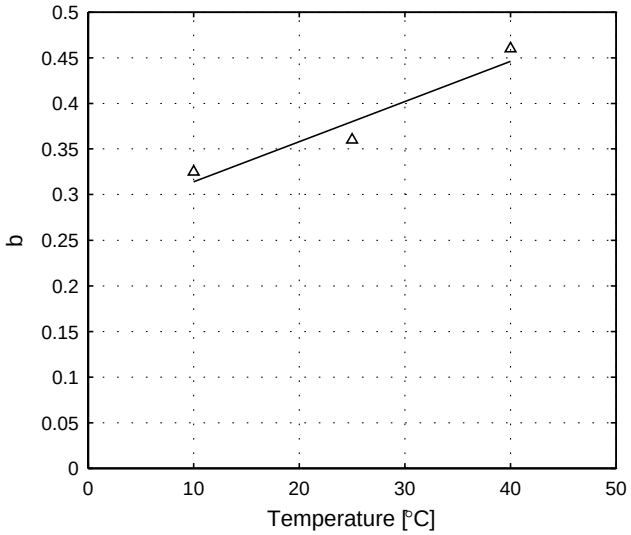

Figure 4.10. Factor *b* with respect to temperature.

$$b(T) = 0.27+0.004 \cdot T \tag{4.14}$$

Factors c_1 and c_2 were determined experimentally.

4.2 Experiment Setup

Experiment setup consists of the actuator, the current driver, a displacement meter, computer with data acquisition board and control software. These are introduced in Chapter 2 with an exception of current driver, which will be discussed here.

4.2.1 Current Driver

The current driver consists of a voltage amplifier, a current meter and a feedback controller, Figure 4.11. The voltage amplifier and the current meter are the same for all the experiments, but the feedback controller varies.

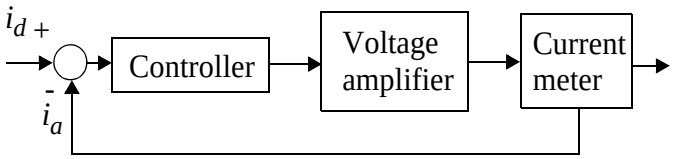

Figure 4.11. Schematics of the current drive; i_d is desired current and i_a actual current.

In Section 4.3.1 and Section 4.3.3, and in Papers I and III, a PID controller is used running at a frequency of 250 Hz with the PID parameters at P=0.001, I=0.5 and D=1e-5. The controller is discretised using Tustin's approximation [80]. In Section 4.3.2 and in Paper II, the utilized controller is a PID-like controller with an additional integrator running at 2 kHz. Equation (4.15) presents the transfer function of the controller

$$Cr(s) = \frac{K_1 s^2 + K_2 s + K_3}{s^2}, \tag{4.15}$$

where K_1, K_2 and K_3 are the controller parameters (for the actuator in question with a chosen current range, the parameter values are K_1=0.00001, K_2=0.3 and K_3=2).

4.3 Results

This section presents the summary of the main results for the control methods presented in Section 4.1. The complete description of the results is given in Papers I-III. Section 4.3.1 presents the results for the control method based on the Power Loss Model. Results of the control method utilizing the Actuator Current Model are presented in Section 4.3.2, while results of the temperature compensation for the Power Loss Model are presented in Section 4.3.3.

Since hysteresis and drift are the main causes of inaccuracy in the control of piezoactuators, their compensation is the main focus of the experiments.

4.3.1 Power Loss Model

This section introduces the results of the control method based on the Power Loss Model. The model parameters used in these experiments are a=16 m/C, R=21 GΩ, c_1=3.4e7 A^{-1}, and C=120 nF. To show that the method has not only been tuned for a certain velocity, a decaying ramp signal is applied (Figure 4.12). The ramp time remains constant, and therefore, by decreasing the displacement, speed is decreased as well. The experiments show that the maximum inaccuracy is 10µm.

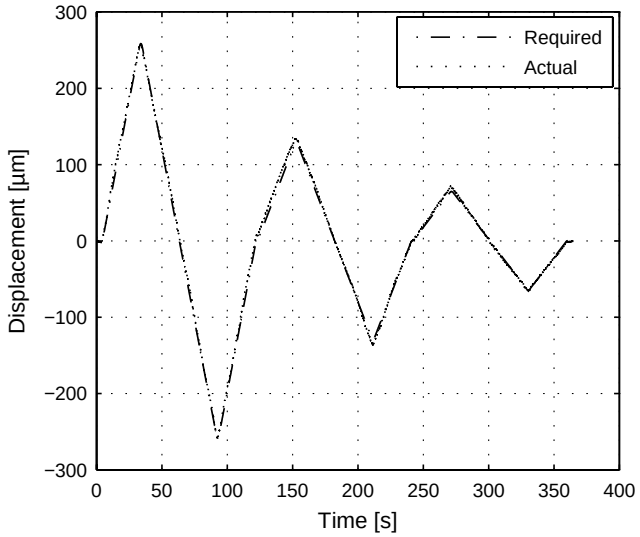

Figure 4.12. A decaying ramp curve.

The results of the hysteresis test are demonstrated in Figure 4.13. The maximum hysteresis is approximately 1.5%.

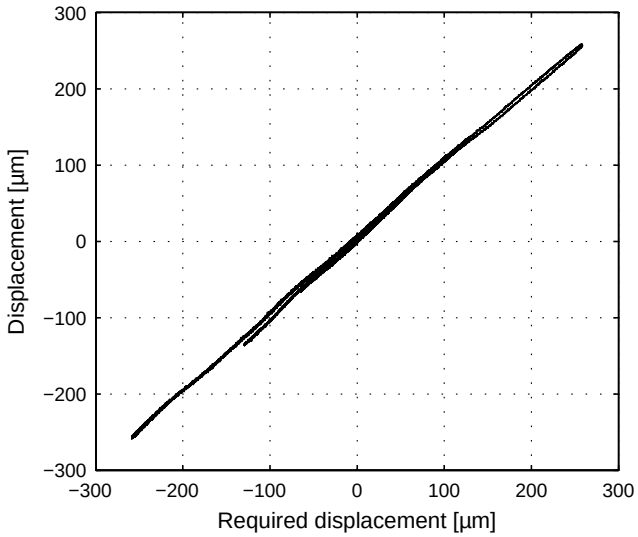

Figure 4.13. The hysteresis of the decaying ramp curve.

Repeatability was tested by running a ramp curve 20 times. The test showed very good results: The displacement drifted only 2% in nearly 80 minutes, while the peak-to-peak value remained practically constant, increasing by only 0.5% during the time period.

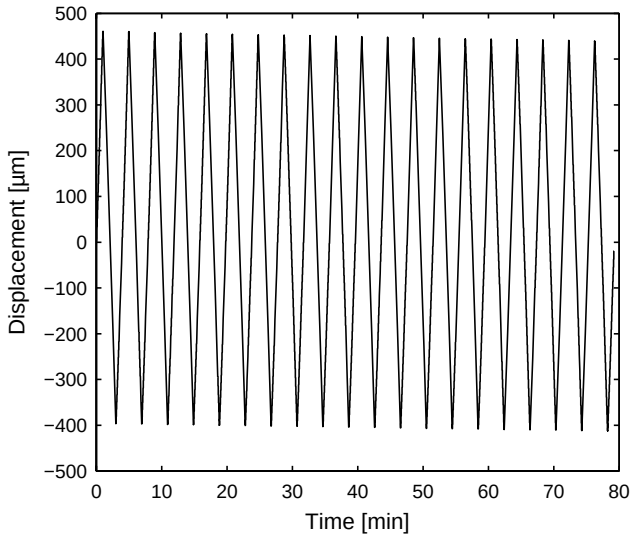

Figure 4.14. Ramp curve driven 20 times.

Figure 4.15 shows the drift. The displacement stays within 1.5% over two minutes. This displacement error caused by drift is one-tenth in comparison to open-loop voltage control.

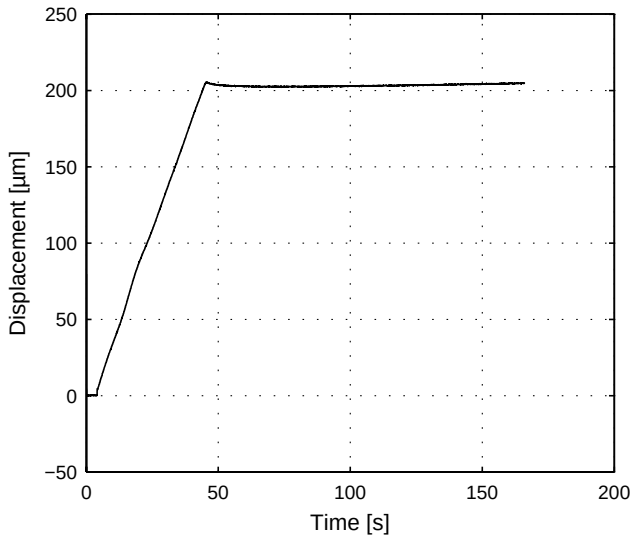

Figure 4.15. Drift.

4.3.2 Actuator Current Model

This section presents experimental results of the control method utilizing the Actuator Current Model. Even though the control method is intended to the control of the actuator velocity, the displacement results will be presented; this is due to the reference measuring system. Since it is measuring the displacement with a certain noise level, velocity should be obtained by differentiation, and this would result in a relatively noisy signal. Therefore, it is more convenient to accumulate the velocity control signal and examine the results with respect to displacement.

The performance of the control method is validated with several displacement ramp curves with varying frequency and amplitude. The tested trajectories include steady states for drift characterisation. All trajectories have been driven a minimum of five times, and the results in this section present typical results. The model parameters used in experiments are G=1.3e-11 Ω^{-1}, a=38 m/C, r=1e5, and k=1e3.

Experiments show that the hysteresis for the displacement ramp curves without steady states is less than 1.5%. The drift in steady state experiments is about 1%. Results for an experiment with a 16-minute lasting periodical trajectory consisting of several motion velocities and steady states with varying times is presented here. Figure 4.16 displays the required displacement, the actual displacement and the difference between them magnified ten times. As can be seen, the outcome follows well the required trajectory. Over the 16 minute time period the maximum inaccuracy is about ±1.5 µm.

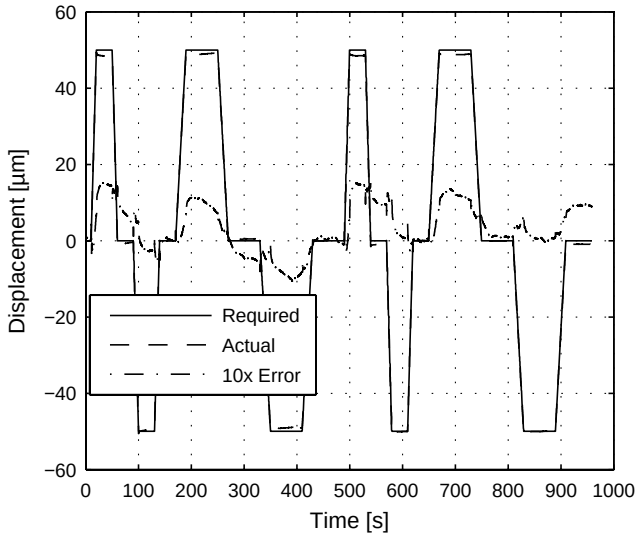

Figure 4.16. Displacement trajectory with steady state phases of variable lengths.

The steady state behaviour is presented in more detail in Figure 4.17. After a small decay in the beginning of the steady state, the displacement remains quite constant with a slight increase in the displacement. Hysteresis is depicted in Figure 4.18 and in more detail in Figure 4.19. The figures show linear behaviour with 1.5% non- linearity.

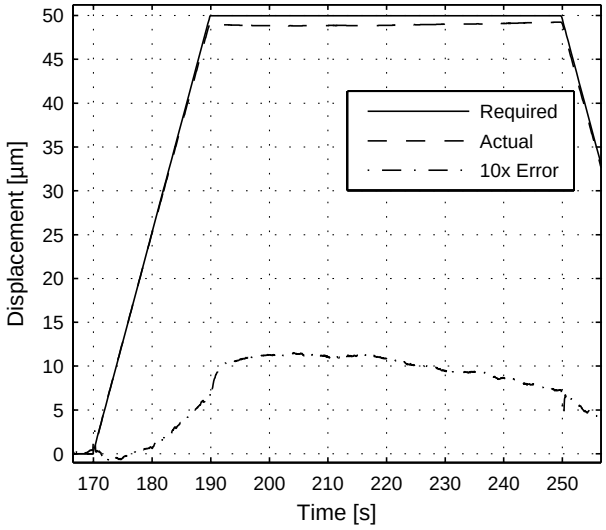

Figure 4.17. Close-up of a steady state phase.

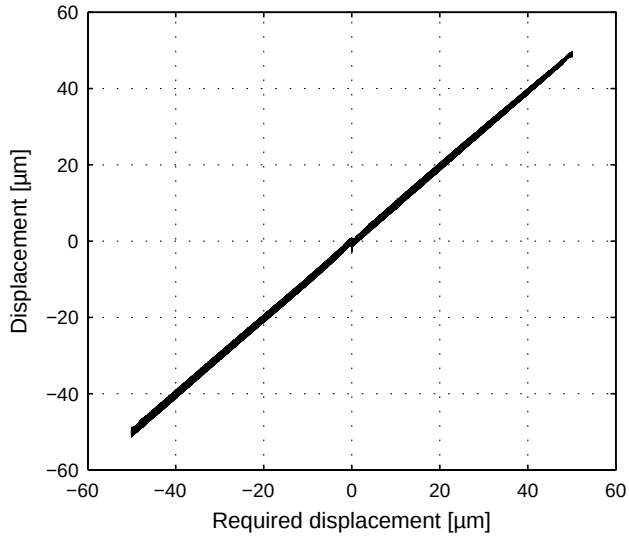

Figure 4.18. Hysteresis of the displacement trajectory with steady state phases of variable lengths.

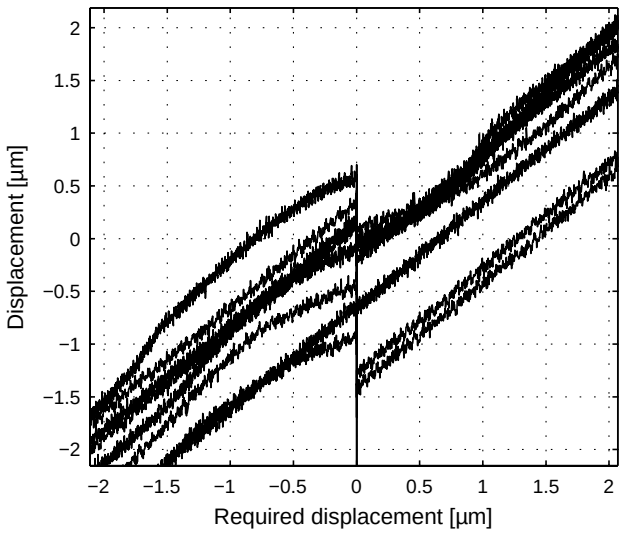

Figure 4.19. Close-up of the hysteresis.

It was discovered that while repeating experiments with a certain trajectory, the output varied slightly. This is due to the remaining offset in the displacement trajectory; after each trajectory, the actuator leaves to a certain position that differs from the starting position. Thus, the starting point of the following displacement trajectory differs from the starting point of the previous trajectory. Maximum difference in the trajectories driven with different starting positions is less than 6%. For a reference, the voltage difference between these same experiments is about 40%.

4.3.3 Temperature Compensation

The temperature compensation was tested in three different environmental conditions; 15°C and 10%, 20°C and 50%, and 35°C and 40% RH. The same trajectories were run with and without environment compensation in all conditions to validate the compensation model. The reference test uses power loss compensation and environment parameters set to room conditions (25°C, 30%). The used trajectories were a decaying displacement ramp curve similar as in Section 4.3.1 for the hysteresis analysis and a drift test. The drift test has a static phase of 100s after a ramp-up. The model parameters used in experiments are a=32 m/C, c_1=1e-10, and c_2=1e4. The linear models $R(T)$ and $b(T)$ including their numerical values was introduced in Section 4.1.3.

At 20°C, 50%, the difference by environmental compensation in comparison to the uncompensated case is relatively small, which is natural considering the temperature difference. At 15°C, 10% RH and at 35°C, 40% RH, the difference is significantly larger.

Figure 4.20 presents the decaying ramp curve at 35°C, 40%. The solid line presents the required trajectory, the dash-dot line the displacement with compensation, and the dotted line without compensation. Figure 4.21 shows the corresponding hysteresis.

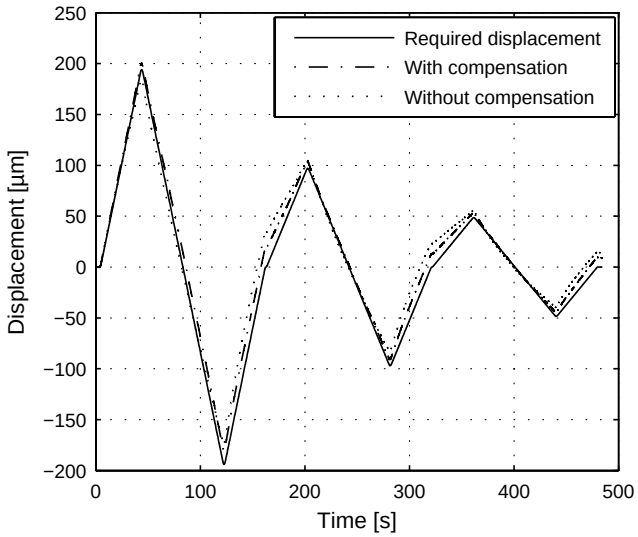

Figure 4.20. Decaying ramp curve driven at 35°C 40% RH.

The hysteresis reduces from 10% to 5% with environmental compensation. The improvement at 15°C, 10% is at the same level; the hysteresis is about half of the uncompensated case. At 20°C, 50%, the hysteresis is similar in both compensated and uncompensated cases, less than 4% of the full displacement.

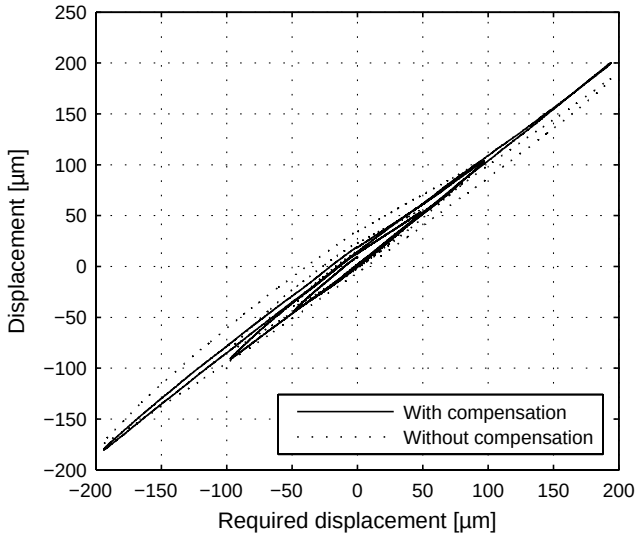

Figure 4.21. Hysteresis of the decaying ramp curve driven at 35°C 40% RH.

In the drift test, the actuator is first driven with a constant speed for 40 seconds and then attempted to keep in its position for 100s.

Figure 4.22 presents drift at 35°C, 40%. As shown, without the compensation the displacement does not reach the required displacement and, in the end, is 25 µm below the desired displacement. With compensation, the displacement overshoots but later follows the required trajectory as desired. Further studies on overshooting will be needed. Mechanical properties of the actuator are the most probable cause for the overshoot.

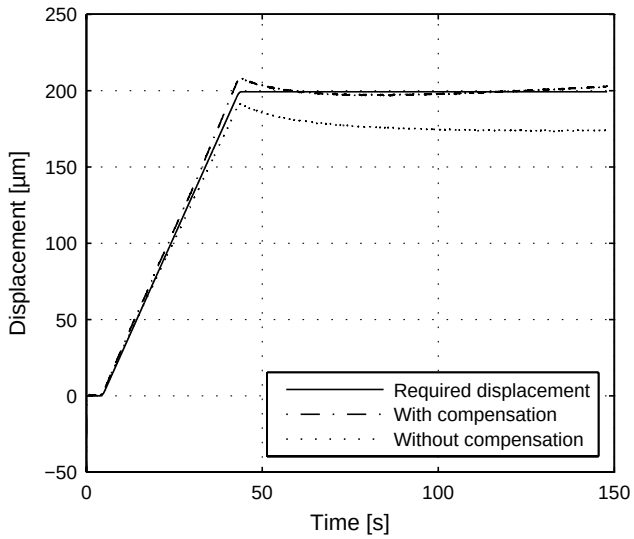

Figure 4.22. Drift at 35°C, 40% RH.

At 15°C, 10%, the uncompensated test results are nearly 20 µm above the desired trajectory, while the results with the compensation are within a couple of micrometers. At 20°C, 50%, the drift results with and without compensation are close to each other: the compensated case is slightly below the required trajectory, and the uncompensated is slightly above the desired displacement, Figure 4.23.

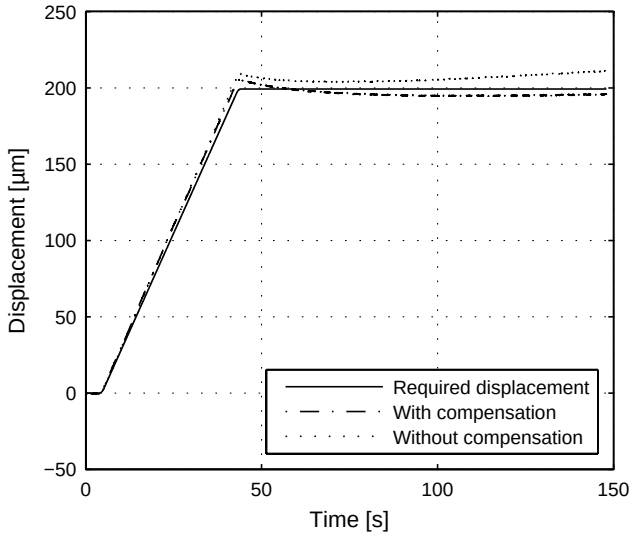

Figure 4.23. Drift at 20°C, 50% RH.

4.4 Discussion

This section discusses the control methods and results presented in the previous sections. Differences in the control setup are discussed first, then some imperfections in the results are addressed. The imperfections include the small decay in the beginning of the static phase, effect of starting position on the displacement, and the source of uncertainty. After these, performance of current meter is discussed. Finally, differences in Power Loss Model and Actuator Current Model are discussed from a practical point of view.

While comparing the results of the different methods, differences in the testing setup have to be considered. The greatest difference in the setups is the current driver, presented in Section 4.2.1. The used control frequency of the PID controller for the current driver is 250 Hz in the experiments with the Power Loss Method including the Temperature Compensation. Experiments with the Actuator Current Model are performed with a current driver including a PID-like controller with an additional integrator and running at 2 kHz. Therefore, the performance of the Power Loss Model is partly reduced by the current driver, since the difference between actual and desired current is greater. This is partly compensated by a slower desired motion and rounded corners in signal shapes. Another difference between the current drivers is the possibility to utilize the actuator voltage information in Actuator Current Model, which was not an option in the

experiments with the Power Loss Model. Therefore, the long-term stability might be poorer in these experiments than the control method could otherwise perform.

In the results at the beginning of the static phases, there is a small decay in the displacement. There are several possible reasons for this: The primary hypotheses include peaking of the current while changing the velocity, a mechanical spring effect of the cantilever, and a drift in the electro-mechanical properties of the actuator. The peaking is rather difficult to totally avoid, since the current meter has a cut-off frequency of 40 Hz. Different controller parameters of the current drive were tested in order to reduce the peaking of the current, but a similar tendency in the output displacement remained in the beginning of the static phase. The latter two hypotheses--the mechanical spring effect and the drift in electromechanical properties--seem therefore to be more probable reasons for this behaviour.

The displacement decay in the beginning of the static phase could be avoided by implementing dynamic features into the actuator models or by designing an advanced controller for the current drive that behaves differently depending on the desired current value and the change in the current values.

Another imperfection was discovered with the Actuator Current Model: The starting position of the actuator has a small effect on the displacement. This is not tested with the Power Loss Model, but it is likely that it has a similar property. Results with the Actuator Current Model show a 6% difference between the different trajectories depending on the starting position. However, this is significantly smaller than in the open-loop voltage control, where the difference can be more than 25%. This starting position effect might suggest that the capacitance $C(d)$ presented as a function of displacement in Section 3.4, should instead be considered as a function of position. However, it is still unclear whether the deviation in the displacement is due to other properties of piezo actuators or could be avoided by using a more complex actuator model.

Temperature has an effect on the performance of the current control methods, which can partly be compensated for with the developed temperature compensation. The temperature compensation experiments suffered from an unidentified source of uncertainty in the test setup. This was decreasing the repeatability and, thus, decreasing the accuracy of the model. The source of uncertainty can result from (i) the inaccuracy in the estimated voltage, (ii) the actuator wears out, or (iii) inaccuracies in the measurement system; (laser displacement meter, current meter, or the data acquisition system). Although the highest temperature studied here in 40°C, it is likely that the linear compensation method could perform also at higher temperatures up to about 100°C. It has been demonstrated that below this temperature the relation between current and voltage is quite linear, but becomes non-linear at higher temperatures [37].

Overall, these feedforward control methods are suitable for velocity control, but long-term position control can lead to inaccuracy due to summation of control errors. Therefore, the performance of the current meter plays an important role in the control methods. The important parameters of the current meter are not only the creep properties and the repeatability but also its range, since the current range practically limits the motion speed range.

Different actuators might require considerably different model parameters. Therefore, the time consumed for each actuator model is important. Finding parameters for the Power Loss Model requires an iterative process and is quite time consuming. Creation of the Actuator Current Model is more simpler and time efficient. The Power Loss Model, on the other hand, offers information, aside from the required currents, about the actuator power losses. This can be a benefit in some applications. Although the Power Loss Model is quite simple and time efficient to create, a question remains whether the model creation could be further accelerated and automated. This might be achievable by carefully designing the model structure and by optimizing the measurements of the actuator.

4.5 Conclusion

The displacement control methods have been discussed in this chapter. Two feedforward charge control methods have been presented: the Power Loss Model and the Actuator Current Model. For the first one, also a temperature compensation is developed.

The control method based on the Power Loss Model estimates and compensates for the power losses occurring in the actuator, such as dielectric, piezoelectric, and mechanical losses. The compensation is done by an additional current. Temperature compensation is added to the Power Loss Model by experimentally finding the model parameters that are influenced by temperature variation and then creating a linear approximations for these changes.

The Actuator Current Model estimates the required current for the actuator to move with the desired velocity. Aside from the desired velocity, the actuator voltage is an input for the Actuator Current Model. The model is straightforward to create, requiring far fewer experiments than the Power Loss Model. This results in an easier and faster implementation of the Actuator Current Model in comparison to the Power Loss Model. The Actuator Current Model is also more adaptive to different types of actuators than the Power Loss Model due to its flexibility.

From the hardware point of view, these methods require (i) a high voltage current driver or (ii) a current meter, along with a voltage amplifier and a controller, as was done in this work.

Both discussed methods show very good results: the hysteresis is less than 2% and the drift about 1% in constant temperature. These results are common for both methods. Temperature changes affect the electrical and mechanical properties of the piezoelectric actuators. The effect of humidity is smaller until a high level of humidity is reached. Temperature changes decrease the accuracy of the control methods. The presented temperature compensation improves the control performance in varying temperatures close to the performance in constant temperature. The results would, therefore, indicate that the motion of piezo actuators is a function of current, voltage, and temperature; thus, history knowledge seems unnecessary in order to overcome the hysteresis and drift in sensorless control of piezoelectric actuators. The Power Loss Model shows the capability of predicting the power losses quite accurately and can therefore be utilized also in power considerations in application areas where power is a critical issue such as space and mobile applications.

In comparison to feedback charge control methods, the current control method enables hysteresis and drift free control of the displacement in static cases and at low frequency, which is not the case with feedback charge control methods, as discussed in Section 1.3.4. However, for the current control to cover also higher frequencies, where the feedback charge control works at its best, the measurement range of the current meter should be from some nanoamperes up to hundreds of milliamperes. Therefore, an intriguing question is whether the feedforward and feedback charge control could be combined in such a way that the best parts of the both individual methods would be included and the result would cover full frequency spectrum.

5. Force Estimation

This chapter discusses the usability of current measurement in force estimation and control, Paper IV. Since the input current and voltage knowledge contain sufficient information to predict the displacement of a piezoelectric actuator in the absence of external forces, as shown in the previous chapter, and the effect of force on the displacement of a piezoactuator is well known, by combining the displacement measurement into the actuator model with current and voltage inputs, a force can be estimated.

This chapter presents a force estimation method that enables simultaneous actuation and force estimation using piezoelectric actuators. The method combines the actuator input voltage and the current together with the displacement to form a force estimator. The force estimator contains a non-linear actuator model to approximate the present external force without the use of force sensors. The measured position can simultaneously be utilized in feedback position control to enable precise microrobotic operations.

The rest of the chapter is organized as follows: Section 5.1 presents the force estimation method, experiment setup is introduced in Section 5.2, and results are presented in Section 5.3. Discussion and conclusions are provided in Section 5.4.

5.1 Force Estimation Method

This section presents the proposed force estimation method. The method should estimate the external force without any force measurement. By writing Equation (3.10) with respect to the external force $F_{ext}(t)$ in a constant temperature, it follows:

$$F_{ext}(t) = g(i(t), V(t), d(t)), \tag{5.1}$$

where $i(t)$ is current, $V(t)$ actuator voltage and $d(t)$ displacement.

This would suggest that by measuring the actuator input current and the voltage, and the resulting displacement, the force could be estimated. This could be done simultaneously with the traditional position control of the actuator. Figure 5.1 presents the block diagram of the proposed force estimation method.

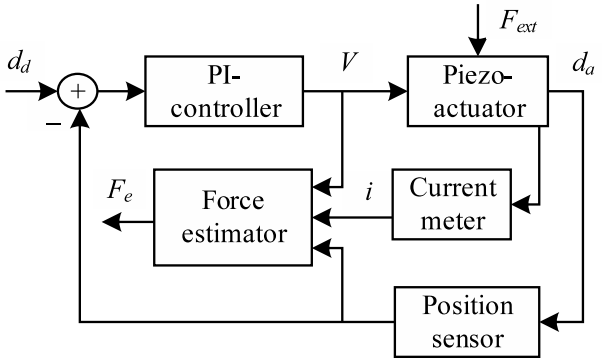

Figure 5.1. Block diagram of the proposed force estimation method.

In the figure, d_d and d_a present the desired and actual displacements. V presents the voltage and i the current. F_{ext} presents the external force and F_e the estimated force. The used PI controller is presented in more detail in Section 5.2.1.

Another approach could be to utilize the actuator velocity instead of the position, thus the actuator model structures presented in Chapter 4 and in Papers I-III could be utilized. The drawback of this approach is the poor availability of precise velocity sensors in comparison to position sensors. The velocity is possible to calculate from the actuator position by differentiation, but the drawback in this approach is the poor resulting signal to noise ratio due to the sensor noise. For off-line measurement, this can be avoided by proper signal filtering, but for on-line application, the delay between the actual velocity and the measured velocity might became too large.

5.1.1 Force Estimator

This section discusses the Force Estimation Model. The model has three inputs: voltage V, current i, and actuator displacement d, and one output, external force estimation F_e.

There are many possibilities for the model type and structure. Analytical modelling is one approach requiring good knowledge of the actuator functions and physics. Semi-physical or a grey-box type of modelling is another approach, where one option could be to adapt some model structures from Chapter 4. In this work, a neural network is chosen for the model. It has many favourable properties, as discussed in Section 2.1.2, of which the availability of powerful software tools for creating and training is not the least significant. Feedforward backpropagation network is chosen for the force estimation model having 10 tansig-function nodes in the hidden layer, Figure 5.2. All node functions contain bias values. Training data are obtained by driving the trajectory presented in Figure 5.3 with several different static loads: 0 N, 34 mN, 61 mN and 90 mN.

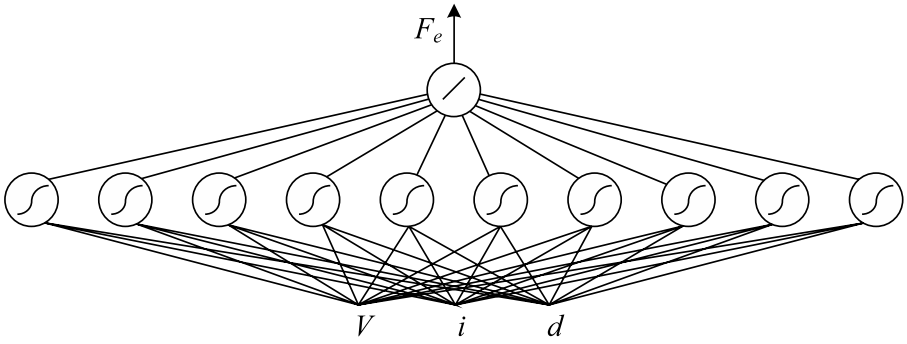

Figure 5.2. Structure of force estimator neural network.

Figure 5.4 combines the trajectories driven with different loads to the same figure. The figure presents actual loads and training results. Continuous line presents the actual load, and the dashed line the force estimation of the model.

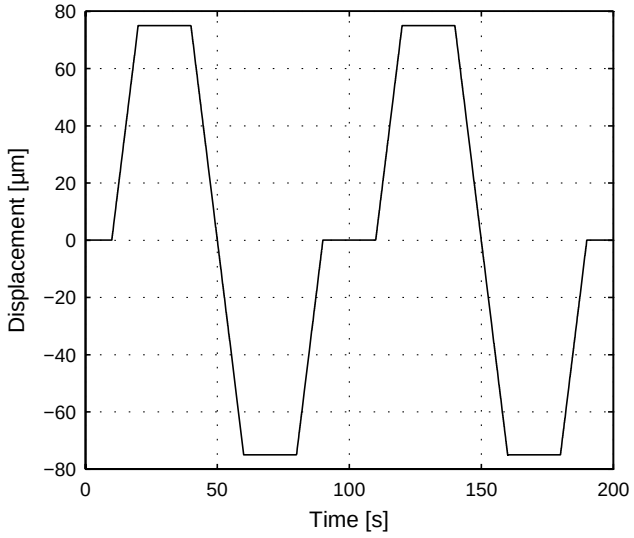

Figure 5.3. Displacement trajectory for obtaining the training data.

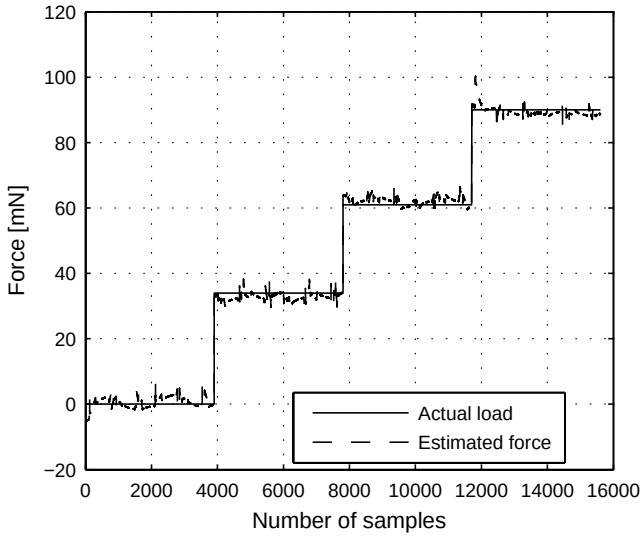

Figure 5.4. Training results, continuous line presents the actual load and the dashed line the force estimation.

5.2 Experimental Setup

Experimental setup consists of the actuator, a current meter, a displacement meter, computer with data-acquisition board, and control software. These are introduced in Chapter 2 with the exception of position controller, which will be discussed here.

5.2.1 Position Controller

The simultaneous position control during the force estimation consists of the voltage amplifier, a position sensor and a PI controller, with a gain of 0.1 and an integrator gain of 3. The used control frequency was 2 kHz.

5.3 Results

This section presents the experimental results of the force estimator. All experiments are carried out five times, and the results in this section present typical results.

The trajectory shown in Figure 5.3 is driven with the following static loads: 0 N, 22 mN, 47 mN, and 77 mN. These are combined into the same figure as was done in Figure 5.4 by presenting only actual loads and the corresponding estimated forces, Figure 5.5.

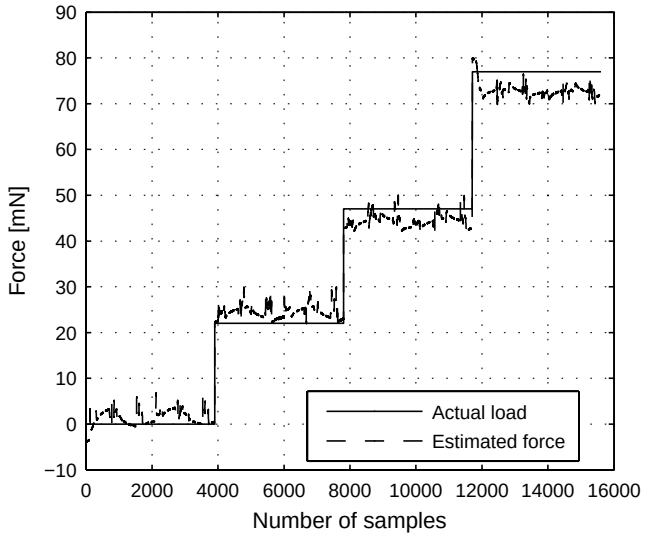

Figure 5.5. Results of static force measurements.

The force estimation gives a relatively good approximation of the actual force. Some variation, however, occurs during different phases of the trajectory. Some error is also present in the estimated forces. With the three lightest loads, the error is 2 - 3 mN, but with the heaviest load, the error is slightly over 4 mN. The average absolute value of the error between the actual load and the estimated force is 2.8 mN, and the median error is close to this at 2.83 mN. The maximum error during the experiments is slightly below 8 mN. The applicable force range of the estimator is in minimum 0 - 90 mN, which is the range of the loads used for the training. This, in combination with the maximum error of 8 mN, results in a total estimation accuracy of better than 9% of the full scale.

The actuator is driven using the same trajectory against a plastic cantilever, introduced in Chapter 2, to test how the force estimator follows a varying force. Results of this experiment are presented in Figure 5.6, the continuous line presenting the displacement of the actuator, and the dashed line the estimated force. Unfortunately, the actual force is unknown in this experiment and, therefore, only qualitative validation is possible. The results show that the shape of the estimated force is as it should be for a spring-type force. This indicates that the force estimator can follow varying loads.

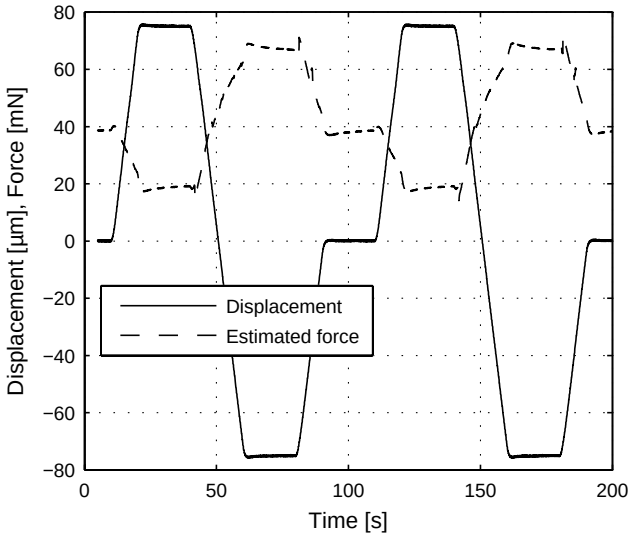

Figure 5.6. The piezoactuator driven against a plastic cantilever.

To obtain a rough estimate on the actual force in this experiment, another force estimation is created. This is based on the Hooke's Law, presented in Equation (2.1), to which an offset is added. The spring constant and the offset are approximated by finding a best fit so that the measured actuator displacement would be the spring elongation distance, and the estimated force would be the spring force. Since the values of the fitted curve are as close as possible to the force values of the estimator, quantitative conclusion cannot be made. However, the shape of the curve should be accurate to some extent, with an assumption that the deformation of the plastic cantilever is fully reversible and, thus, the force follows the spring force equation. The fitted values for the spring constant k_s and for the offset are 0.33 mN/µm and 42 mN.

The comparison between the fitted curve and the estimated force indicates the existence of both hysteresis and drift in the force estimator or in the cantilever, Figure 5.7.

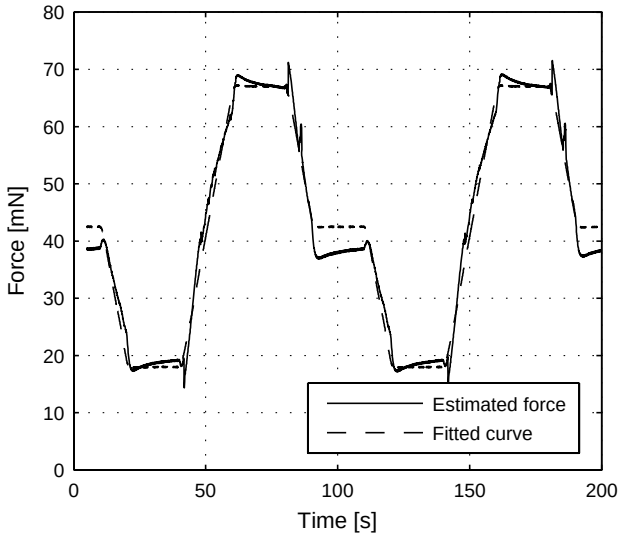

Figure 5.7. Estimated force and a fitted spring force curve.

5.4 Discussion and Conclusion

Although the force estimation model is straightforward to create and gives relatively good results, there is some room for further optimization of both the implementation of the model and the model structure. The model implementation could be improved by increasing the complexity of the training data, which, at present, is relatively simple. This would also solve the present overtraining risk of the neural network. A special attention should be at the static cases, as stressed in Section 4.1.2 with displacement control. The model structure could be improved by modelling motion and no-motion separately and, thus, obtain better tunability of the submodels. By optimizing the model structure, the performance of a force estimation method combining current, voltage, and displacement could be closer to the accuracy of the models presented in Chapter 4. These models contained about 2% of non-linearities. The force estimation of piezoelectric actuators contains quite complex phenomena and is, therefore, possible that many uncertainties remain even in more sophisticated model structures. Thus, one approach could be to use modelling approaches which are taking these uncertainties into account.

The proposed force estimation method is able to estimate both static and varying external forces with relatively good accuracy. The obtained accuracy is better than 10% of the full scale. This is not as good as the performance of separate force sensors but adequate in many microrobotic tasks. The main benefits of the sensorless force estimation method proposed here are: (i) the simplification and (ii) enabling further miniaturization of the mechanics compared to systems with separate force sensors, and (iii) enabling force sensing in applications where it has been unreachable. The force estimation enables also force control.

6. Self-Heating

This chapter introduces a method to quantify self-heating by a current measurement and how this can be utilized in the compensation of the effects of self-heating on displacement. Issues influencing self-heating include; the frequency and the amplitude of the driving voltage, the size, or more specifically the volume-area ratio of the actuator, the actuator material, and the used frequency with respect to resonance frequency, as discussed in Chapter 1. Some of these issues are also experimentally verified in Paper V. According to the experiments, the peak-to-peak value of the consumed current is a good indication of the temperature rise of the actuator. This can be used for the protection of the actuator from overheating, or it can be used to compensate for the changes in the displacement induced by the self-heating.

The rest of the chapter is organized as follows: In Section 6.1, the effect of self-heating on current consumption is introduced. Section 6.2 presents the effect of self-heating on the displacement. Section 6.3 introduces a compensation method for the displacement variations. Section 6.5 presents some application areas for the proposed methods. Conclusions are drawn at the end of the chapter.

6.1 Self-Heating and Current Consumption

This section presents how the current consumption is affected by heat generation. Naturally, the most severe effects of self-heating are damage in the actuator or destruction of its periphery. Some milder effects include thermal expansion of the actuator and changes in its displacement that can, however, also be of high significance. This section introduces how the current measurement can be used to quantify the amount of self-heating. The driving frequencies have been selected as such that some heating occurs but risks for overheating and depolarization are low. The used frequencies are low in comparison to actuator resonance frequencies introduced in Section 2.4.6. Therefore, the non-linear effect of the resonant frequency proximity on power consumption is not encountered [45].

When the actuator is controlled by a voltage and is heating up, it is noticeable that the current consumption is increasing along the temperature rise. This is in good agreement with [37], where polarization switching is shown to enhance at higher temperatures. Thus,

in this case, the voltage with a constant amplitude results in larger polarization at higher temperatures and this can be seen from the current measurement. Figure 6.1 presents the current (grey line) and temperature (black line) values from a test driven with Piezo 1 (presented in Chapter 2) at 200 V and 100 Hz.

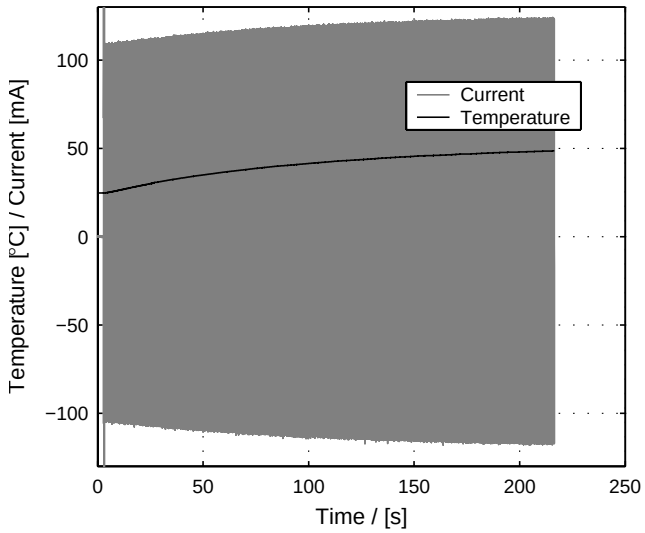

Figure 6.1. Influence of self-heating on the current.

The connection of the current consumption with the actuator temperature is depicted more clearly in Figure 6.2, where the temperature and the peak-to-peak values of the current are shown. The offset value of the peak-to-peak current is removed. In the beginning, the peak-to-peak current value is 205 mA (at 25 °C), and it increases more than 10%, while the temperature increases approximately 25 degrees.

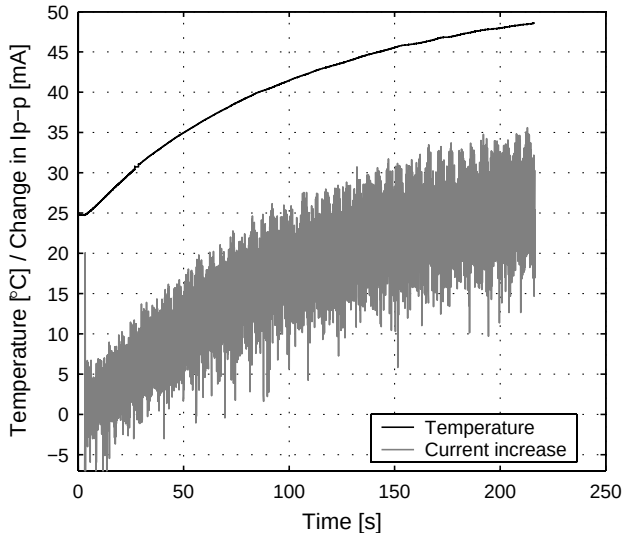

Figure 6.2. Temperature and change in peak-to-peak current value.

To quantify the relation between the current increase and the temperature rise, more measurements were carried out with two actuators: Piezo 1 and Piezo 3, presented in

Chapter 2. Piezo 1 was tested with three frequencies: 100 Hz, 120 Hz, and 180 Hz; and Piezo 3 with two frequencies: 500 Hz and 700 Hz. A 200 V triangular control signal is used in the measurements. Each test was repeated five times. Table 1 presents the results. Current increase is given as percentages of the original peak-to-peak current. According to the results, the average current increase per degree is 0.5%/°C, and a standard deviation 0.03%/°C in these 25 tests. The measured temperature rise varied from 15 °C up to 44 °C. According to these results, the current consumption can be utilized in the measurement of the actuator temperature change.

Table 1: Average results from the measurements.

Stack no.	Freq.	Temperature increase	Current increase in %	Current increase per °C
Piezo 1	100 Hz	16 °C	8 %	0.49 %/°C
Piezo 1	120 Hz	19 °C	10 %	0.50 %/°C
Piezo 1	180 Hz	29 °C	15 %	0.52 %/°C
Piezo 3	500 Hz	27 °C	13 %	0.46 %/°C
Piezo 3	700 Hz	43 °C	21 %	0.48 %/°C
			Average	0.49 %/°C

6.2 Effect of Self-Heating on Displacement

Since the increase in current is most likely due to the enhancement of polarization switching, as discussed in the previous section, and polarization, on the other hand, correlates with strain [15], self heating should increase the displacement. This effect was studied using Piezo 1 by driving it with a sine wave (200 V / 100 Hz).

Figure 6.3 presents the results, with the black line representing the temperature and the grey line the displacement. The thermal expansion of the actuator, being slightly more than 5 µm and approximately 0.03% of the actuator length, can be seen quite nicely in the figure.

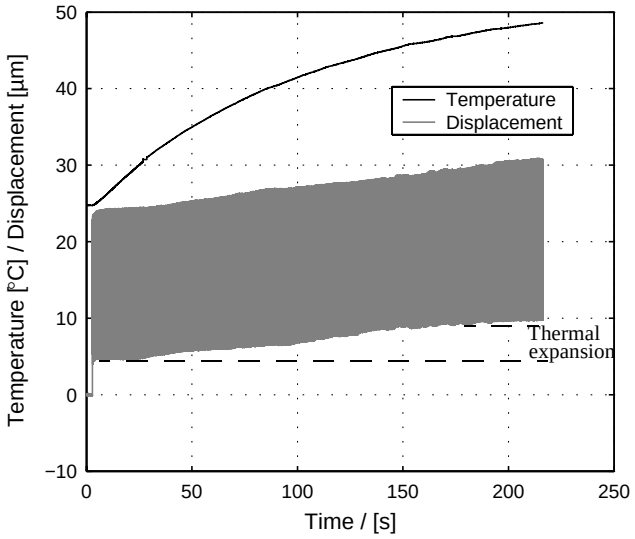

Figure 6.3. Influence of self-heating on the displacement.

In addition to the thermal expansion of the actuator, the amplitude of the displacement changes, increasing from 19.0 µm to 20.5 µm, as was expected. The change corresponds to 8% of the original amplitude (taken from the averages of the first and the last 1000 displacement cycles).

The amplitude increase is illustrated in Figure 6.4, where few displacement cycles from the beginning and in the end of the experiment have been captured to the same figure. The offset has been removed to show the difference in the amplitude more clearly.

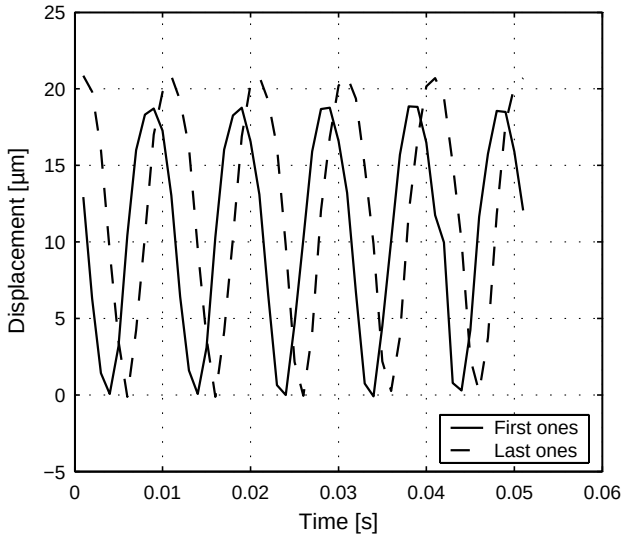

Figure 6.4. Five displacement cycles from the beginning (continuous) and in the end (dashed) of the test.

6.3 Compensation Method

Section 6.1 showed that self-heating is possible to measure without a temperature sensor using the consumed current. The effect of self-heating on the displacement was presented in the previous section. In this section, the emphasis will be on the compensation of the increase in the displacement amplitude induced by self-heating using information on the current consumption of the actuator.

The control goal is to keep the displacement amplitude constant. Since the displacement is proportional to polarization and, thus, to charge, as discussed in Section 1.3, by controlling the charge flow, the displacement amplitude is expected to remain constant. The approach is to keep the peak-to-peak current constant when the actuator is driven by a reciprocating signal, resulting in self-heating.

Figure 6.5 presents the block diagram of the proposed control method; an actuator current i is measured, and converted into a peak-to-peak current I_{pp}. A controller adjusts the amplitude A in order to maintain the current I_{pp} at a set point current I_{sp}. The set point current equals to the peak-to-peak current at the beginning, $I_{sp} = I_{pp\ at\ t\ zero}$. In the block diagram, f presents frequency, V voltage and d displacement.

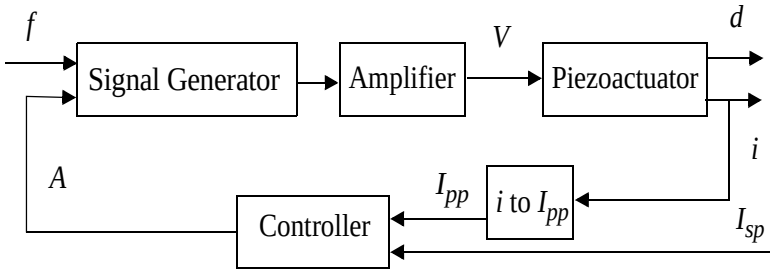

Figure 6.5. The block diagram of the proposed control method.

6.4 Compensation Results

The devices utilized in the experiment are the current meter, the PC with the data acquisition board, the laser position sensor, the signal generator, and the piezo amplifier presented in Chapter 2. A manual control is utilized in the experiments.

The proposed method is experimented with two actuators in the same conditions as in previous section: (200 V triangular wave, Piezo 1: 100 Hz, 120 Hz, 180 Hz; Piezo 3: 500 Hz, 700 Hz). Each test was repeated five times. For a reference, the same experiments were done also without the compensation.

Table 2 presents the results. Error is the relative difference between the original displacement amplitude and the final displacement amplitude. The temperature increase is the average value in the tests; in the compensated case, the temperature is typically a

couple of degrees lower; in the uncompensated case, a couple of degrees higher than the average.

Table 2: Average results from the experiments.

Stack no.	Freq.	Temperature increase	Error without compensation	Error with compensation
Piezo 1	100 Hz	16 °C	3 %	0.7 %
Piezo 1	120 Hz	19 °C	4 %	0.7 %
Piezo 1	180 Hz	28 °C	6 %	3 %
Piezo 3	500 Hz	25 °C	4 %	1.1 %
Piezo 3	700 Hz	39 °C	9 %	3 %
		Average	5.2 %	1.7 %

As can be seen, the results are far better when the compensation is used; the differences between the displacement amplitudes in the beginning and at the end are, on average, three times smaller with compensation than without compensation.

Figure 6.6 shows typical results from the first tests (Piezo 1, 100 Hz): The displacement amplitude of the uncompensated case increases until a certain point, while the displacement amplitude of the compensated case remains quite constant. The difference in the origin of the compensated and uncompensated cases is likely due to some remaining heat in the uncompensated case after the previous measurement. The actuator was cooled down between measurements with an air fan, and even though the surface of the actuator was at room temperature, the temperature of the inner body of the actuator could have been slightly higher. This decreases the displacement error of the uncompensated case and, by eliminating the remaining heat, the results would be even better than presented now.

In the experiments, where the compensated result differed significantly from the original and was as large as 3%, (Piezo 1 180 Hz and Piezo 3 700 Hz), the compensation decreased the displacement amplitude, and the final amplitude was smaller than in the beginning. It therefore seems that, in some cases, the proposed compensation method too effectively decreases the increased displacement amplitude due to self-heating.

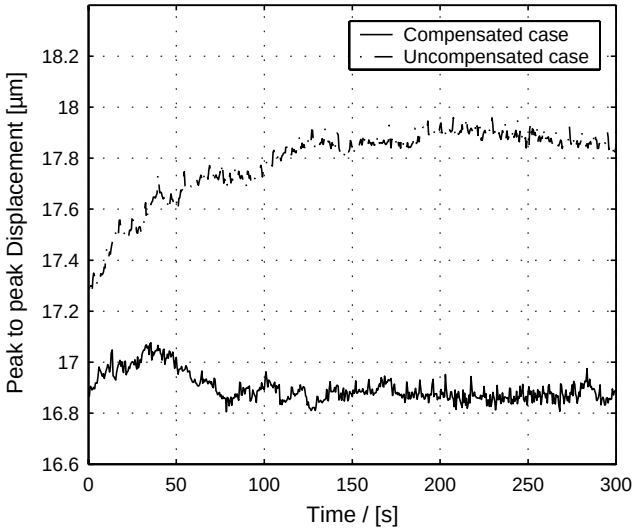

Figure 6.6. Typical results from the first test (Piezo 1, 100Hz), the uncompensated case with a dash-dot line and the compensated case with a continuous line.

6.5 Discussion and Application Areas

This section discusses first the temperature estimation method and its applications, then the proposed compensation method and its applications are addressed. Some indications can be found in the literature how the temperature estimation method would perform at temperatures higher than experimented in this thesis. Experiments with pyroelectric current [37] suggests that the temperature - current relation might become non-linear as the temperature increases near the Curie temperature. It is expected that the current would first increase even more and then at the very proximity of the Curie temperature the current would decrease rapidly. Based on their measurements, this effect would be expected to start about 50 °C below the Curie temperature with soft PZT actuators.

The temperature estimation by measuring the peak-to-peak current could be used as a safety feature preventing overheating, or as a trigger to start an additional cooler. An interesting application could also be found in piezoelectric pumps, where it might be possible to detect the media inside the pump due to their different cooling capability.

The proposed self-heating compensation method can be utilized in applications, which use a periodic control signal and where the overall performance can be increased by controlling the actuator amplitude more precisely. They include different piezoelectric pumps, liquid dispensers, and motors, for example. The compensation method should also be suitable for motors working at resonant or antiresonance frequencies. Further studies are, however, needed for applications, where the actuator driving frequency varies and is occasionally driven at resonance. There the large variation in mechanical losses [71] might require some modifications to the compensation method.

Piezoelectric stepper motors working with high frequencies could benefit open-loop accuracy by using the compensation method. Then the step size would be more constant, and dependency on the temperature would be decreased. Naturally, the load would remain as the main source of inaccuracy in piezo motors. In robotic applications where high accuracy is required, feedback sensors are naturally used, but a current measurement could give valuable information of the temperature of the motor.

Piezoelectric pumps can be used in applications where a constant flow is required, but an implementation of a flow sensor would be impossible due to the size/price requirements. Such application would benefit from the proposed compensation.

6.6 Conclusion

Current measurement can be used for determining the state of self-heating in a piezoelectric actuator without temperature measurement. The linear approximation is expected to work up to approximately 50 °C below Curie temperature with soft PZT actuators. Furthermore, based on the current measurement, a compensation method for the reduction of displacement variations is proposed induced by self-heating. The displacement error of an actuator driven by a high-frequency reciprocating signal reduces, in average, down to one part in three when the proposed compensation is used.

7. Other Applications

This chapter presents other applications where current measurement and the equations presented in Chapter 3 could be utilized. The issues presented in this chapter are not studied in detail in this work but are discussed on an idea level with an exception of one already demonstrated example. Some of the topics presented in the chapter are simple and easy to utilize while the others require more research to create feasible methods. All the presented ideas are related to measurements, but are here divided according to their applications to fault diagnostics and condition monitoring in Section 7.1 and measurements in Section 7.2.

7.1 Fault Diagnostics and Condition Monitoring

Fault diagnostics is important in high throughput systems, where the time while the system is not running can be measured in money. Systems with build-in diagnostics can be fixed in a shorter time in comparison to “dummy” systems, where the first task of maintenance is locating the failure. An optimal self-diagnostic system would give warning well before a critical failure in the system. This would highly increase the system reliability.

By having a current measurement as a part of the control setup, various self-diagnostic features can be implemented. They include detection of: 1. a broken wire, 2. dielectric breakdown, 3. a depolarised actuator, and 4. aging or wearing of the actuator. These are discussed in the following.

1. The simplest case is a detection of broken wire. When no current runs into the actuator regardless on the voltage input, a broken wire can be diagnosed. 2. Also relatively simple is the case of an actuator suffering from a dielectric breakdown; then the current can be many magnitudes larger than with a normal actuator. 3. A depolarised actuator, on the other hand, might have an almost-normal voltage-current relation but showing no movements. Therefore, this might be difficult to diagnose without the use of displacement measurement. 4. When the actuator is aging or wearing out, the piezoelectric properties change gradually with time; to monitor the changes, accurate actuator models are required. This might also require some additional sensors such as displacement, temperature, and force sensors, to obtain the best diagnostic performance.

An example of an application where current measurement has already been tried and found to be useful is monitoring of the poling process [36]. In the poling process, the resulting polarization is affected by the poling time, the electric field, and temperature. It was discovered, that the shape of the current curve measured during the poling process can describe when or if a full polarization has occurred. Furthermore, it was discovered that the resulting polarization can be estimated by the current measurement of the pyroelectric effect.

7.2 Temperature and Impact Measurements

This section discusses some measurements that the current measurement can enable in addition to the displacement, external force, and self-heating measurements introduced in Chapters 4-6. According to Equation (3.10), among the possible measurements only temperature estimation is left outside the scope of this work. It is likely that the temperature estimation could be accomplished similarly as force estimation in Chapter 5. It would require either a constant load or relatively little varying load in comparison to the actuator blocking force or usage of external force sensors. The method would then estimate the temperature of the operating environment of the actuator. However, temperature measurement is simple using thermistors; therefore, the temperature estimation of the operating environment using piezoactuators does not seem feasible.

More feasible measurement would be impact detection under sensorless displacement control. When the piezoactuator is controlled using the methods presented in Chapter 4, an impact can be detected from the current measurement as a peak. Although current is controlled in the position control methods, controller of the current drive is not fast enough to eliminate current peaks caused by impacts. The current peak size is likely to correlate with the impact strength.

8. Conclusion

This work has studied the utilization of the actuator input current measurement in several control applications. These applications include displacement control, and force and self-heating estimation. To utilize current measurement, a general actuator model is proposed that suggests that current, voltage, displacement, external force, and temperature are linked to each other through piezoelectric actuation mechanisms and pyroelectric effect. This model is then utilized in different control applications. The experimental results indicate that the proposed actuator model is feasible. Furthermore, the results show that the current measurement provides valuable information that can be utilized in displacement control, and in force and self-heating estimation, among others. The obtained information from the current measurement can replace one sensor in many cases and thus decrease the complexity of the system.

The results of displacement control utilizing current measurement show very good results: Hysteresis is less than 2% and drift about 1% in constant temperature. Temperature changes decrease the control performance. However, the temperature compensation method proposed in the thesis improves the control performance in varying temperatures close to the performance in constant temperature.

The results of the external force estimation method show that the method is capable of estimating constant and varying external forces while the actuator is under simultaneous position feedback control. The achieved accuracy is better than 10% of the full force scale. Therefore, force sensing without the use of separate force sensors is feasible, which opens new applications for force sensing in microrobotics. The results show that by adding current measurements into a typical micropositioning control scheme, force estimation and force control are feasible.

Current measurement is showed to be useful in the estimation of the amount of self-heating. The peak-to-peak current can be used to estimate the temperature rise when the actuator is driven with periodical voltage of a constant amplitude. On the other hand, the increase in the motion amplitude due the temperature rise can be compensated for by decreasing the amplitude of the input voltage such that the peak-to-peak current remains constant.

Other possible usages for current measurement in the control of piezoelectric actuators include fault diagnostics. It is suggested that several different actuator failure types could be distinguished from each other by combining the current measurement with the other available information.

References

1. K. Abidi, A. Sabanovic, and S. Yesilyurt, “Sliding-mode based force control of a piezoelectric actuator,” *Proceedings of the IEEE International Conference on Mechatronics, 2004. ICM '04*, pp. 104 - 108, June 2004.
2. H. J. M. T. A. Adriaens, W. L. de Koning, and R. Banning, “Modeling piezoelectric actuators,” *IEEE/ASME Transactions on Mechatronics*, 5 (2000) 4, 331-341.
3. Agilent Technologies Inc., “33120A Function generator user's guide”, March 2002.
4. APC International Ltd., “Guidance for designing mechanisms using servocell,” http://www.americanpiezo.com/servocell/design.html, July 2003.
5. E. Benes, M. Groschl, W. Burger, and M. Schmid, “Sensors based on piezoelectric resonators,” *Sensors and Actuators A: Physical*, 48 (1995) 1, 1-21.
6. D. Berlincourt, B. Jaffe, H. Jaffe, and H.H.A. Krueger, “Transducer properties of lead titanate zirconate ceramics,” *IRE Transactions on Ultrasonic Engineering*, 7 (1960) 1, 1-6.
7. B. Bhikkaji, M. Ratnam, Andrew J. Fleming, and S. O. R. Moheimani, “High-performance control of piezoelectric tube scanners,” *IEEE Transactions on control systems technology*, 15 (2007) 5, 853-866.
8. J.-M. Breguet, “Actionneurs ‘Stick and Slip’ pour micro-manipulateurs,” Doctoral Thesis, EPFL Switzerland, no 1756 (1998).
9. W. Cady, *Piezoelectricity*, Vol. 2, New York: Dover Publishers, (1964), pp. 699-702.
10. S. H. Chang, C. K. Tseng, and H. C. Chien, “An ultra-precision $XY\Theta_Z$ piezo-micropositioner part II: Experiment and performance,” *IEEE Transactions on Ultrasonics, Ferroelectrics, and Frequency Control*, 46 (1999) 906-912.

11. J. H. Cho, R. F. Richards, D. F. Bahr, and C. D. Richards, “Efficiency of energy conversion by piezoelectrics,” *Applied Physics Letters*, 89 (2006) 10, id. 104107.

12. G. S. Choi, H.-S. Kim, and G. H. Choi, “A study on position control of piezoelectric actuators,” *Proceedings of the IEEE International Symposium on Industrial Electronics*, Guimaraes, Portugal, pp. 851-855, July 1997.

13. R. H. Comstock, “Charge Control of Piezoelectric Actuators to Reduce Hysteresis Effects,” U.S. Patent 4,263,527, 1981.

14. D. Croft, G. Shedd, and S. Devasia, “Creep, hysteresis, and vibration compensation for piezoactuators: Atomic force microscopy application,” *Journal of Dynamic Systems Measurement and Control-Transactions of the ASME*, 123 (2001) 35-43.

15. D. Damjanovic, in *The Science of Hysteresis*, Vol. 3, I. Mayergoyz and G. Bertotti (Eds.), New York: Elsevier, 2005, pp. 345-429.

16. C. Dörlemann, P. Muß, M. Schugt, and R. Uhlenbrock, “New high speed current controlled amplifier for PZT multilayer stack actuators,” *Actuator 2002; 8th International Conference on New Actuators*, Bremen, Germany, pp. 454-457, June 2002.

17. S. Fahlbusch and S. Fatikow, “Force sensing in microrobotics systems - an overview,” *IEEE International Conference on Electronics, Circuits and Systems*, vol.3, pp 259 - 262, September 1998.

18. S. Fatikow and U. Rembold, *Microsystem Technology and Microrobotics*. Berlin Heidelberg: Springer-Verlag, 1997, p. 138.

19. A. Ferreira, J. Agnus, N. Chaillet, and J.-M. Breguet, “A smart microrobot on chip: design, identification, and control,” *IEEE/ASME Transactions on Mechatronics*, 9 (2004) 3, 508-519.

20. A. Ferreira, J. Agnus, N. Chaillet, and J.-M. Breguet, “Corrections to A Smart Microrobot on Chip: Design, Identification and Control,” *IEEE/ASME Transactions on Mechatronics*, 11 (2006) 3, 366.

21. A. J. Fleming and S. O. R. Moheimani, “Precision current and charge amplifiers for driving highly capacitive piezoelectric loads,” *Electronics Letters*, 39 (2003) 3, 282-284.

22. L. Fontanella, G. Frattini, G. Ricotti, and G. Pedrazzini, “Single chip, self supplied, voltage and charge mode double 80V piezoelectric actuator driver,” *Proceedings of the 25th European Solid-State Circuits Conference, ESSCIRC '99*, Duisburg, Germany, pp. 94- 97, September 1999,

23. K. Furutani, M. Urushibata, and N. Mohri, “Improvement of control method for piezoelectric actuator by combining induced charge feedback with inverse transfer function compensation,” *Proceedings of the 1998 IEEE International Conference on Robotics & Automation*, Leuven, Belgium, pp. 1504- 1509, May 1998.

24. T. Galante, J. Frank, J. Bernard, W. Chen, G. A. Lesieutre, and G. H. Koopmann, “Design, modeling, and performance of a high force piezoelectric inchworm motor,” *Journal of Intelligent Material Systems and Structures*, 10 (1999) 962-972.

25 P. Ge and M. Jouaneh, “Tracking control of a piezoceramic actuator,” *IEEE Transactions on Control Systems Technology*, 4 (1996) 209 - 216.

26 M. Guan and W.-H. Liao, “Studies on the circuit models of piezoelectric ceramics,” *Proceedings of 2004 International Conference on Information Acquisition*, Heifei, China, pp. 26-31, June 2004.

27 Y. Haddab, N. Chaillet, and A. Bourjault, “A microgripper using smart piezoelectric actuators,” *Proceedings of the 2000 IEEE/RSJ International Conference on Intelligent Robots and Systems*, Takamatsu, Japan, pp. 659-664, October 2000.

28 T. Higuchi, Y. Yamagata, K. Furutani, and K. Kudoh, “Precise positioning mechanism utilizing rapid deformations of piezoelectric elements,” *Proceedings of IEEE Micro Electro Mechanical Systems, an Investigation of Micro Structures, Sensors, Actuators, Machines and Robots*, Napa Valley, California, USA, pp. 222-226, February 1990.

29. D. Hughesy and J. T. Wenz, “Preisach modeling of piezoceramic and shape memory alloy hysteresis,” *Smart Materials and Structures*, 6 (1997) 287-300.

30. IEEE Standard on Piezoelectricity, 176-1987, January 1988.

31. T. Ikeda, *Fundamentals of Piezoelectricity*, New York: Oxford University Press, 1990, p. 1.

32 J. S. R. Jang, C. T. Sun, and E. Mizutani, *Neuro-Fuzzy and Soft Computing: a Computational Approach to Learning and Machine Intelligence*, New Jersey: Prentice-Hall, 1997.

33. L. Jones, E. Garcia, and H. Waitest, “Self-sensing control as applied to a PZT stack actuator used as a micropositioner,” *Smart Materials and Structures*, 3 (1994) 147-156.

34 P. Kallio and J. Kuncová-Kallio, “Capillary pressure microinjection of living adherent cells: Challenges in automation,” *Journal of Micromechatronics*, 3 (2006) 189-220.

35 P. Kallio, M. Lind, Q. Zhou, and H. N. Koivo, “A 3 DOF piezohydraulic parallel micromanipulator,” *Proceedings of the 1998 IEEE International Conference on Robotics & Automation*, Leuven, Belgium, pp. 1823-1828, May 1998.

36. T. M. Kamel, F. X. N. M. Kools, and G. de With, “Poling of soft piezoceramic PZT,” *Journal of the European Ceramic Society,* 27 (2007) 6, 2471-2479.

37. T. M. Kamel and G. de With, “Pyroelectricity versus conductivity in soft lead zirconate titanate (PZT) ceramics,” *Journal of Materials Research,* 22 (2007) 12, 3448-3454.

38 F. Khorrami, “Adaptive nonlinear control for end-effector position tracking of multi-link flexible manipulators with embedded active materials,” *Proceedings of the 33rd Conference on Decision and Control*, Lake Buona Vista, Florida, USA, pp. 103-108, December 1994.

39. E. S. Kolesar and C. S. Dyson, “Object imaging with a piezoelectric robotic tactile sensor,” *Journal of Microelectromechanical Systems*, 4 (1995) 2, 87-96.

40. P. Krejci and K. Kuhnen, “Inverse control of systems with hysteresis and creep,” *IEE Proceedings on Control Theory and Applications*, Berlin, Germany, pp. 185-192, May 2001.

41 S.-S. Ku, U. Pinsopon, S. Cetinkunt, and S. Nakajima, “Design, fabrication, and real-time neural network control of a three-degrees-of-freedom nanopositioner,” *IEEE/ ASME Transactions on Mechatronics*. 5 (2000) 273-280.

42. C. Lee, T. Itoh, and T. Suga, “Self-excited piezoelectric PZT microcantilevers for dynamic SFM—with inherent sensing and actuating capabilities,” *Sensors and Actuators A*, 72 (1999) 179–188.

43. G. A. Lesieutre, L. Fang, G. H. Koopmann, S. P. Pai, and S. Yoshikawa, “Heat generation of a piezoceramic induced strain actuator embedded in a glass/epoxy composite panel,” *Proceedings of SPIE Volume: 2717, Smart Structures and Materials 1996: Smart Structures and Integrated Systems*, pp. 267-275, May 1996.

44. J.-F. Li, K. Takagi, M. Ono, W. Pan, R. Watanabe, A. Almajid, and M. Taya, “Fabrication and evaluation of porous piezoelectric ceramics and porosity–graded piezoelectric actuators,” *Journal of the American Ceramic Society,* 86 (2003) 1094-1098.

45. C. Liang, F. Sun, and C. A. Roger, “Electro-mechanical impedance modeling of active material systems,” *Smart Materials and Structures*, 5 (1996) 2, 171-186.

46. Z. Lu, P. C. Y. Chen, and W. Lin, “Force sensing and control in micromanipulation,” *IEEE Transactions on Systems, Man, and Cybernetics—part C: Applications and Reviews*, 36 (2006) 713-724.

47. J. A. Main, D. V. Newton, L. Massengill, and E. Garcia, “Efficient power amplifiers for piezoelectric applications,” *Smart Materials and Structures*, 5 (1996) 6, 766-775.

48. K. Makihara, J. Onoda, and K. Minesugi, “A self-sensing method for switching vibration suppression with a piezoelectric actuator,” *Smart Materials and Structures*, 16 (2007) 455-461.

49. Marco Systemanalyse und Entwicklung GmbH, “Piezoceramic stack actuators,” http://www.marco.de/E/D/pa/ps/007.html, September 2007.

50. Matlab R2006b, “Neural network toolbox, user manual.”

51. Mel Mikroelektronik, http://www.melsensor.de/, June 2005.

52. W. J. Merz, “Domain formation and domain wall motions in ferroelectric BaTiO3 single crystals,” *Physical Review*, 95 (1954) 3, 690 - 698.

53. S. O. R. Moheimani, “A survey of recent innovations in vibration damping and control using shunted piezoelectric transducers,” *IEEE Transactions on Control Systems Technology*, 11 (2003) 4, 482- 494.

54. M. Nagai, N. Endo, and T. Yamada, “Fundamental characteristics of linear ultrasonic motor driven by travelling wave,” *IEEE International Workshop on Intelligent Motion Control*, Istanbul, Turkey, pp. 649-654, August 1990.

55 C. V. Newcomb and I. Flinn, “Improving the Linearity of Piezoelectric Ceramic Actuators,” *Electronics Letters*, 18 (1982) 442-444.

56. C. Niezrecki, D. Brei, S. Balakrishnan, and A. Moskalik, “Piezoelectric actuation: state of the art,” *The Shock and Vibration Digest*, 33 (2001) 4, 269-280.

57. Noliac A/S, “Plate stacks (SCMA-P),” Catalog 2003.

58. R. Perez, J. Agnus, J.-M. Breguet, N. Chaillet, H. Bleuler, and R. Clavel, “Characterisation and control of a 1DOF monolithic piezoactuator (MPA),” *Proceedings of SPIE Volume 4568: Microrobotics and Microassembly III*, Boston, USA, pp. 151-161, October 2001.

59. Physik Instrumente (PI) GmbH & Co. “Temperature effects,” http:// www.physikinstrumente.de/products/prdetail.php?secid=4-38, July 2003.

60. Piezo Systems Inc., “Piezo linear amplifier, catalog #7,” pp. 4-5, 2006.

61. J. L. Pons, *Emerging Actuator Technologies – A Micromechatronics Approach*, John Wiley & Sons, 2005, p. 53.

62. T. Ritala, “GMC-RT - user manual”, Internal report TUT/ACI, June 2004.

63. C. B. Sawyer and C. H. Tower, “Rochelle Salt as a Dielectric,” *Physical Review,* 35 (1930) 3, 269 - 273.

64. G. E. Simmers, J. R. Hodgkins, D. D. Mascarenas, G. Park, and H. Sohn, “Improved piezoelectric self-sensing actuation,” *Journal of Intelligent Material Systems and Structures,* 15 (2004) 941-953.

65. H. A. Sodano, D. J. Inman, and G. Park, “A review of power harvesting from vibration using piezoelectric materials,” *The Shock and Vibration Digest*, 36 (2004) 3, 197–205.

66. D. Song and C. J. Li, “Modeling of piezo actuator's nonlinear and frequency dependent dynamics,” *Mechatronics,* 9 (1999) 4, 391-410.

67. S. Takahashi, S. Hirose, K. Uchino, and K.-Y. Oh, “Electro-mechanical characteristics of lead-zirconate-titanate ceramics under vibration-level change,” *9th IEEE International Symposium on Applications of Ferroelectrics*, University Park, PA, USA, pp. 377-382, August 1994.

68. T. Takigami, K. Oshima, Y. Hayakawa, and M. Ito, “Application of self-sensing actuator to control of a soft-handling gripper,” *Proceedings of the IEEE International Conference on Control Applications,* Trieste, Italy, pp. 902-906, September 1998.

69. J. F. Tressler, S. Alkoy, and R. E. Newnham, “Piezoelectric Sensors and Sensor Materials,” *Journal of Electroceramics*, 2 (1998) 4, 257-272.

70. H. S. Tzou and J. J. Hollkamp, “Collocated independent modal control with self-sensing orthogonal piezoelectric actuators (theory and experiment),” *Smart Materials and Structures*, 3 (1994) 277-284.

71. K. Uchino and S. Hirose, “Loss mechanisms in piezoelectrics: How to measure different losses separately,” *IEEE Transactions on Ultrasonics, Ferroelectrics, and Frequency Control*, 48 (2001) 307-321.

72. C. Wallenhauer, B. Gottlieb, A. Kappel, T. Schwebel, J. Rucha, and T. Lüth, “Accurate load detection based on a new piezoelectric drive principle employing phase-shift measurement,” *Journal of Microelectromechanical Systems,* 16 (2007) 2, 344-350.

73. L. Xu, S.-F. Ling, B. Lu, H. Li, and H. Hu. “Sensing capability of a PZT-driven cantilever actuator,” *Sensors and Actuators A,* 127 (2006) 1–8.

74. K. Yao, K. Uchino, Y. Xu, S. Dong, and L. S. Lim, “Compact piezoelectric stacked actuators for high power applications,” *IEEE Transactions on Ultrasonics, Ferroelectrics, and Frequency Control*, 47 (2000) 819-825.

75. S. Yarlagadda, M. H. W. Chan, H. Lee, G. A. Lesieutre, and D. W. Jensen, “Low temperature thermal conductivity, heat capacity, and heat generation of PZT,” *Journal of Intelligent Material Systems and Structures*, 6 (1995) 757-764.

76. K. A. Yi and R. J. Veillette, “A charge controller for linear operation of a piezoelectric stack actuator,” *IEEE Transactions on Control Systems Technology*, 13 (2005) 4, 517-526.

77. S. Zhang, R. Xia, L. Lebrun, D Anderson, and T. R. Shrout, “Piezoelectric materials for high power, high temperature applications,” *Materials Letters*, 59 (2005) 27, 3471-3475.

78. Q. Zhou, A. Albut, C. Corral, P. Esteban, P. Kallio, B. Chang, and H. N. Koivo, “A microassembly station with controlled environment” *Proceedings of SPIE Vol. 4568, Microrobotics and Microassembly III*, B. J. Nelson, J.-M. Breguet, Eds., Boston, USA, pp. 252 - 260, 2001.

79. Q. Zhou, C. Corral, P. Esteban, A. Albut, and H. N. Koivo, “Environmental influence on microassembly,” *IEEE/RSJ International Conference on Intelligent Robots and Systems, IROS'02*, Lausanne, Switzerland, pp. 1760-1765, October 2002.

80 K. J. Åström and B. Wittenmark, *Computer-Controlled Systems: Theory and Design*, 3rd ed., New Jersey: Prentice-Hall, 1997, p. 295.

Publications

I

Paper I

P. Ronkanen, P. Kallio, and H. N. Koivo, “Current control of piezoelectric actuators with power loss compensation,” *IEEE/RSJ International Conference on Intelligent Robots and Systems (IROS)*, Lausanne, Switzerland, pp. 1948-1953, October 2002.

Proceedings of the 2002 IEEE/RSJ
Intl. Conference on Intelligent Robots and Systems
EPFL, Lausanne, Switzerland • October 2002

Current Control of Piezoelectric Actuators with Power Loss Compensation

Pekka Ronkanen[1], Pasi Kallio[1], Heikki N. Koivo[2]

[1]*Tampere University of Technology, Tampere, Finland, Pekka.Ronkanen@tut.fi, Pasi.Kallio@tut.fi*
[2]*Helsinki University of Technology, Helsinki, Finland, Heikki.Koivo@hut.fi*

Abstract

This paper introduces a feedforward charge control method, which controls the displacement by the amount of current fed to the actuator. The method includes estimation and compensation of the power losses occurring in the actuator. Power losses are estimated with an experimentally created dynamic model, that does not include the load and self heating effects.

Even though the method is based on feedforward control, the amount of current is controlled in closed loop, using a precise current measurement and a PID controller.

Experiments with a piezo bender show promising results; the hysteresis was nearly reduced to one part in twenty and drift to one part in ten, in comparison to open-loop voltage control. The proposed method can predict the power losses quite accurately and can therefore be utilized not only for the control but also for power estimation in applications where power consumption is critical.

1. Introduction

Piezoelectric actuators are widely used in applications requiring high resolution and accuracy. Their favorable dynamic properties extend the application areas into high speed areas such as vibration control. However, large hysteresis, drift, self-heating and load effects decrease the open-loop positioning accuracy. If a high accuracy is required, these non-linearities have to be compensated for. The compensation is usually accomplished by means of four different control principles: *feedforward voltage control*, where non-linear models are typically used [1], [2], [3]; *feedback voltage control*, where various sensors are used; *feedforward charge control*, where the operating current is controlled [4] and *feedback charge control*, where charge is measured and controlled [5], [6], [7].

Piezoelectric actuators are commonly controlled by using a voltage as an input signal. Since the primary electrical property of piezoelectric actuators is capacitance, it also includes the relationship between charge Q and voltage V:

$$C = \frac{Q}{V} \tag{1}$$

If capacitance C was constant, using voltage or charge as an input signal would give the same result. However, since the deformation of the material results in a change in the capacitance, a charge as a control signal gives results different from those that a voltage gives. The greatest difference of charge control is the reduction of hysteresis and drift. Experiments indicate that hysteresis is likely to be reduced at least to one fifth of the original [5]. Even better results were achieved in [6], where the hysteresis was reduced down to 2%.

Summarizing the advantages and disadvantages of the charge control: The main benefit is reduction of hysteresis. The disadvantages include additional electric circuits needed and thus, the increased complexity of the control hardware.

Charge control circuits can be divided into two groups: feedback and feedforward circuits. The first one utilizes feedback voltage charged to a capacitor in series with a piezoelectric actuator [5] and [6]. In another feedback method, the charge of the subsidiary electrodes is measured and used in the feedback [7]. These electrodes are additional layers of the actuator, to which a charge proportional to internal charge is induced.

Current drives utilize feedforward control. A charge can obtained by integrating a known current over a period of time. Constant current has been used over a variable period of time in [4] to obtain a certain displacement of a piezoelectric actuator.

This work concentrates in controlling the current fed into the actuator. Altough it is similar to the work of [4], the difference is that in [4] constant current is used and power losses were neglected. The results were also reported quite indistinctly. The contribution of this paper is that any current may be used, and the power losses are taken into account.

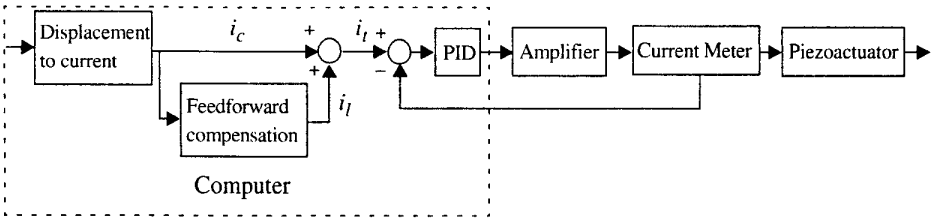

Figure 1: Control setup for current control.

The paper is organized as follows. Section 2 presents the control principle. In Section 3, the control setup is introduced. Section 4 and Section 5 discuss static and dynamic piezo operations, respectively. In Section 6, power loss compensation is presented. Section 7 presents the results of the work. Conclusions are drawn at the end of the paper.

2. Control Principle

The charge of the actuator can be obtained by integrating the current fed into the actuator. The relationship between the position and the current is as follows:

$$\delta(t) = a \cdot \int_0^t i(t)dt, \tag{2}$$

where $\delta(t)$ is the displacement, a a constant and $i(t)$ the current at time $t > 0$.

Solving for current i from (2) indicates that it can be used in control corresponding to velocity:

$$i(t) = \frac{1}{a} \cdot \frac{d}{dt}\delta(t) = \frac{v(t)}{a}, \tag{3}$$

where $v(t)$ is the speed of the actuator.

These equations neglect the power losses that occur in the actuator. As previously described, the capacitance is the dominant electrical property of the piezoelectric actuators. As is well-known, all capacitors have an internal resistance that causes a leakage current. Moreover, motion consumes power as in all actuators. The goal is to create a method that takes into account those losses, and compensates for them by feeding additional current to the actuator. Then the total current can be expressed as

$$i_t(t) = i_c(t) + i_l(t), \tag{4}$$

where $i_t(t)$ is the total current, $i_c(t)$ the current that causes charging and $i_l(t)$ the current used to compensate for the power losses. For convenience, external forces are neglected.

3. Control Setup

The first control experiments with the proposed control scheme were carried out by using devices available at Tampere University of Technology, instead of investing in expensive high voltage current drives. The components used are a normal piezo amplifier, a sensitive current meter with a voltage output and a computer with a data acquisition system. The control setup is shown in Fig. 1.

The *displacement to current* and the *feedforward compensation* blocks are the actual targets of interest in this work. The displacement to current block converts the displacement to the current as presented in Equation (3). The feedforward compensation block compensates for the power losses that occur in the actuator, whichwill be presented in Section 6. Section 4 and Section 5 create the basis for the feedforward compensation by discussing the static and dynamic piezo operations. The feedback loop in Fig. 1 is required to drive a certain current into the actuator with a normal voltage amplifier.

The current measurement has to be very sensitive. The following experiments demonstrate that the current must be controlled at a nanoampere precision in static operations. The current meter used was a 160B Digital Multimeter by Keithley Instruments (USA). The maximum resolution of this device is 10 pA.

Actuator used in the experiment was a piezoelectric bender NB 40x10x0.6-21 by Tokin (Japan).

4. Static Operations of Piezoelectric Actuators

A capacitor parallel with a resistor can be used to model the impedance of these actuators. A frequency dependent impedance of such a combination is

$$X_s(j\omega) = \frac{X_C(j\omega) \cdot R}{X_C(j\omega) + R}, \tag{5}$$

where $X_C(j\omega)$ is capacitive impedance, R is resistance and ω is frequency.

By taking the absolute value (5) becomes

$$X_s = \frac{R}{\sqrt{(\omega RC)^2 + 1}}, \quad (6)$$

where C is capacitance.

This frequency dependence should be taken into account in practice, if the movements are so fast that the component would still be charging when the polarity of the input signal changes. In other words, the target would be changed, before the goal displacement has been reached. It would lead to unsatisfying control design if this occurred. Therefore, we assume the motion speed to be low enough so that we can neglect the frequency dependent term and determine only R.

Since the value of R is over the MΩ range, it needs to be determined by means other than the normal Ohm meter. It was experimentally discovered that a 5 nA current was required to hold the piezobender in position after driving a 300 nA current to the piezo for a period of 40 seconds. The corresponding voltage was 105 V. The internal resistance can be calculated from these measured values according to Ohm's law, giving 21 GΩ as a result. The measurements of the experiment are shown in Fig. 2.

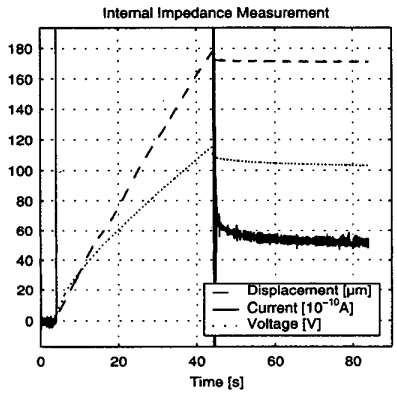

Figure 2: Current consumption in static operation.

5. Dynamic Operations of Piezoelectric Actuators

In dynamic operations, the piezoelectric actuator consumes power. The approach here is to generate a model for the internal impedance that describes the power losses occurring in the actuator. This can be achieved by at first finding suitable impedance values experimentally for two different currents. Then a relationship between current and impedance is formed to match the values together with the static 21GΩ in such a way that the accuracy of the formula will also be sufficient with other current and speed values. This impedance value can then be used to calculate the additional current needed for the actuator.

The test plan was to run a displacement ramp curve with ±300 nA and ±100 nA, and to evaluate various values of the internal impedance. By changing the impedance value, the estimated power losses and leakage current change accordingly. They are then compensated with the additional current.

For these experiments, a rough voltage value was required in order to calculate the leakage current from the impedance. This is estimated by using the actuator capacitance and the current for charging i_c.

The evaluation of whether the impedance is too small or too large can be made by observing the velocity of the movement. When an impedance value is too large, the additional current $i_l(t)$ will be too small and the power losses will consume part of the current meant for charging. This will result in a smaller velocity. It can be seen in Fig. 3, curve (1), where the velocity decreases when the charge increases. When the current $i_c(t)$ changes polarity; the direction of the velocity changes and its absolute value is increased, curve (2) in Fig. 3. Since the positive $i_l(t)$ is too small (added to the negative $i_c(t)$), the resulting negative total current is too large and respectively the velocity increases.

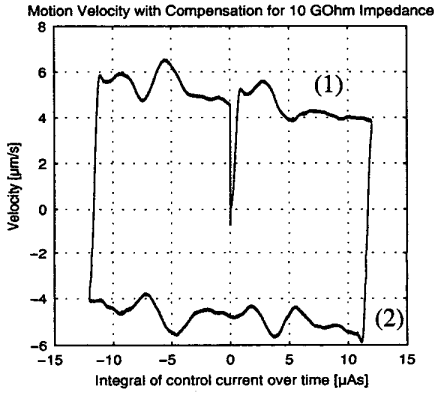

Figure 3: The velocity of the displacement ramp curve, when the impedance is estimated to be too large.

The change in the velocity is opposite to too small an impedance value, as can be seen in Fig. 4.

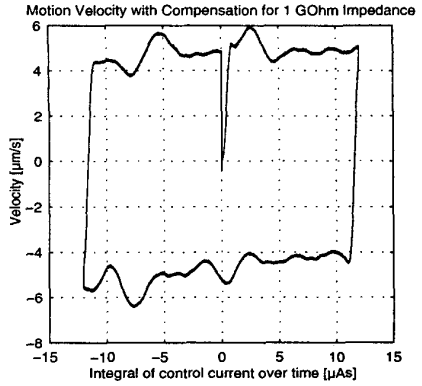

Figure 4: The velocity of the displacement ramp curve, when the impedance is estimated to be too small.

Fig. 5 presents an ideal velocity graph, when the impedance is set to an ideal value. The velocity remains constant at 5 µm/s throughout the displacement ramp curve.

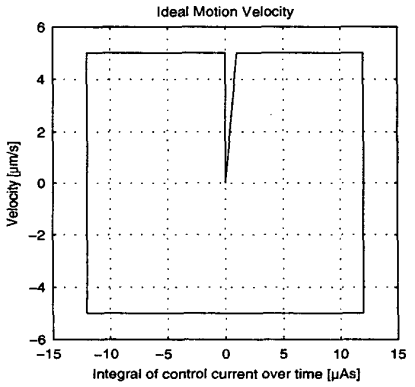

Figure 5: Ideal velocity of the displacement ramp curve.

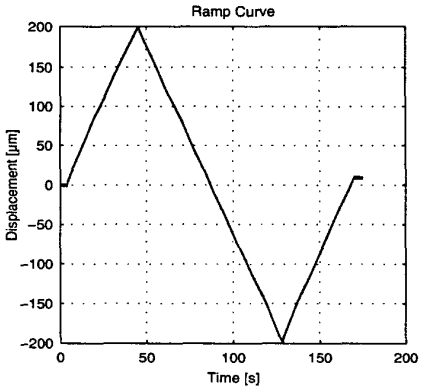

Figure 6: Displacement ramp curve driven with ±300 nA current.

Fig. 6 shows the displacement ramp curve driven with ±300 nA (see Eq. (2)) with a compensation for 2GΩ.

The experimental results of the tests described previously are presented in the following table.

Table 1: Experimental impedance values.

Current	Impedance
±300 nA	2 GΩ
±100 nA	6 GΩ

The final objective is to create a model in which resistance would be 21 GΩ, when current intersects zero, and get as close to 6 GΩ at 100 nA and to 2 GΩ at 300 nA as possible. The following empirical models, (7) to (11), were tried. They are all asymptotically approaching zero.

$$X = R \cdot e^{-|ci|} \tag{7}$$

$$X = R \cdot b^{-|ci|} \tag{8}$$

$$X = \frac{R}{|c \cdot i| + 1} \tag{9}$$

$$X = \frac{R}{\sqrt{(ci)^2 + 1}} \tag{10}$$

$$X = \frac{R}{ci^2 + 1}, \tag{11}$$

where b and c are constants, X is the impedance representing the cause of power losses, and R the internal resistance. The results are shown in Fig. and the sums of square errors are given in Table 2.

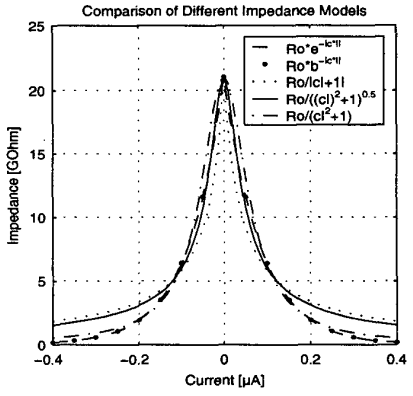

Figure 7: Comparison between different impedance models.

Table 2: Sums of square errors of different equations.

Equation	(7)	(8)	(9)	(10)	(11)
SSE / $G\Omega^2$	2.1	2.1	0.18	0.0052	1.2

The best result was achieved with (10). This equation has the smallest error between the model and the experimental values, when $c = 3{,}4 \cdot 10^7\ A^{-1}$. Then (10) becomes

$$X = \frac{21G\Omega}{\sqrt{(3{,}4 \cdot 10^7 \cdot i)^2 + 1}} \tag{12}$$

6. Feedforward Compensation

Based on (12), a feedforward compensation block shown in Fig. 1 can be designed. This block will compensate for the power losses that occur in the piezoelectric actuator by feeding additional current into it. It will not, however, take into account the effect of external loads. With an input value of the current desired to be charged to the actuator, the output of the block is the current that needs to be driven into the actuator in order to reach the goal.

When Ohm's law is substituted into the (4), we obtain

$$i_t(t) = i_c(t) + i_l(t) = i_c(t) + \frac{V(t)}{X} \tag{13}$$

The capacitors voltage-current relationship and (10) are substituted into (13) to obtain:

$$i_t(t) = i_c(t) + \frac{\frac{1}{C}\int_0^t i_c(t)dt}{\frac{R}{\sqrt{(c \cdot i_c(t))^2 + 1}}} \tag{14}$$

$$= i_c(t) + \frac{1}{RC} \cdot \sqrt{(c \cdot i_c(t))^2 + 1} \cdot \int_0^t i_c(t)dt$$

The voltage $V(t)$ can also be measured directly from the output of the PID controller. This requires that the amplifier amplification is taken into account, and the equation is simplified

$$i_t(t) = i_c(t) + \frac{V(t)}{R} \cdot \sqrt{(c \cdot i_c(t))^2 + 1} \tag{15}$$

where $i_t(t)$ and $i_c(t)$ are the currents, $V(t)$ a voltage, R an internal resistance of the actuator, and c a constant.

7. Results and Discussion

This section introduces the results of the developed feedforward charge control method. To show that the method has not only been tuned for a certain motion speed, a decaying ramp signal is applied (Fig. 8). The ramp time remains constant and therefore, by decreasing the displacement, the speed is decreased as well. The maximum inaccuracy was 10µm.

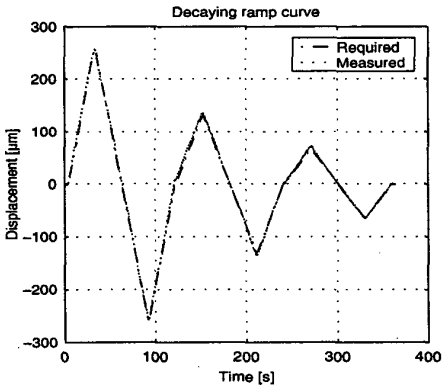

Figure 8: A decaying ramp curve.

The results of the hysteresis test are demonstrated by Fig. 9. The maximum hysteresis is approximately 1.5%.

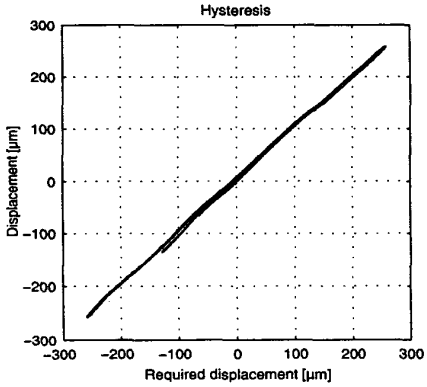

Figure 9: The hysteresis of the decaying ramp curve.

Repeatability was tested by running a ramp curve 20 times. The test showed good results, the displacement drifted only 2% in nearly 80 minutes, while the peak to

peak value remained practically constant, increasing only by 0.5% during the time period.

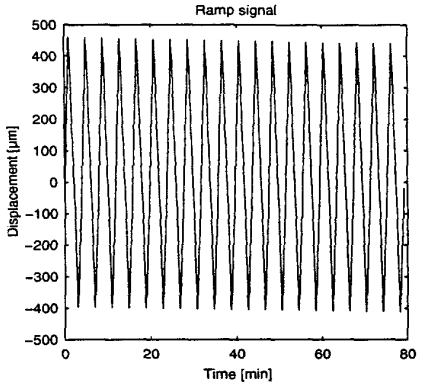

Figure 10: Ramp curve driven 20 times.

Fig. 11 shows the drift. The displacement stays within 1.5% over the time period of two minutes, which is one tenth in comparison to open loop voltage control.

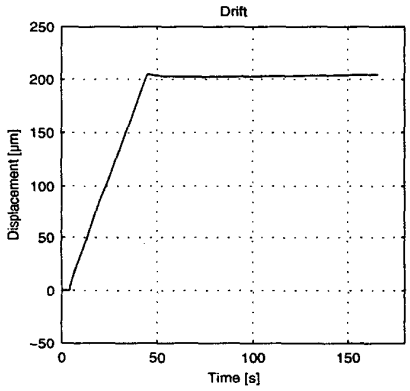

Figure 11: Drift.

Long term operations with varying inputs may lead to undesired results in feedforward control. It is should be noted that several other variables can also effect the results. Therefore different actuators of same dimensions might require parameters, whose values van deviate considerably from the ones presented here.

8. Conclusion

A new current control scheme was developed by estimating and compensating for the power losses occurring in the actuator. They were compensated by an additional current. The method gives very promising results. The hysteresis reduced from 27% to 1.5%. The elimination of the drift was remarkable, reducing from 15% to 1.5%. Current control method shows the capability of predicting the power losses quite accurately and can therefore be utilized also in the power considerations in application areas where power is a critical issue. They include space and mobile applications, since the method gives a good approximation of the driving current without measurements. Future work includes implementing the compensation for load and temperature effects related to piezoactuators.

References

[1] Ge, P. & Jouaneh M. 1996. *Tracking Control of a Piezoceramic Actuator.* IEEE Transactions on Control Systems Technology, Vol. 4, No. 3, May.

[2] Croft, D., Shedd, G. & Devasia, S. 2000. *Creep, Hysteresis, and Vibration Compensation for Piezoactuators: Atomic Force Microscopy Application.* Proceedings of the American Control Conference, Chicago, Illinois, June 2000.

[3] Choi, G. S., Kim, H.-S. & Choi, G. H. 1997. *A Study on Position Control of Piezoelectric Actuators.* Proceedings of the IEEE International Symposium on Industrial Electronics, Guimaraes, Portugal, July 7-11, 1997. Vol. 3.

[4] Newcomb, C. V. & Flinn, I. 1982. *Improving the Linearity of Piezoelectric Ceramic Actuators.* Electronics Letters, Vol. 18, No. 11, May.

[5] Comstock, R. H. 1981. *Charge Control of Piezoelectric Actuators to Reduce Hysteresis Effects.* U.S. Patent 4,263,527.

[6] Perez, R., Agnus, J., Breguet, J.-M., Chaillet, N., Bleuler, H. & Clavel, R. 2001. *Characterisation and Control of a 1DOF Monolithic Piezoactuator (MPA).* Proceedings of SPIE Volume 4568: Microrobotics and Microassembly III, Boston, USA, October 2001.

[7] Furutani, K., Urushibata, M. & Mohri, N. 1998. *Improvement of Control Method for Piezoelectric Actuator by Combining Induced Charge Feedback with Inverse Transfer Function Compensation.* Proceedings of the 1998 IEEE International Conference on Robotics & Automation, Leuven, Belgium, May 1998.

II

Paper II

P. Ronkanen, P. Kallio, M. Vilkko, and H. N. Koivo. ”Displacement control of piezoelectric actuators using current and voltage,” Submitted to *IEEE/ASME Transactions on Mechatronics*.

Displacement Control of Piezoelectric Actuators Using Current and Voltage

Pekka Ronkanen, Pasi Kallio, *Member, IEEE*, Matti Vilkko, *Member, IEEE*, Heikki N. Koivo, *Senior Member, IEEE*

***Abstract*— This paper introduces a feedforward charge control scheme, which controls the velocity of a piezoelectric actuator by the amount of current fed to the actuator. The method utilizes an actuator model to estimate the current needed for the desired motion velocity. Actuator voltage information is utilized as an input for the model, which is separated in two phase combining individual models for a motion phase and a static phase.**

The method is verified by a series of experiments having a variable motion velocities and amplitudes. During the experiments, the current is fed to the actuator by a current driver consisting of a voltage amplifier, a precise current meter and a controller.

The results show significant improvement in comparison to open loop voltage control; the hysteresis is less than 2% and the drift about 1%. This indicates that the motion of piezo actuators is a function of current and voltage and does not depend considerably on the motion history. Therefore, a sensorless control to overcome the hysteresis and drift would be feasible.

***Index Terms*— piezoelectric actuator; charge control; current control**

I. Introduction

Piezoelectric actuators are widely used in applications that require high resolution and accuracy. Their favourable dynamic properties extend the application areas into high speed areas such as vibration control. However, large hysteresis, drift, temperature, self- heating, and load effects decrease the open-loop positioning accuracy. If a high accuracy is required, these non-linearities have to be compensated for. The compensation is usually accomplished by means of four different control principles: feedforward voltage control, where non-linear models are typically used [1], [2], [3], [4]; feedback voltage control, where various sensors are used; feedforward charge control, where the operating current is controlled [5], [6], [7]; and feedback charge control, where charge is measured and controlled [8], [9], [10].

Piezoelectric actuators are commonly controlled by using voltage as an input signal. The main benefit achieved using charge control is the reduction of hysteresis and drift. Experiments indicate that hysteresis is likely to be reduced at least to one fifth of the original [8], [9], [10]. The disadvantages include the need for additional electric circuits and, thus, the increased complexity of the control hardware.

Charge control circuits can be divided into two groups: feedback and feedforward circuits. The first one utilizes feedback voltage charged to a capacitor in series with a piezoelectric actuator [8] and [9]. In another feedback method, the charge of subsidiary electrodes is measured and used in the feedback [10]. The electrodes are additional layers of the actuator, to which a charge proportional to internal charge is induced.

Current drives utilize feedforward control. A charge can be obtained by integrating a known current over a period of time. Constant current has been used over a variable period of time in [5] to obtain a certain displacement of a piezoelectric actuator but without taking into account power losses. The authors introduced in [6] a feedforward charge control method where any current may be used and the power losses are estimated and compensated for. Extension including temperature and humidity effects on the control scheme was introduced later in [7]. Both results were good; hysteresis and drift were reduced remarkably. However, the impedance model of the actuator, that the method is based on, is very laborious to create. Another drawback is the long term stability, since the voltage information used in context with the impedance model was estimated, and not actually measured.

This work proposes a method which simplifies the creation of actuator model. The goal is to create a current control method using a simple actuator model that could be specified for each actuator with a minimum effort. This means that the required number of experiments and the consumed time should be minimized for the model parameter estimation. Another goal is to keep the structure of the control method sufficiently simple such that the control algorithms could be implemented using only simple arithmetic operations.

The rest of the paper is organized as follows; Section II

Manuscript received October 22, 2007. This work was supported in part by the Graduate School in Electronics, Telecommunications and Automation (GETA).

P. Ronkanen is with the Institute of Automation and Control at the Tampere University of Technology, 33720 Tampere, Finland (phone: 358-3-3115 3369; fax: 358-3-3115 2340; e-mail: Pekka.Ronkanen@tut.fi).

P. Kallio is with the Institute of Automation and Control at the Tampere University of Technology, 33720 Tampere, Finland.

M. Vilkko is with the Institute of Automation and Control at the Tampere University of Technology, 33720 Tampere, Finland.

H. N. Koivo is with the Control Engineering Laboratory at the Helsinki University of Technology, 02150 Espoo, Finland.

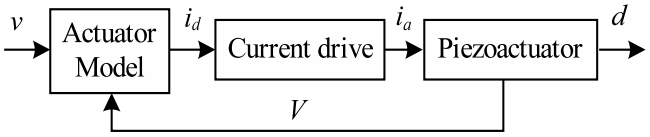

Fig. 1. Block diagram of the proposed method, v is the desired velocity, i_d the desired current, i_a the actual current and V the voltage.

presents the proposed control architecture and Section III describes the experiment setup. Results are presented in Section IV. Discussion and conclusion are at the end of the paper in Sections V and VI.

II. Control Architecture

This section proposes the modified current control method for piezoelectric actuators. The basic approach is to control the velocity of the actuator using current and voltage. The method can be categorized as feedforward charge control using also voltage information. Fig. 1 presents the control block diagram.

A. Actuator model

This section proposes a structure for the actuator model. The model should estimate the current that the actuator requires in order to move with a desired velocity.

From [6] we can derive that the velocity of a piezoelectric actuator can be described as a function of current and voltage:

$$v(t) = f(i(t), V(t)), \tag{1}$$

where $v(t)$ is velocity of the actuator, $i(t)$ current, and $V(t)$ voltage. This can be presented with respect to current:

$$i(t) = g(v(t), V(t)). \tag{2}$$

Moreover, we can derive from the same source that in a special case when the velocity equals zero, the current can be presented as a function of voltage:

$$i(t)_v = g(V(t))\big|_{v(t)=0}. \tag{3}$$

According to these two equations, we create a structure for the actuator model. Equation (3), being only a special case of Equation (2), is included in the model to have better long-term stability and tunability of the actuator model. This leads to an actuator model architecture with two components where one part is modelling actuator motion and the other part is modelling the actuator in a static operation mode. Besides the motion and static models, a mode selector is included for switching between the two models. Fig. 2 presents the structure of the actuator model architecture.

The motion model is used for the approximation of the desired current in motion and the static model for the approximation of the desired current when the actuator should hold still. The following sections present the actuator model parts in more detail.

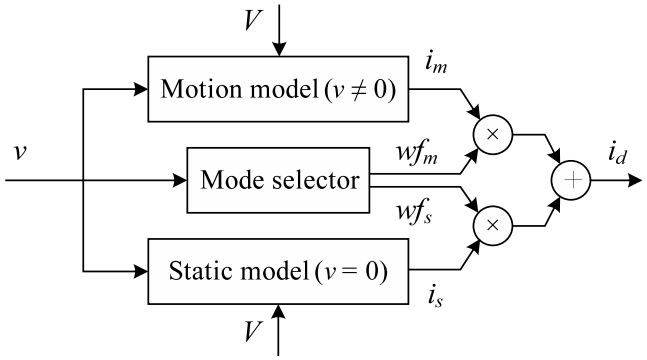

Fig. 2. Structure of the actuator model.

1) Motion model

This section discusses the motion part of the actuator model. As presented in [6], the dependency among actuator velocity, current, and voltage is nonlinear. Therefore, a nonlinear mapping is required. In order to minimize the manual labour in the model creation, a method which is supported by software tools should be selected.

One of this type of well established methods are neural networks [11]; tools for creating and training neural networks exist in commercial softwares. The goal was to create as simple model as still feasible, since it would result in faster training and implementation of the model and it would require less computation in actual control.

Training data have been obtained by driving random current to the actuator while the actuator velocity and the voltage have been recorded. Various feedforward backpropagation networks were created, trained and evaluated using NNTool of Matlab®. It was discovered that a simple 2*1 feedforward backpropagation network can model the actuator quite accurately, and in order to significantly improve the model performance, the neural network model should be far more complex than this. The model structure is as follows

$$i_m = w_2 \tanh\left(w_{11} \cdot v + w_{12} \cdot V + b_1\right) + b_2, \tag{4}$$

where w_{11}, w_{12}, w_2, b_1, and b_2 are constants, and i_m is motion model current.

2) Static model

This section presents the static part of the actuator model. It is included to enhance the model performance when the actuator is desired to hold its location or when the desired motion velocity is very small. Linear relationship between current and voltage can be found from electrical models of piezoelectric actuators with a zero frequency, e.g. [12]. Also our previous work with current control in the static case utilized a linear model between voltage and current [6]. The current fed to the actuator is considered to have two sub-currents; charging current i_c and power loss current i_l, Equation (5). The charging current charges the actuator and

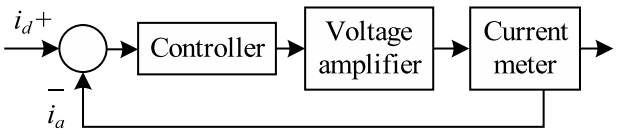

Fig. 3. Schematics of the current drive.

results in motion. The power loss current is for power losses, such as for leakage current.

$$i_s(t) = i_c(t) + i_l(t), \tag{5}$$

where i_s is static model current, i_c charging current, and i_l power loss current.

Required charging current is presented in Equation (6).

$$i_c(t) = \frac{v(t)}{a}, \tag{6}$$

where a is a constant describing the relation between velocity and charging current.

Now, power loss current can be simplified from [6] to a linear relationship between current and voltage, Equation (7), since the power losses of no-motion case and very slow motions are desired to be compensated.

$$i_l(t) = GV(t), \tag{7}$$

where G is a constant describing the conductance of the actuator. In addition to the electrical conductance of the actuator, other effects such as drift in electrical capacitance due to mechanical drift may influence the value of the constant and can be included in practical cases.

3) Mode selector

This section presents the mode selector used to switch between the two models, the motion model and the static model.

In order to avoid a jump in the actuator model output due to a difference in the outputs of the two submodels, the mode selector should perform a smooth transition between the two models. A simple way to enable this is to create weight functions for the two models, which define how much each model should be taken into account. This approach is derived from fuzzy logic methodology. To avoid "if" and "then" -clauses in the controller, the weight functions should be continuous over the used velocity range. The following equation presents the weight function used for the static model.

$$wf_s = \frac{1}{k(rv)^2 + 1}, \tag{8}$$

where k defines the shape of the weight factor, r normalizes the velocity according to the selected velocity range, $-1 \le rv \le 1$, and v is the velocity. The weight function for the motion model becomes

$$wf_m = 1 - wf_s. \tag{9}$$

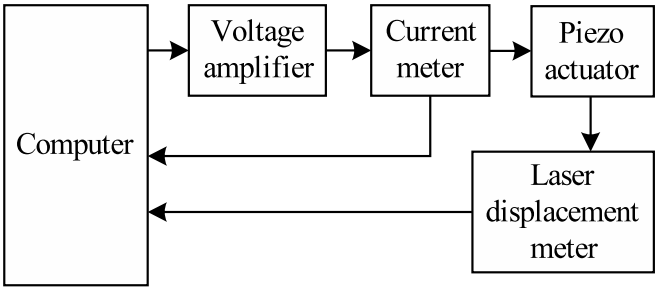

Fig. 4. Experiment setup.

III. Description of the Experiment

This section describes the control implementation and the experiment setup. The implementation of the control scheme requires control software, a data-acquisition board with analog inputs and outputs, a current driver, and a piezo actuator.

The implementation of the control software is done using Matlab, with a real-time xPC Target toolbox. Data-acquisition is performed using a National Instruments AD-board model with two analog outputs (PCI-6052E).

In order to drive the desired current into the actuator, a current driver is needed. Due to the lack of such a device in our laboratory, this is created using a voltage amplifier (Piezo Systems EPA 102), a current meter (Keithley 160B), and a controller implemented in the same control software as the actuator model. Fig. 3 presents the schematics of the current drive. The utilized controller is a PID controller with an additional integrator. Equation (10) presents the transfer function of the controller.

$$C(s) = \frac{K_1 s^2 + K_2 s + K_3}{s^2}, \tag{10}$$

where K_1, K_2, and K_3 are the controller parameters (for the actuator in question with a chosen current range the parameter values are 0.00001, 0.3 and 2 respectively.)

The entire experiment setup is presented in Fig. 4. The laser displacement meter is M5L/0,5 from Mel Mikroelektronik with a range of ±250 µm. The piezo actuator used in the experiments is a bimorph bender NB38*4*0.6 from Tokin.

The following steps are performed in order to create a model of a certain actuator; first the motion model is created: (i) Driving a random current to the actuator, each random current value is driven for several seconds. Displacement and voltage are recorded. (ii) The data is processed for the neural network toolbox by filtering and calculating the actuator velocity. (iii) The neural network is created and trained.

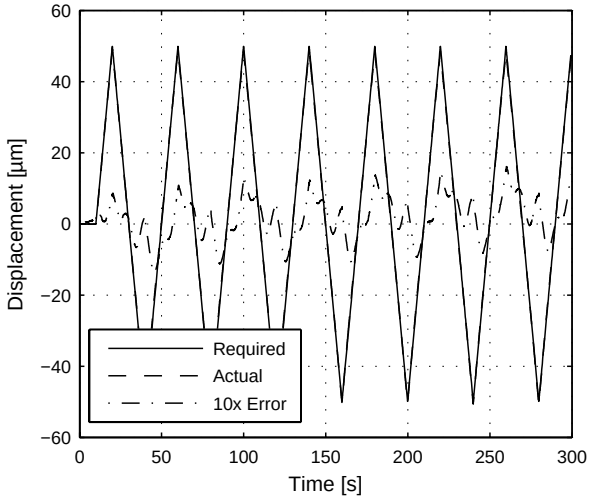

Fig. 5. 100 µm displacement ramp curves with a 40 s time period.

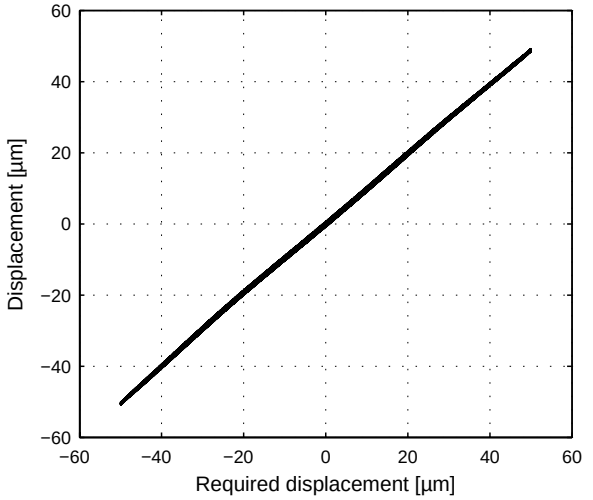

Fig. 6. Hysteresis of 100 µm displacement ramp curves with a 40 s time period.

In the second step, the static model is to be created. (i) Resistance of the actuator is measured or approximated. (ii) A few conductance values in the proximity of the corresponding resistance value are tested in static experiments and the best is chosen. (iii) Constant a in the static model is approximated from the motion model or it is experimentally determined. In these experiments, a value of 1.25e-11 1/Ω was used for the conductance G, and a value of 37.6 m/As was used for the constant a.

The third step determines the parameters of the mode selector: (i) Desired velocity range is selected and parameter r is calculated. (ii) Desired shape is determined for the weight factor. In these experiments, a value of 1000 was used for the shape factor k.

IV. Results

This section presents experimental results of the proposed control method. Even though the control method is intended to the control of the actuator velocity, the results will present displacement. This is due to the reference measuring system. Since it is measuring the displacement with a certain noise level, velocity should be obtained by differentiation and this would result in a relatively noisy signal. Therefore, it is more convenient to accumulate the velocity control signal and examine the results with respect to displacement.

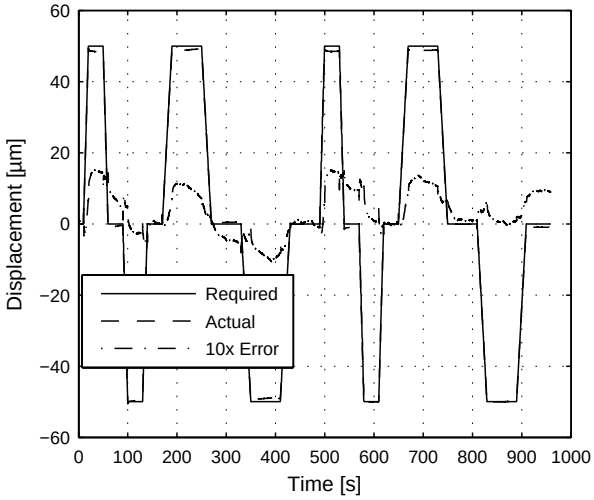

Fig. 7. Displacement trajectory with steady state phases of variable lengths.

Several displacement ramp curves with varying frequency and amplitude will be presented. The tested trajectories include also steady states for drift characterization. All trajectories have been driven for a minimum of five times and the results in this section present typical results.

A. Performance in constant velocity experiments

Fig. 5 presents results of a displacement ramp curve with an amplitude of 100 µm with a cycle time of 40 s repeated for several times. The total time of the experiment is 300 s. The figure presents the required displacement, the actual displacement, and their difference magnified by 10 times. The maximum inaccuracy is about 1.5 µm, i.e. 1.5 %. Fig. 6 presents the actual displacement with respect to the required displacement. As can be seen, the outcome is quite linear and relatively accurate. Hysteresis is less than 1.5 % of the total displacement amplitude.

B. Performance in steady states and variable velocity experiments

A longer trajectory having steady states of different lengths and variable velocities is presented in the following figures. Fig. 7 presents the required displacement and the actual displacement. As can be seen, the outcome follows well the required trajectory for the 16 minutes that the experiment lasts. During the 16-minute time period the maximum inaccuracy is about ±1.5 µm.

The steady state behaviour is presented in more detail in Fig. 8. A typical drift behaviour is noticeable; the

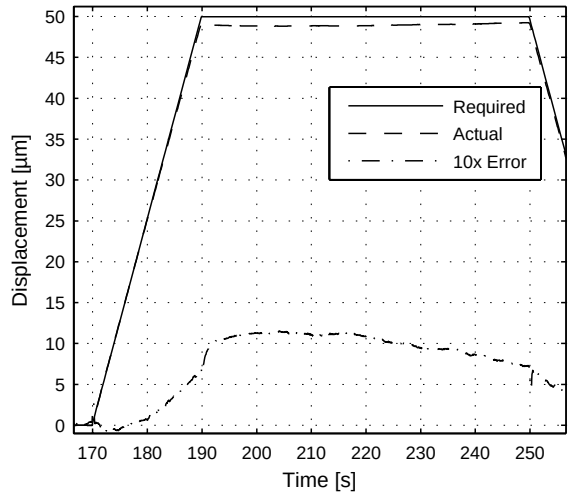

Fig. 8. Close-up of a steady state phase.

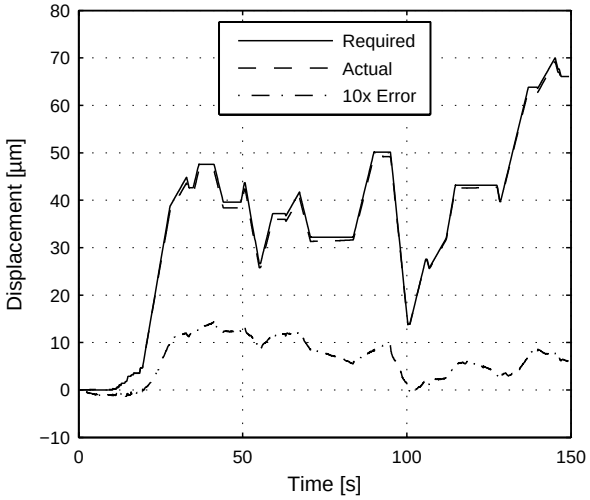

Fig. 10. Displacement trajectory obtained from cell injections.

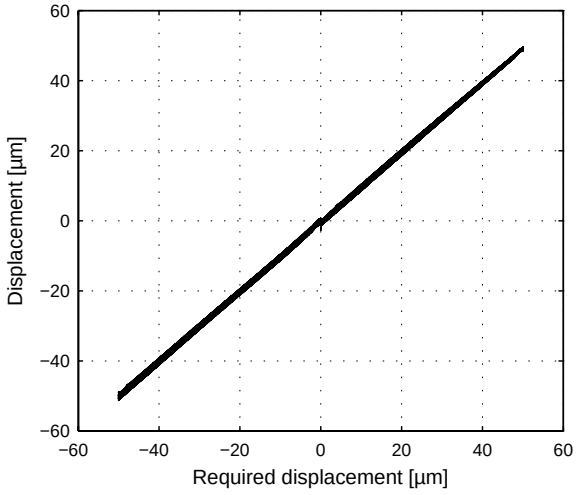

Fig. 9. Hysteresis of the displacement trajectory with steady state phases of variable lengths.

displacement is for the first few seconds decaying, before stabilizing. The static model is tuned in such a way that the displacement is slightly increasing to the end of the steady state, to overcome the decay at the beginning of the steady state. Hysteresis is presented in Fig. 9. The figure shows linear behaviour with 1.5 % non-linearity.

C. Performance in cell injection applications

The suitability of the method for real life control applications was tested with a trajectory obtained from living cell injections. The cell injections were performed with a MANiPEN micromanipulator [13] using a joystick as an operator input device in an injection session, where two cells were injected. The input trajectory during the injection was recorded and then later used as an input for these experiments. The trajectory is presented in Fig. 10 with a result using the proposed control method. The maximum inaccuracy during the 150 seconds is less than 1.5 µm and during 70 % of the time, inaccuracy is less than 1 µm.

V. DISCUSSION

The displacement of piezoelectric actuator follows closely the required trajectories by using the proposed control method. The starting position has a small effect on the end displacement. Another imperfection can be found in the beginning of the static phases. There is a small decay in the displacement. This section discusses the ways to eliminate these remaining errors.

It was discovered during the cell injection application experiments, that the starting position has a small effect on the end displacement. Results show a maximum difference of 6 % between different trajectories. However, this is significantly smaller than in the open-loop voltage control, where the difference can be more than 25 %. It is still unclear, whether the deviation in the displacement is due to the properties of piezo actuators or can it be avoided by using a more complex actuator model.

There are several possible reasons for the small decay in the displacement in the beginning of the static phase. The primary hypotheses include peaking of the current while changing the motion speed, a mechanical spring effect of the cantilever and a drift in the electro- mechanical properties of the actuator. Different controller parameters of the current drive were tested in order to reduce the peaking of the current, but a similar tendency in the output displacement remained in the beginning of the static phase. The peaking is rather difficult to avoid totally, since the current meter has a cut-off frequency of 40 Hz, and the controller is running at 2 kHz. The latter two hypotheses - the mechanical spring effect and the drift in electromechanical properties - seem therefore to be more probable reasons for this behaviour.

The displacement decay in the beginning of the static phase could be avoided by implementing a dynamic feature into the static model or by designing an advanced controller for the current drive that behaves differently depending on the

desired velocity and the change in the velocity.

The present mode selector is computationally simple, but requires some manual work for optimization. The optimization process could be easier by using a method which is supported by software tools, such as a radial-base function network. However, this method results in computationally more complex actual control.

The performance of the current meter plays an important role in the proposed control method, since the controlled current adds up in the actuator. The important parameters of the current meter are not only the creep properties and the repeatability but also its range, since the current range practically limits the motion speed range.

The importance of the static model was demonstrated by using solely the motion model with trajectories consisting of stationary parts. The results were poor, as the drift was beyond any acceptable limits. This shows that the accuracy of the actuator model is very important at the proximity of the zero velocity. This can be ensured using the chosen model structure, where the motion and static part are independent.

VI. Summary and conclusion

A new control method has been presented. This method uses current to control the speed of a piezoelectric actuator but, since the relationship between current and speed is not linear over the entire actuator motion range, information about an actuator voltage is also utilized. Voltage along with desired velocity acts as an input to an actuator model consisting of a motion model and a static model. The output of the actuator model is current that is fed to the actuator in order to obtain the desired velocity.

As a hardware point of view, to enable driving of the desired current, the method requires (i) a high voltage current driver or (ii) a current meter, a voltage amplifier, and a controller, as was done in this work.

The proposed actuator model is straightforward to create requiring far less experiments than the previous models in this control category. The control algorithms are so simple that the control method could also be utilized in simpler control environments.

The method shows very good results: The hysteresis is less than 2 % and the drift about 1 % in experiments containing variable velocities and motion amplitudes in motion phases, and variable time periods in static phases. The results would therefore indicate that the motion of piezo actuators is a function of current and voltage; thus, history knowledge seems unnecessary in order to overcome the hysteresis and drift in sensorless control of piezoelectric actuators.

References

[1] P. Ge and M. Jouaneh, "Tracking control of a piezoceramic actuator," *IEEE Transactions on Control System Technology*, 4 (1996) 209 - 216.

[2] D. Croft, G. Shedd, and S. Devasia, "Creep, hysteresis, and vibration compensation for piezoactuators: Atomic force microscopy application," *Journal of Dynamic Systems Measurement and Control-Transactions of the ASME*, 123 (2001) 35-43.

[3] G. S. Choi, H.-S. Kim, and G. H. Choi, "A study on position control of piezoelectric actuators," *Proceedings of the IEEE International Symposium on Industrial Electronics*, Guimaraes, Portugal, pp. 851-855, July 1997.

[4] L. Chuntao and T. Yonghong, "A neural networks model for hysteresis nonlinearity," *Sensors and Actuators, A: Physical*, 112 (2004) 49-54.

[5] C. V. Newcomb and I. Flinn, "Improving the linearity of piezoelectric ceramic actuators," *Electronics Letters*, 18 (1982) 442-444.

[6] P. Ronkanen, P. Kallio, and H. N. Koivo, "Current control of piezoelectric actuators with power loss compensation," *IEEE/RSJ International Conference on Intelligent Robots and Systems (IROS)*, Lausanne, Switzerland, pp. 1948-1953, October 2002.

[7] P. Ronkanen, P. Kallio, Q. Zhou, and H. N. Koivo, "Current control of piezoelectric actuators with environmental compensation," *Micro.Tec 2003, 2nd VDE World Microtechnologies Congress*, Munich, Germany, pp. 323-328, October 2003.

[8] R. H. Comstock, "Charge Control of Piezoelectric Actuators to Reduce Hysteresis Effects," U.S. Patent 4,263,527, 1981.

[9] R. Perez, J. Agnus, J.-M. Breguet, N. Chaillet, H. Bleuler, and R. Clavel, "Characterisation and control of a 1DOF monolithic piezoactuator (MPA)," *Proceedings of SPIE Volume 4568: Microrobotics and Microassembly III*, Boston, USA, pp. 151-161, October 2001.

[10] K. Furutani, M. Urushibata, and N. Mohri, "Improvement of control method for piezoelectric actuator by combining induced charge feedback with inverse transfer function compensation," *Proceedings of the 1998 IEEE International Conference on Robotics & Automation*, Leuven, Belgium, pp. 1504- 1509, May 1998.

[11] J. S. R. Jang, C. T. Sun, and E. Mizutani, *Neuro-Fuzzy and Soft Computing: a Computational Approach to Learning and Machine Intelligence*, New Jersey: Prentice-Hall, 1997.

[12] M. Guan and W.-H. Liao, "Studies on the circuit models of piezoelectric ceramics," *Proceedings of 2004 International Conference on Information Acquisition*, Heifei, China, pp. 26-31, June 2004.

[13] P. Kallio and J. Kuncová-Kallio, "Capillary pressure microinjection of living adherent cells: Challenges in automation," *Journal of Micromechatronics*, 3 (2006) 189-220.

Pekka Ronkanen received the M.Sc. degree in electrical engineering from Tampere University of Technology, Tampere, Finland in 2002. He joined the Institute of Automation and Control at Tampere University of Technology in 2000 as a research assistant. Currently he is pursuing a Dr.Tech. degree in the Micro- and Nanosystems Research Group at the Institute. His main research interests are active materials and micromechatronics, their control issues and applications in biomedical engineering.

Pasi Kallio (M'03) received the M.S. degree in electrical engineering and the D.Tech. degree in automation from Tampere University of Technology, Tampere, Finland in 1994 and in 2002, respectively. He joined the Institute of Automation and Control at Tampere University of Technology in 1995. Currently he is a Senior Research Scientist and the head of the Micro- and Nanosystems Research Group at the Institute. His main research interests are active materials, microrobotics and microfluidics, and their application in the development of automatic systems for cell manipulation, cell cultivation and medical diagnostics.

Matti Vilkko (M'05) received his M.Sc. degree in electrical engineering in 1989, Lic.Tech degree in 1993 in electrical engineering and D.Tech degree in 1999 in automation engineering from Tampere University of Technology, Tampere, Finland. From 1989 to 1999 he was a researcher in Institute of Automation and Control (ACI), Tampere university of Technology. His research focused on scheduling and optimization of hydro- thermal power production. From 2000 to 2003 he had a research and development management positions in Patria Ailon Inc and Ailocom Inc. Currently he is a senior researcher in ACI. His current research interest is in the areas of modelling, simulation and system identification.

Heikki N. Koivo (S'67–M'71–SM'86) is a Professor of Control Engineering at Helsinki University of Technology (HUT). He received his BSEE degree from Purdue University, Indiana, the MS degree in Electrical Engineering and the Ph.D. degree in Control Sciences from University of Minnesota. Before joining HUT in 1995, he served in various academic positions at the University of Toronto and at Tampere University of Technology, Finland.

Dr. Koivo's research interests include study of complex systems, adaptive and learning control, mechatronics, microsystems and wireless communication systems. He has authored more than three hundred scientific publications. He has been the principal investigator in more than one hundred research projects. Dr. Koivo is a member of the Editorial Board of *Journal of Intelligent and Fuzzy Systems*, *Intelligent Automation and Soft Computing*, and *Journal of Systems and Control Engineering*. He was Associate Editor of IEEE TRANSACTIONS ON ROBOTICS AND AUTOMATION and member of the Administrative Council of the IEEE Robotics and Automation Society. He is a Fellow of the Finnish Academy of Technology.

III

Paper III

P. Ronkanen, P. Kallio, Q. Zhou, and H. N. Koivo, “Current control of piezoelectric actuators with environmental compensation,” *Micro.Tec 2003, 2nd VDE World Microtechnologies Congress*, Munich, Germany, pp. 323-328, October 2003.

Current Control of Piezoelectric Actuators with Environmental Compensation

Pekka Ronkanen[1], Pasi Kallio[1], Quan Zhou[2], Heikki Koivo[2], [1]Tampere University of Technology, [2]Helsinki University of Technology, Finland

Abstract

This paper introduces an environmental compensation method for a feedforward charge control scheme, which controls the displacement of a piezoelectric actuator by the amount of current fed to the actuator. The method uses an impedance model of the actuator to estimate the needed current and controls then the current in a closed loop using precise current measurement and a PID controller.

In the basic scheme, power losses occurring in the actuator are estimated and compensated for, but environment, load and self-heating effects are neglected. This paper extends the control scheme by introducing temperature and humidity compensation to the feedforward model.

The experiments with a piezoelectric bender show promising results. Compared to an open loop voltage control, hysteresis can be reduced from 30% down to 2-4% by power loss compensation in constant environmental conditions. In varying conditions, the performance reduces if the environmental effects are not compensated for. As an example, at 35°C 40% RH (relative humidity), the hysteresis can be reduced from 10 % to 5 % by introducing the environmental compensation into the feedforward charge control scheme. The more the environmental conditions vary, the greater is the improvement in performance.

1 Introduction

Piezoelectric actuators are widely used in applications that require high resolution and accuracy. Their favourable dynamic properties extend the application areas into high speed areas such as vibration control. However, large hysteresis, drift, temperature, self-heating and load effects decrease the open-loop positioning accuracy. If a high accuracy is required, these non-linearities have to be compensated for. The compensation is usually accomplished by means of four different control principles: feedforward voltage control, where non-linear models are typically used [1], [2], [3]; feedback voltage control, where various sensors are used; feedforward charge control, where the operating current is controlled [4], [5] and feedback charge control, where charge is measured and controlled [6], [7], [8].

Piezoelectric actuators are commonly controlled by using voltage as an input signal. The main benefit achieved using charge control is the reduction of hysteresis and drift. Experiments indicate that hysteresis is likely to be reduced at least to one fifth of the original [5], [6], [7]. The disadvantages include the need for additional electric circuits and thus, the increased complexity of the control hardware.

Charge control circuits can be divided into two groups: feedback and feedforward circuits. The first one utilizes feedback voltage charged to a capacitor in series with a piezoelectric actuator [6] and [7]. In another feedback method, the charge of subsidiary electrodes is measured and used in the feedback [8]. The electrodes are additional layers of the actuator, to which a charge proportional to internal charge is induced.

Current drives utilize feedforward control. A charge can be obtained by integrating a known current over a period of time. Constant current has been used over a variable period of time in [4] to obtain a certain displacement of a piezoelectric actuator but without taking into account power losses. The authors introduced in [5] a feedforward charge control method where any current may be used and the power losses are estimated and compensated for. The results were splendid; both hysteresis and drift reduced remarkably.

Temperature and humidity effects on piezoelectric actuators are relatively little studied; manufacturers have made some studies on how temperature affects e.g. the maximum displacement [9], the piezoelectric effect, and the thermal expansion of the ceramics [10]. The effects of temperature and humidity on the maximum displacement of a piezoelectric bender were reported in [11]. The displacement varied with both the temperature and the humidity.

This work concentrates on the compensation of the temperature and humidity effects in the proposed current control. In this paper, the proposed method is modified such that the effects of temperature and humidity changes are taken into account. Experiments are made in an environment controlled chamber introduced in [12].

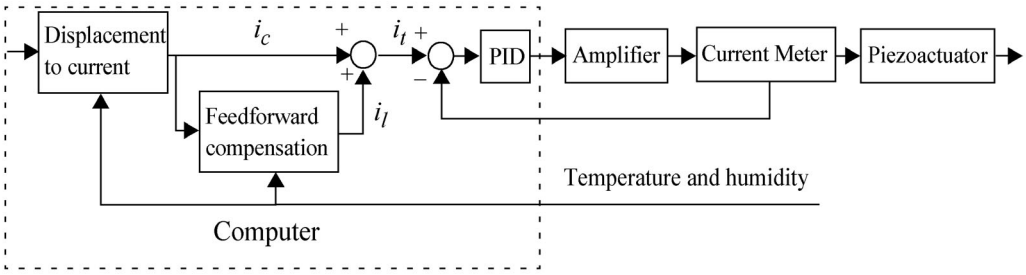

Fig. 1 Control setup for current control.

The paper is organized as follows. Section 2 presents the control principle and Section 3 the control setup. Section 4 discusses the environmental effects and their compensation. Section 5 presents the results of the work. Conclusions are drawn in the end of the paper.

2 Control Principle

The control principle was introduced in [5], where the relationship between the displacement, velocity and current was presented as follows:

$$i(t) = \frac{1}{a} \cdot \frac{d}{dt}\delta(t) = \frac{v(t)}{a} \quad , \tag{1}$$

where $\delta(t)$ is the displacement, a is a constant, $i(t)$ is the current and $v(t)$ is the velocity.
Since part of the current is consumed by power losses, it is divided into two components: $i_c(t)$ charges the actuator, and $i_l(t)$ compensates for the power losses. Thus, the total current $i_t(t)$ is as already presented in the earlier work:

$$i_t(t) = i_c(t) + i_l(t) \quad , \tag{2}$$

The compensation current $i_l(t)$ is determined based on the voltage $V(t)$ over the actuator and a dynamic impedance model $X(i_c)$, which is a function of the charging current $i_c(t)$.

$$i_l(t) = \frac{V(t)}{X(i_c)} \tag{3}$$

In [5], the dynamic impedance model was determined experimentally to describe the power losses but environment effects were neglected. Figure 2 presents the impedance with respect to the charging current $i_c(t)$. In this paper, a small modification has been made to the impedance model (compared with [5]) to improve the performance on higher currents.

To compensate for environment effects, we assume the parameter a in Equation (1) and the impedance model $X(i_c)$ in Equation (3) to be temperature and humidity dependant factors $a(T,H)$ and $X(i_c,T,H)$. Temperature and humidity dependence will be discussed in Section 4 in more details.

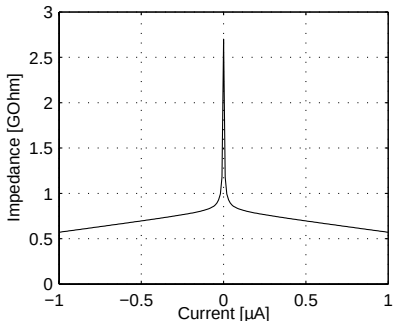

Fig. 2 Charging current – impedance relation.

3 Control Setup

The hardware components used in the control scheme are a regular piezo amplifier, a sensitive current meter with a voltage output and a computer with a data acquisition system. The current meter used was a 160B Digital Multimeter by Keithley Instruments (USA). The maximum resolution of this device is 10 pA. The control setup including hardware and software components is shown in Figure 1.

The *displacement* to *current* and the *feedforward compensation* blocks are the actual targets of interest in this work. The displacement to current block converts the displacement to the current (Equation (1)). The feedforward compensation block compensates for the power losses that occur in the actuator (Equation (3)). The feedback loop in Figure 1 is required to assure that the desired current is driven into the actuator using a regular voltage amplifier.

The actuator used in the experiment was a piezoelectric bender NB 40x10x0.6-21 by Tokin (Japan).

4 Environmental Compensation

The internal impedance model presented [5] can be written with a small modification in such a way, that the previous constants will become the functions of temperature and humidity:

$$X(i_c,T,H)=\left(\frac{1-b(T,H)}{\sqrt{(c(T,H)\cdot i_c(t))^2+1}}\right. \quad (4)$$
$$+\left(1+s(T,H)\cdot|i_c(t)|\right)\cdot b(T,H)\Big)$$
$$\cdot R(T,H)$$

where $b(T,H)$, $c(T,H)$ and $s(T,H)$ are factors describing how the impedance varies with the charging current. Parameters $b(T,H)$ and $s(T,H)$ describe the relation at higher currents and $c(T,H)$ at lower currents. $R(T,H)$ is the static impedance.

The effects of temperature and humidity on the internal impedance $X(i_c,T,H)$ and the actuation velocity parameter $a(T,H)$ were studied in six different environmental conditions; 10°C 30% RH (relative humidity), 25°C 5% RH, 25°C 30% RH, 25°C 55% RH, 25°C 80% RH and 40°C 30% RH. When the humidity rose to 80%, the behaviour of the actuator changed drastically and the testing with the same setup was out of question. In other conditions, static and dynamic impedance values were found experimentally by the trial and error method described in [5]. The impedance values (in GΩ) with 5 different currents in the 5 environment conditions are given in a table below.

Temp Hum	Stat Imp	60nA Imp.	100nA Imp.	180nA Imp.	250nA Imp.
10°C 30%	4	1.2	1.3	1.2	1.2
25°C 5%	3	0.9	1	1.1	1.1
25°C 30%	2	0.8	0.9	0.9	0.9
25°C 55%	3	0.8	1	1	1
40°C 30%	1.2	0.5	0.6	0.5	0.5

The impedance change with respect to humidity change was rather small, until the humidity reached 80% and the behaviour of the actuator changed drastically. However, the effect of the temperature change can be seen clearly, since the impedance is many times greater at 10°C than at 40°C. As can be seen in Figure 3, the relation is quite linear.

The relation between the temperature and the static impedance at 30% of relative humidity is as follows

$$R=-0.09\,G\Omega/_{\circ C}\cdot T+4.7G\Omega \quad (5)$$

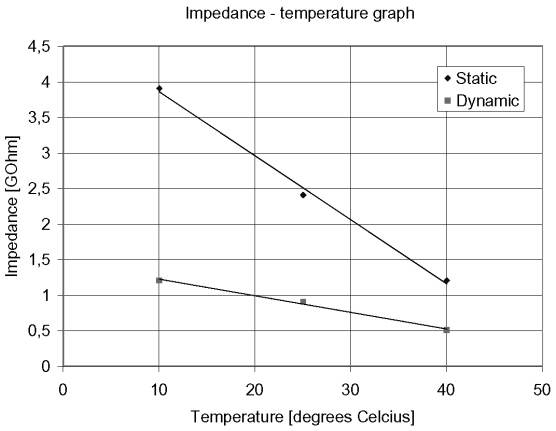

Fig. 3 Impedance with respect to temperature.

The effect of humidity is rather small, therefore $R(T,H)$ is basically described by Equation (5). The results in the table are rounded and therefore, the effect of humidity appears greater than it actually is.

Temperature dependency of the parameter $b(T,H)$ is presented in Figure (4) and Equation (6) describes the trend line.

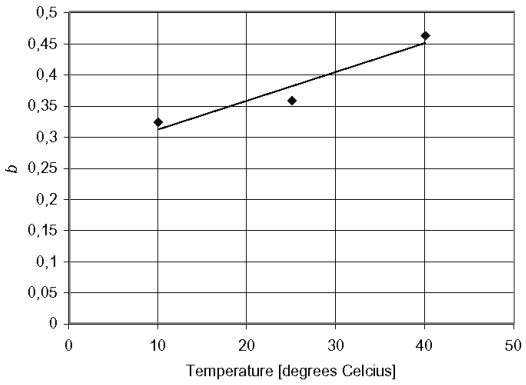

Fig. 4 Change of parameter b with respect to temperature.

$$b(T)=0.27+0.004\cdot T \quad (6)$$

According to the measurements, the parameters $s(T,H)$ and $c(T,H)$ are constants in the studied temperature and humidity range.

By combining the parameter equations with Equation (4), we obtain

$$X(i_c,T,H)=\left(\frac{1-(0.27+0.004\cdot T)}{\sqrt{(1e^{10}\cdot i_c(t))^2+1}}\right. \quad (7)$$
$$+\left(1+1e^{4}\cdot|i_c(t)|\right)\cdot(0.27+0.004\cdot T)\Big)$$
$$\cdot\left(4.7G\Omega-0.09\,G\Omega/_{\circ C}\cdot T\right)$$

Equation (7) will then be used together with Equations (1)-(3) to compensate for power losses. The valid temperature range for the models is 10-40°C and humidity level below 60%.

The velocity parameter $a(T,H)$ can be considered constant at the studied temperatures and levels of humidity. At 40°C the velocity decreases some percents. Based on measurement data, the value of 0.03µm/s/nA will be used as the value of the actuation velocity parameter a. The voltage over the actuator $V(t)$ is estimated with an integral of the charging current $i_c(t)$ and the actuator capacitance, as in [5].

5 Results and Discussion

The developed model was tested in three different environmental conditions; 15°C 10% RH, 20°C 50% RH and 35°C 40% RH. The same trajectories were run with and without environment compensation in all conditions to validate the compensation model. The reference test uses power loss compensation and environment parameters set to room conditions (25°C 30% RH).

A decaying displacement ramp curve was used for the hysteresis analysis and a drift test. The decaying ramp curve has three ramps where the displacement decreases 50% from the previous one. The first ramp has amplitude of 200 µm, while the amplitude of the third ramp is 50 µm. The time used for each ramp remains constant.

At 20°C 50% RH, the difference by environmental compensation in comparison to the uncompensated case is relatively small, which is quite natural considering the temperature difference. At 15°C 10% RH and at 35°C 40%, RH the difference is more obvious.

Figure 5 presents the decaying ramp curve at 35°C 40% RH. The solid line presents the required trajectory, dash-dot line the displacement with compensation, and the dotted line without compensation. Figure 6 presents the corresponding hysteresis.

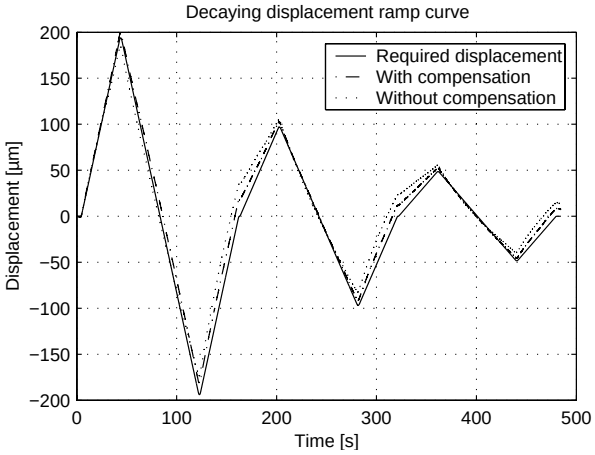

Fig. 5 Decaying ramp curve at 35°C 40% RH.

The hysteresis reduces from 10% to 5% with environmental compensation. The improvement at 15°C 10% RH is quite similar; the hysteresis is about half of the uncompensated case. At 20°C 50% RH the hysteresis is similar in both compensated and uncompensated cases; less than 4% of the full displacement.

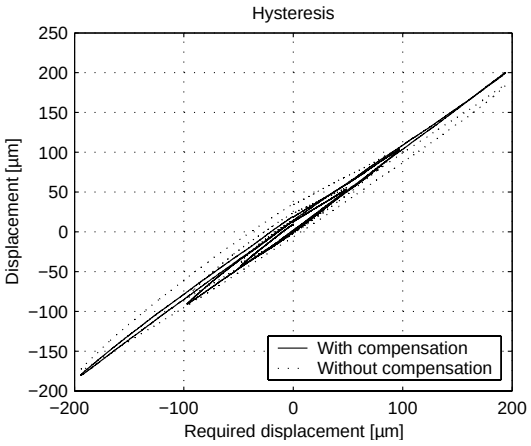

Fig. 6 Hysteresis of the decaying ramp curve driven at 35°C 40% RH.

In the drift test, the actuator is first driven with a constant speed for 40 seconds and then attempted to keep in its position for 100s.

Figure 7 presents drift at 35°C 40% RH. As can be seen, without the compensation the displacement does not reach the required displacement and in the end is 25 µm below the desired displacement. With compensation, the displacement overshoots, but later follows the required trajectory as desired. Further studies on overshooting would be in place, mechanical properties of the actuator are the most probable cause for this.

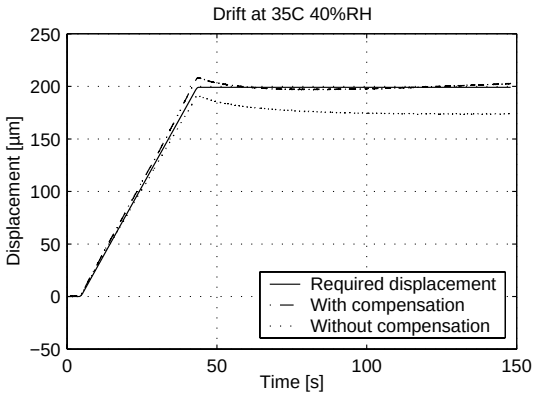

Fig. 7 Drift at 35°C 40% RH.

At 15°C 10% RH, the uncompensated test results are nearly 20 µm above the desired trajectory, while the results with compensation are within a couple of micrometers. At 20°C 50% RH, the drift results with and without compensation are close to each other: the compensated case is slightly below the required

trajectory and the uncompensated is slightly above the desired displacement, Figure 8.

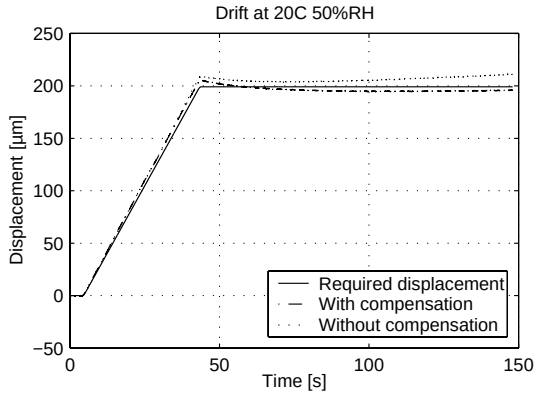

Fig. 8 Drift at 20°C 50% RH.

The environmental compensation improved the performance of the actuator compared to the uncompensated case. However, there was an as yet unidentified source of uncertainty in the test setup that was decreasing the repeatability and thus decreasing the accuracy of the model. This can result from (i) the inaccuracy in the estimated voltage, (ii) actuator wear out or (iii) inaccuracies in the measurement system; (laser displacement meter, current meter or the data acquisition system). When this problem is solved, the results should improve still with a more accurate model.

6 Conclusion

Environmental compensation for the current control method of piezoelectric actuators was developed by experimentally studying how power losses vary in different environmental conditions. This was then modeled and compensated for with an additional current. The method improves the actuator performance. By using power loss compensation in constant temperature, the hysteresis is reduced from approximately 30% to 2-4%. When the method is used in changing environment conditions, performance reduces. For example in 35°C 40% RH the hysteresis is 10%. By introducing environment compensation, the hysteresis decreases to 5%. The further the conditions vary from normal office conditions, the better the results are. Similar results were obtained in drift tests.

To summarize the results from the piezo actuator point of view, the power losses increase when the temperature increases. The effect of humidity is smaller, until a high level of humidity is reached.

Future work includes implementing the compensation for self heating and load effects, as well as improving repeatability and studying current control with several different actuator types and actuators.

7 References

[1] Ge, P. & Jouaneh M. 1996. Tracking Control of a Piezoceramic Actuator. IEEE Transactions on Control Systems Technology, Vol. 4, No. 3, May.

[2] Croft, D., Shedd, G. & Devasia, S. 2000. Creep, Hysteresis, and Vibration Compensation for Piezoactuators: Atomic Force Microscopy Application. Proceedings of the American Control Conference, Chicago, Illinois, June 2000.

[3] Choi, G. S., Kim, H.-S. & Choi, G. H. 1997. A Study on Position Control of Piezoelectric Actuators. Proceedings of the IEEE International Symposium on Industrial Electronics, Guimaraes, Portugal, July 7-11, 1997. Vol. 3.

[4] Newcomb, C. V. & Flinn, I. 1982. Improving the Linearity of Piezoelectric Ceramic Actuators. Electronics Letters, Vol. 18, No. 11, May.

[5] Ronkanen, P., Kallio, P. & Koivo, H. Current Control of Piezoelectric Actuators with Power Loss Compensation. 2002 IEEE/RSJ International Conference on Intelligent Robots and Systems, IROS'02. Lausanne, Switzerland, October 2002.

[6] Comstock, R. H. 1981. Charge Control of Piezoelectric Actuators to Reduce Hysteresis Effects. U.S. Patent 4,263,527.

[7] Perez, R., Agnus, J., Breguet, J.-M., Chaillet, N., Bleuler, H. & Clavel, R. 2001. Characterisation and Control of a 1DOF Monolithic Piezoactuator (MPA). Proceedings of SPIE Volume 4568: Microrobotics and Microassembly III, Boston, USA, October 2001.

[8] Furutani, K., Urushibata, M. & Mohri, N. 1998. Improvement of Control Method for Piezoelectric Actuator by Combining Induced Charge Feedback with Inverse Transfer Function Compensation. Proceedings of the 1998 IEEE International Conference on Robotics & Automation, Leuven, Belgium, May 1998.

[9] APC International Ltd. *Guidance for Designing Mechanisms Using Servocell*. http://www.americanpiezo.com/servocell/design.html. 10.7.2003.

[10] Physik Instrumente (PI) GmbH & Co. *Temperature Effects*. http://www.physikinstrumente.de/products/prdetail.php?secid=4-38. 10.7.2003.

[11] Zhou, Q., Corral, C., Esteban, P., Albut, A. & Koivo, H. *Environmental Influence on Microassembly*. IEEE/RSJ International Conference on Intelligent Robots and Systems, IROS'02. Lausanne, Switzerland, October 2002.

[12] Zhou, Q., Albut, A., Corral, C., Esteban, P., Kallio, P., Chang, B. & Koivo, H. *A Microassembly Station with Controlled Environment*. Microrobotics and Microassembly III, Bradley J. Nelson, Jean-Marc Breguet, Editors, Proceedings of SPIE Vol. 4568, pp. 252 - 260, Boston, USA, 2001.

Paper IV

IV

P. Ronkanen, P. Kallio, and H. N. Koivo, “Simultaneous actuation and force estimation using piezoelectric actuators,” *IEEE International Conference on Mechatronics and Automation (ICMA)*, Harbin, China, pp. 3261-3265, August 2007.

Proceedings of the 2007 IEEE
International Conference on Mechatronics and Automation
August 5 - 8, 2007, Harbin, China

Simultaneous Actuation and Force Estimation Using Piezoelectric Actuators

Pekka Ronkanen, Pasi Kallio
Tampere University of Technology
Tampere, Finland
{Pekka.Ronkanen & Pasi.Kallio}@tut.fi

Heikki N. Koivo
Helsinki University of Technology
Helsinki, Finland
Heikki.Koivo@hut.fi

***Abstract*—This paper introduces a force estimation method that enables simultaneous actuation and force estimation using piezoelectric actuators. The method combines an actuator input voltage and a current together with a displacement measurement to a force estimator. The force estimator contains a nonlinear actuator model to approximate the present external force without the use of force sensors. The measured displacement can simultaneously be utilized in feedback control to enable precise microrobotic operations.**

The results show that the method enables estimation of both static and varying forces under simultaneous position feedback control. Experimented displacement trajectories contain both stationary and mobile phases. The achieved accuracy in force estimation according to experiments is better than 10% of the full force scale. Therefore force sensing without the use of separate force sensors is feasible, which opens new applications for force sensing in microrobotics.

***Index terms*—Piezo actuator; force sensing; sensorless; simultaneous actuation; current.**

I. INTRODUCTION

Micromanipulation techniques are widely used in research of several fields. Common for the majority of the cases is the required operator. For the micromanipulation techniques to be exploited in high volumes in areas such as industrial and biological applications, the role of the operator should be reduced to minimum. This can be achieved by increasing the automation level [1].

Previously the research has focused on the development of microrobots, -manipulators and tools. This has led to a situation, where the performance of the devices and tools would support fully automated systems, but the knowledge about the target is inadequate. Therefore, the research trend has recently shifted towards techniques, that gather more knowlegde about the objects to be manipulated and about the operating environment. These techniques include machine vision and various sensor developments, such as force sensors. These are not competitive techniques, but rather complimentary.

Contact sensing is one of the most important actions for example in pick and place from an operational point of view. The most generic method to sense this event is the application of force sensors. Many other methods are based on certain target properties, such as on conductivity. Also in biological applications such as in manipulation tasks related to cell cultivation and microdissection of tissues, force and contact sensing are required to enable full automation.

There are various methods to measure forces; many of the most suitable methods for micromanipulation are listed in review articles such as [2] and [3]. These methods include strain gauges, use of piezoresistive, piezoelectric and piezomagnetic effects, capacitive sensors and optical sensors [2], [3]. Perhaps the most convenient of these methods are the ones based on the piezoelectric effect, since it enables simultaneous sensing and actuation. This simplifies the mechanisms and enables further miniaturizing of the system in comparison to a setup with a separate actuator and force sensor.

Using piezoelectric materials for actuation is very common in microrobotics. This is due to their high resolution and favorable dynamic properties. However, large hysteresis, drift, temperature, self-heating and load effects decrease the open-loop positioning accuracy. Therefore, typically one of the following control methods is used to increase the positioning accuracy: feedforward voltage control, feedback voltage control, feedforward charge control and feedback charge control.

Simultaneous sensing and actuation using piezoelectric materials is not as rare as one could imagine; the mass quartz balance is perhaps the best example of this. The mass quartz balance is vibrating and a shift in the resonance amplitude is measured and this is proportional to the measured mass. Other examples can be found, where piezoceramics is actuated by ac voltage for sensing purposes, such as [4] and [5]. This sensing method gives good results when masses or other mechanical properties of objects are needed to be measured. For a more general use in microrobotics this method cannot be utilized, since it requires a certain motion to be generated for the measurement. In microrobotics, the motion trajectories can not be specified in advance and they can have some static positions as well.

Another approach is proposed in [6], where a sliding-mode based force control method is presented. It is based on a non-linear electromechanical model of the actuator and a displacement measurement using strain gauges. Force is estimated using the actuator input voltage, the output

displacement and the non-linear actuator model. The difference between the model output and the real displacement is used to approximate the external force. The obtained results are quite good, but as the paper points out, any inaccuracy in the model will cause errors in the force estimation.

It has been shown that the input current and voltage knowledge contain sufficient information to predict the displacement of a piezoelectric actuator in the absence of external forces [7].

The goal of this work is to study the feasibility of utilizing current measurement in the external force estimation.

The rest of the paper is organized as follows; Section II presents the force estimation method and Section III describes the experiment setup. Results are presented in Section IV. Conclusion is at the end of the paper in Section V.

II. Force Estimation Method

This section presents the proposed force estimation model. The model should estimate the external force without any force measurement.

From [8] we can derive that the displacement of a piezoelectic actuator can be described as a function of current and voltage:

$$d(t) = f(i(t), V(t)), \quad (1)$$

where $d(t)$ is displacement of the actuator, $i(t)$ current and $V(t)$ voltage. This applies when the external force is constant.

Linear dynamic system can be modeled by a two-port model [9], as presented in Fig. 1.

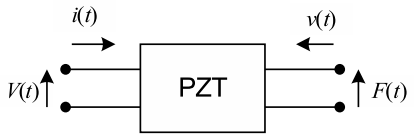

Fig. 1: Two-port model of piezoelectric actuator. F(t) presents the force and v(t) the actuator velocity. Redrawn from [9].

The two-port model together with the general knowledge about the load effect on piezoactuators suggests to include the force $F(t)$ in (1):

$$d(t) = f(i(t), V(t), F(t)) \quad (2)$$

Solving for $F(t)$ gives:

$$F(t) = g(i(t), V(t), d(t)) \quad (3)$$

This would suggest that by measuring the actuator input current and voltage, and the resulting displacement, the force could be estimated. This could be done simultaneously with a traditional position control of the actuator. Fig. 2 presents the block diagram of the proposed force estimation method.

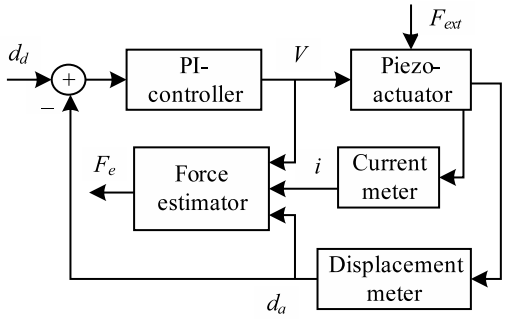

Fig. 2: Block diagram of the proposed force estimation method.

In the figure, d_d and d_a present the desired and actual displacements. V presents the voltage and i the current. F_{ext} presents the external force and F_e the estimated force.

The displacement can be measured in various ways. Strain gauges are perhaps the most popular in many applications, but other sensors such as capacitive, optical and Hall sensors can be used as well.

A. Force estimator

This section discusses the force estimation model. The model has three inputs: voltage V, current i and actuator displacement d, and one output, external force F.

In order to minimize the manual labor in the force estimator creation, a modeling method which is supported by software tools should be selected. One of this type of well established methods is neural networks [10]; powerful tools for creating and training neural networks exist in commercial softwares.

Training data is obtained by driving the trajectory presented in Fig. 3 with several different static loads: 0 N, 34 mN, 61 mN and 90 mN.

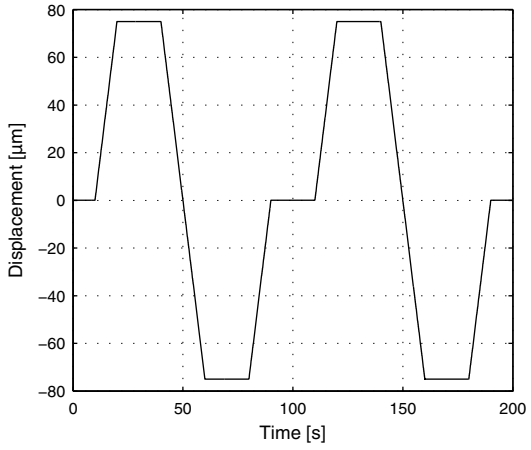

Fig. 3: Displacement trajectory for obtaining the training data.

A 10*1 feedforward backpropagation network is chosen for the force estimation model. Fig. 4 combines the trajectories driven with different loads to the same figure. The figure presents actual loads and training results: continuous line

presents the actual load and the dashed line the force estimation of the model.

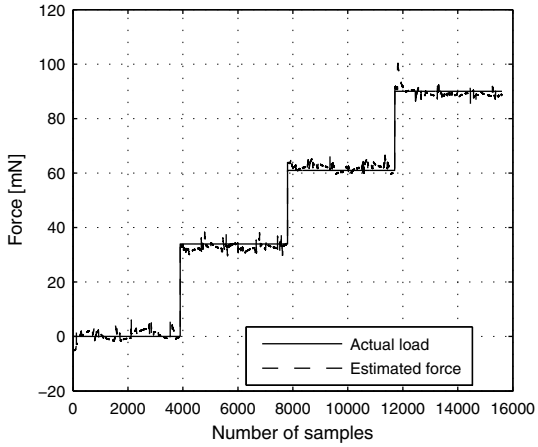

Fig. 4: Training results, continuous line presents the actual load and the dashed line the force estimation.

III. Description of the Experiment

This section describes the control implementation and the experiment setup. The implementation of the force estimation requires control software, a data-acquisition board with analog inputs and outputs, a voltage amplifier (Piezo Systems EPA 102), a current meter (Keithley 160B), a displacement meter and a piezo actuator. Data-acquisition is performed with a National Instruments AD-board (PCI-6052E). The position of the piezoelectric actuator is measured with a laser displacement meter (Mel Mikroelektronik M5L/0,5). The piezo actuator used in the experiments is a bimorph bender NB38*4*0.6 from Tokin.

The control software is implemented using Matlab, with a real-time xPC Target toolbox. The displacement of the piezo actuator was controlled using a PI controller, with a gain of 0.1 and integrator gain of 3. Control frequency used is 2 kHz.

The external force is produced in two ways: (i) by attaching lead weights on to the actuator and (ii) using a plastic cantilever that acts as a spring type of load. Lead weights produce constant force on the actuator, while the force generated by the cantilever is displacement dependent, as is described by the spring force equation:

$$F_{spring} = -k \cdot x, \tag{4}$$

where F_{spring} is the force generated by the spring, k the spring constant and x the distance by which the spring is elongated.

Fig. 5 presents the measurement setup. In the figure, a plastic cantilever pushes the piezoelectric bender downwards. The cross sectional dimensions of the plastic cantilever are 7.5 mm x 1.0 mm and the bending length is 23 mm.

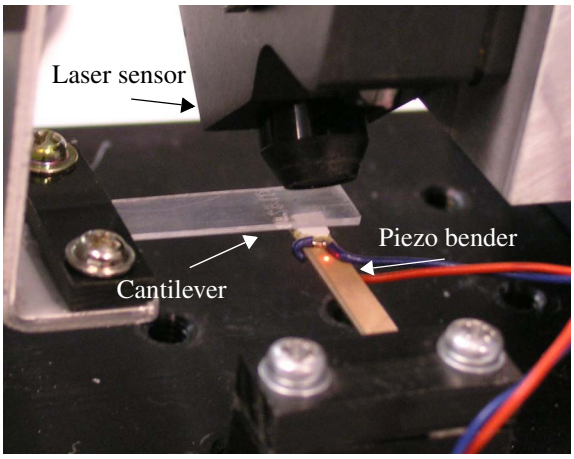

Fig. 5: Measurement setup.

IV. Results

This section presents the experimental results of the force estimator. All experiments are carried out five times and the results in this section present typical results.

The trajectory shown in Fig. 3 is driven with the following static loads: 0 N, 22 mN, 47 mN and 77 mN. These are combined in the same figure as was done in Section 2 by presenting only actual loads and the corresponding estimated forces, Fig. 6.

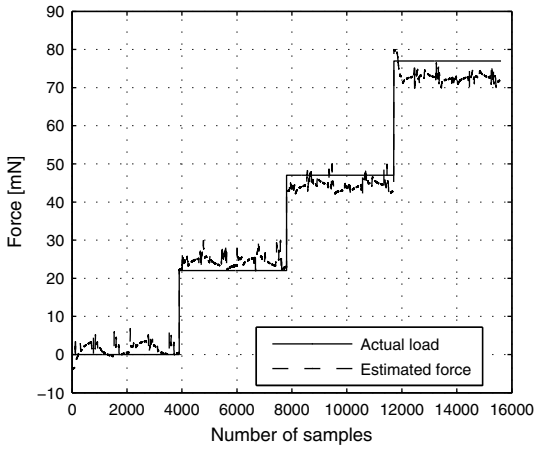

Fig. 6: Results of static force measurements.

The force estimation gives relatively good approximation of the actual force. Some variation, however, occurs during different phases of the trajectory. Some offset is also present in the estimated forces. With the three lightest loads, the offset is 2 - 3 mN, but with the heaviest load the offset is slightly over 4 mN. The average absolute value of the error between the actual load and the estimated force is 2.8 mN and also the median error is very close to this (2.83 mN). The maximum error during the experiments is slightly below 8 mN. The applicable force range of the estimator is in minimum 0 - 90 mN, which is the range of the loads used for the training. This, in

combination with the maximum error of 8 mN, results in a total estimation accuracy better than 9% of the full scale.

The same trajectory is driven against the plastic cantilever to test how the force estimator follows a varying force. Results of this experiment are presented in Fig. 7, continuous line presenting the displacement of the actuator and the dashed line the estimated force. Unfortunately, the actual force is unknown in this experiment and therefore, only qualitative validation is possible. The results show that the shape of the estimated force is as it should be for a spring type of force. This indicates that the force estimator can follow varying loads.

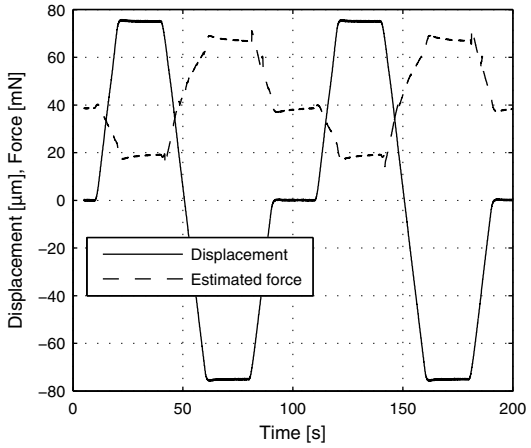

Fig. 7: The piezoactuator driven against a plastic cantilever.

To obtain a rough estimate on the shape of the actual force in this experiment, a fitted curve is created. This curve is based on (4), to which an offset is added. The spring constant and the offset are approximated by finding a best fit so that the measured actuator displacement would be the spring elongation distance and the estimated force would be the spring force. Since the values of the fitted curve are as close to the force values of the estimator as possible, quantitative conclusion cannot be made. However, the shape of the curve should be accurate to some extent, with an assumption that the deformation of the plastic cantilever is fully reversible and thus the force follows the spring force equation. The fitted values for the spring constant k and for the offset are 0.33 mN/µm and 42 mN.

The comparison between the fitted curve and the estimated force indicates the existence of both hysteresis and drift in the force estimator, Fig. 8.

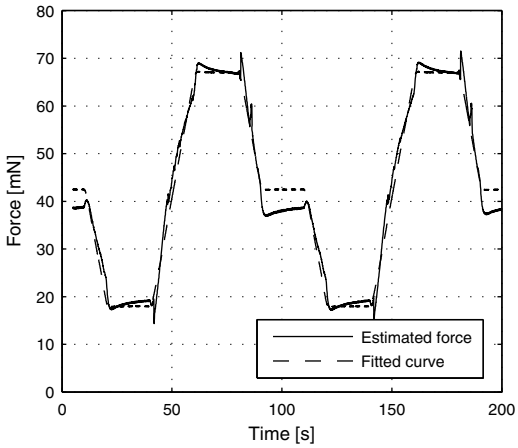

Fig. 8: Estimated force and a fitted spring force curve.

V. Conclusion

The proposed force estimation method is able to estimate both static and varying external forces with relatively good accuracy. The obtained accuracy is better than 10% of the full scale. This is not as good as the performance of separate force sensors, but adequate in many microrobotic tasks. The main benefits of the sensorless force estimation method proposed here are: (i) the simplification and (ii) enabling further miniaturization of the mechanics compared with the systems with separate force sensors, and (iii) enabling force sensing in applications where it has been unattainable before.

Applications, where sensorless force sensing could be utilized, include contact and force sensing in grippers and manipulators, pressure estimation and medium detection in piezoelectric valves and pumps, and force controlled clamps.

Future work includes improving the force estimation model in order to reduce the remaining hysteresis and drift in the system.

References

[1] P. Kallio, and J. Kuncová-Kallio, Capillary Pressure Microinjection of Living Adherent Cells: Challenges in Automation, Journal of Micromechatronics, 3 (2006) 189-220.

[2] S. Fahlbusch and S. Fatikow, Force Sensing in Microrobotics Systems - an Overview, IEEE International Conference on Electronics, Circuits and Systems, 7-10 Sept. 1998, pp 259 - 262 vol.3.

[3] Z. Lu, P. C. Y. Chen and W. Lin, Force Sensing and Control in Micromanipulation, IEEE Transactions on Systems, Man, and Cybernetics—part C: Applications and Reviews, 36 (2006) 713-724.

[4] L. Xu, S.-F. Ling, B. Lu, H. Li and H. Hu. Sensing capability of a PZT-driven cantilever actuator. Sensors and Actuators A 127 (2006) 1–8.

[5] C. Lee, T. Itoh and T. Suga, Self-excited piezoelectric PZT microcantilevers for dynamic SFM—with inherent sensing and actuating capabilities. Sensors and Actuators A 72 (1999) 179–188.

[6] K. Abidi, A. Sabanovic and S. Yesilyurt, Sliding-mode based force control of a piezoelectric actuator, Proceedings of the IEEE International Conference on Mechatronics, 2004. ICM '04. 3-5 June 2004, pp. 104 - 108.

[7] P. Ronkanen, P. Kallio, M. Vilkko and H.N. Koivo. Current Control of Piezoelectric Actuators Using a Two Component Actuator Model with

Voltage Feedback in State Estimation. Submitted to Sensors and Actuators A.

[8] P. Ronkanen, P. Kallio and H. Koivo, Current Control of Piezoelectric Actuators with Power Loss Compensation, IEEE/RSJ International Conference on Intelligent Robots and Systems (IROS), Lausanne, Switzerland, October 2002, pp. 1948-1953.

[9] J. L. Pons, Emerging Actuator Technologies – A micromechatronics Approach, Ed J.Wiley, 2005.

[10] J. S. R. Jang, C. T. Sun and E. Mizutani, Neuro-Fuzzy and Soft Computing: a Computational Approach to Learning and Machine Intelligence, Prentice-Hall, New Jersey, 1997.

Paper V

P. Ronkanen, P. Kallio, M. Vilkko, and H. N. Koivo, “Self heating of piezoelectric actuators: measurement and compensation,” *IEEE International Symposium on Micro-Nanomechatronics and Human Science (MHS)*, Nagoya, Japan, pp. 313-318, November 2004.

V

Self Heating of Piezoelectric Actuators: Measurement and Compensation

Pekka Ronkanen[1], Pasi Kallio[1], Matti Vilkko[1] & Heikki N. Koivo[2]

[1]Tampere University of Technology, Institute of Automation and Control
Korkeakoulunkatu 3, 33720 Tampere, Finland
[2]Helsinki University of Technology, Control Engineering Laboratory
Otaniementie 17, 02150 Espoo, Finland

***Abstract*–This paper introduces the effect of self heating on the displacement of piezoelectric actuators and a novel method to quantify self heating. Issues influencing self heating include; the frequency and the amplitude of the driving voltage, and the size, or more specifically the volume-area ratio of the actuator and they are also discussed. The effect of a load on the heat generation is studied. According to the experiments, the peak-to-peak value of the consumed current is a good indication of the temperature rise of the actuator. This can be used for the protection of the actuator from overheating, or as the authors will propose in the paper, it can be used to compensate for the changes in the displacement induced by the self heating. The displacement error of the heated actuator reduces in average down to one part in three when the proposed compensation is used.**

1. INTRODUCTION

Piezoelectric actuators are widely used in applications requiring high resolution and accuracy. Their favorable dynamic properties extend the application areas into high speed areas such as vibration control. However, large hysteresis, drift, self heating and load effects decrease the open-loop positioning accuracy. If a high accuracy is required, these non-linearities have to be compensated for. The compensation is usually accomplished by means of four different control principles: *feedforward voltage control*, where non-linear models are typically used [1], [2], [3]; *feedback voltage control*, where various sensors are used; *feedforward charge control*, where the operating current is controlled [4], [5] and *feedback charge control*, where charge is measured and controlled [6], [7], [8].

Driving piezoelectric actuators with fast periodic control signals causes intrinsic heat generation in the piezoelectric elements. The increased temperature causes inaccuracy in operation of the piezoelectric actuators due to heat expansion and variation of the characteristics of the element as a function of the temperature, and it can even cause destruction of the element itself.

When a piezoelectric actuator is under a varying electric field, the actuator heats until a steady-state is reached. In the steady-state, the heat generation and the radiation are at the same level [9], [10], [11], [12].

It is suggested that dielectric losses are the main reason for self heating [10], [11], [12], [13]. The heat generation appears to be proportional to the driving frequency and to the square of the amplitude of the driving voltage [12], [13]. Since the actuator produces heat in the entire volume and dissipates it through the surface area, it seems quite obvious that the heat generation is proportional to the volume/area of the actuator [10].

Temperature has an influence on the output of piezoelectric actuators [14]. The outside temperature is rather simple to measure, but intrinsic heat generation requires a sensor attached to the actuator. In some applications, this might be difficult to accomplish.

The goals of this paper are to (i) experimentally study the different aspects affecting self heating; (ii) demonstrate the effect of self heating on the displacement; (iii) provide a novel method for determining the state of self heating in the actuator without temperature measurement and (iv) to provide a method for the compensation of the displacement error of the actuator caused by the heat generation.

Previously issues influencing self heating of piezoelectric actuators have been studied. The contribution of this paper is to provide methods for the quantification of self heating and the compensation of its effects.

A detailed description of the stack actuators used in the paper will be given in the end of the paper in Table 3 and they will be referred in the text as Piezo 1, Piezo 2 and Piezo 3.

The rest of the paper is organized as follows. Section 2 presents the effect of the driving frequency on self heating. In Section 3, the relationship between the driving voltage and self heating is introduced. Section 4 presents the effect of a load on the heat generation. Section 5 discusses the influence of the actuator size on self heating. In Section 6, the effect of self heating on the displacement is studied. Section 7 introduces the relationship between self heating and driving current. Advantage of this is taken in Section 8, where a compensation method for the displacement variations is presented. Section 9 presents some application areas for the proposed methods. Conclusions are drawn at the end of the paper.

2. Effect of Driving Frequency

The effect of the driving frequency was determined by driving the actuators with different frequencies and a constant amplitude of 200 V. In the experiments, the temperature of the actuators was measured. Figure 1 shows the rise in the temperature as a function of the driving frequency.

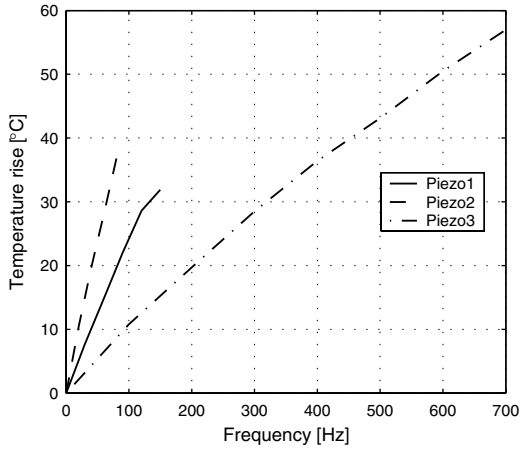

Figure 1: The effect of the driving frequency on self heating.

The heating is proportional to the frequency in all three piezos, as was demonstrated in [12] and [13]. The small decay with Piezo 1 at 150 Hz is caused by the lack of the current driving capability of the piezo amplifier in use.

3. Effect of Driving Voltage

The effect of the amplitude of the driving voltage was evaluated similarly to the frequency test. Now the three actuators were driven with different amplitudes and the actuator temperatures were measured. The frequencies for the actuators were 120 Hz for Piezo 1, 80 Hz for Piezo 2 and 700 Hz for Piezo 3. Figure 2 presents the temperature increase as a function of the driving voltage.

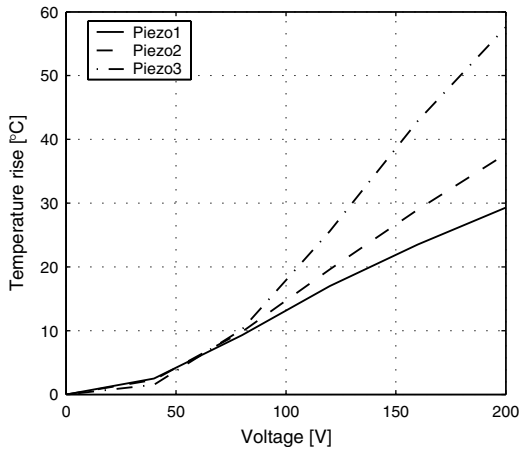

Figure 2: The effect of the driving voltage on self heating.

The results of Piezo 3 resemble most the earlier results presented in [10] and [11], where the heat generation is proportional to the square of the driving voltage. Piezo 1 and Piezo 2, however do not follow the relationship as precisely, and their temperatures remain lower at high voltages than would be expected.

4. Effect of Load

The effect of a load on self heating was tested by measuring the heat generation of Piezo 1 with and without a 100 N spring load (the blocking force of the actuator is stated to be 1500 N). The driving conditions were 200 V / 100 Hz. Figure 3 presents self heating with (dotted lines) and without (dashed lines) the load.

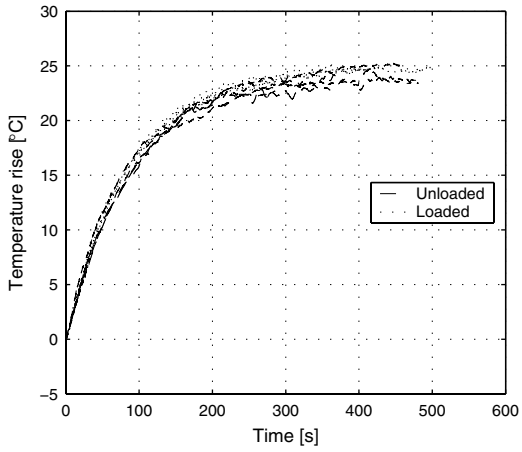

Figure 3: The effect of a load on self heating.

There is a small difference in the steady-state temperature. The temperature rises slightly higher with the load, but the difference is very small. The test was repeated with a 150 N spring load and the result was the opposite: the unloaded actuator heated slightly more than the loaded.

These tests indicate that at least a light loading of the actuator does not increase self heating remarkably. The loads were quite small in comparison to the blocking force of the actuator, and the results might be different with larger loads. It is also noticeable that no feedback was used in the testing. Therefore, the displacement under a load was smaller because of the load. If the displacements were kept constant, the electric field should have been higher in the load cases leading to a greater heat generation.

5. Effect of Size

The three actuators, two (Piezo 1 and Piezo 2) of which are made out of the same material, were driven with the same frequency and voltage (200 V / 80 Hz). Figure 4 presents the results.

The continuous line presents the temperature rise of Piezo 1, the dashed line Piezo 2 and the dash-dot line Piezo 3. Piezo 3 is composed of different material (even though it is soft and it

has high dielectric constant similar to the material of Piezo 1 and Piezo 2, see the end of the paper) and its layer thickness can differ from the other two and therefore, its results cannot be directly compared with the others. It is, however, clear that a large actuator gets more heated than a small one. Due to the scaling effect, the volume/area ratio decreases, when the dimensions are scaled down.

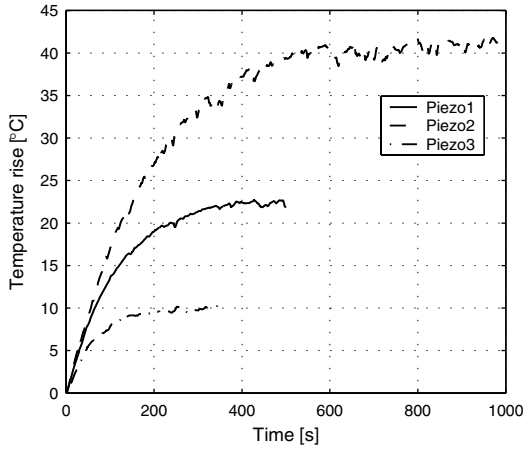

Figure 4: Effect of size on self heating.

Figure 5 presents the increase in the temperature as a function of the actuators' volume/area ratio.

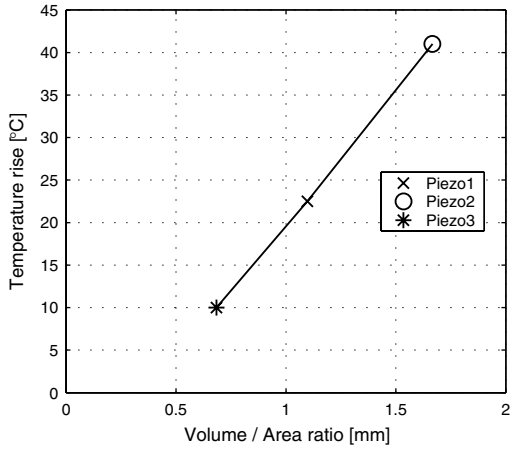

Figure 5: Self heating with respect to the volume/area ratio.

In Figure 5, a linear relation can be observed. The relationship is linear, although one actuator differs from the others. Theoretically, the line should intersect the origin [10].

6. Effect of Self Heating on Displacement

Until this point, the discussion has focused on the issues that influence self heating of piezoelectric actuators. From now on, the emphasis will be on issues, which are affected by the heat generation. Naturally, the damage in the actuator or the destruction of its periphery are the most severe effects. Some milder effects are e.g. thermal expansion of the actuator and changes in its displacement which can, however, be of high significance, too.

The effect of self heating on the displacement was studied using Piezo 1 by driving it with a sine wave (200 V / 100 Hz).

Figure 6 presents the results, the black line presenting the temperature and the grey line the displacement. The thermal expansion of the actuator, being slightly over 5 µm and approximately 0.03 % of the actuator length, can be seen quite nicely in the figure.

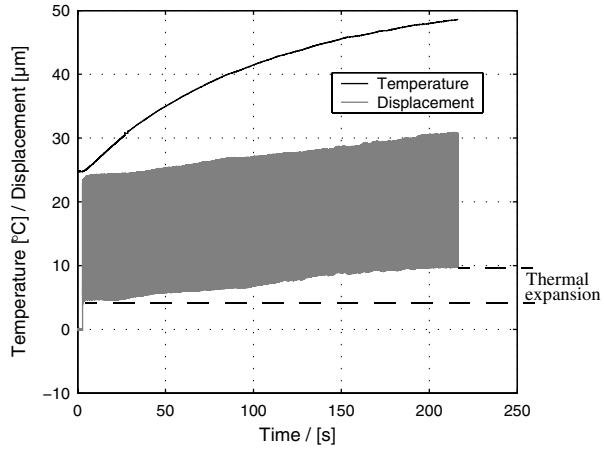

Figure 6: Influence of self heating on the displacement.

In addition to the thermal expansion of the actuator, the amplitude of the displacement changes, increasing from 19.0 µm to 20.5 µm. The change corresponds to 8 % of the original amplitude (taken from the averages of the first and the last 1000 displacement cycles).

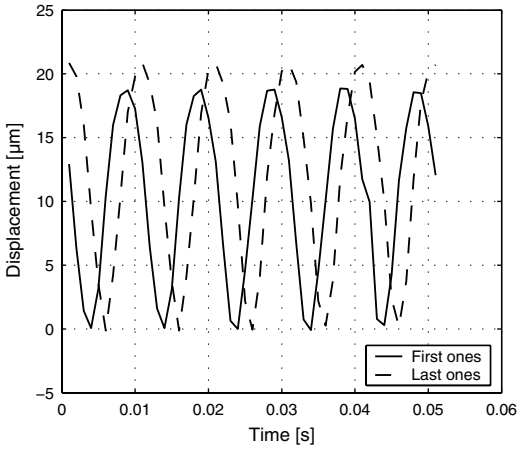

Figure 7: Five displacement cycles from the beginning (continuous) and in the end (dashed) of the test.

The amplitude increase is illustrated in Figure 7, where few displacement cycles from the beginning and in the end of the experiment have been captured to the same figure. The offset

has been removed to show the difference in the amplitude more clearly.

7. Effect of Self Heating on Current Consumption

When the actuator is controlled by a voltage and is heating up, it is noticeable that the current consumption is increasing along the temperature rise. Figure 8 presents the current (grey line) and temperature (black line) values from the test presented in Section 6 (Piezo 1, 200 V / 100 Hz).

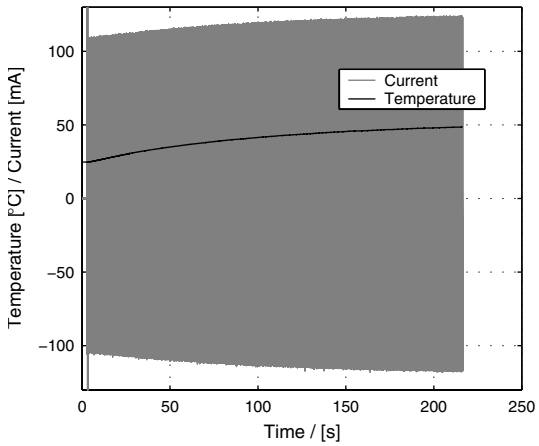

Figure 8: Influence of self heating on the current.

The connection of the current consumption with the actuator temperature is depicted more clearly in Figure 9, where the temperature and the peak-to-peak values of the current are shown. The offset value of the peak-to-peak current is removed. In the beginning, the peak-to-peak current value was 205 mA (at 25 °C), and it increased over 10 %, while the temperature increased approximately 25 degrees.

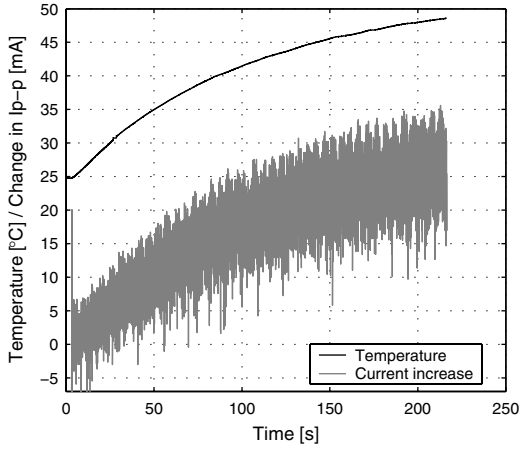

Figure 9: Temperature and change in peak-to-peak current value.

To quantify the relation between the current increase and the temperature rise, more measurements were carried out with two actuators; Piezo 1 and Piezo 3. Piezo 1 was tested with three frequencies; 100 Hz, 120 Hz and 180 Hz, and Piezo 3 with two frequencies; 500 Hz and 700 Hz. 200 V triangular driving signal is used in the measurements. Each test was repeated five times. Table 1 presents the results. Current increase is presented as percents of the original peak to peak current. According to the results the average current increase per degree is 0.5 %/°C, and a standard deviation 0.03 %/°C in these 25 tests. The measured temperature rise varied from 15 °C up to 44 °C. According to these results, the current consumption can be utilized in the measurement of the actuator temperature change.

Table 1: Average results from the measurements.

Stack no.	Freq.	Tempe-rature increase	Current increase in %	Current increase per °C
Piezo 1	100 Hz	16 °C	8 %	0.49 %/°C
Piezo 1	120 Hz	19 °C	10 %	0.50 %/°C
Piezo 1	180 Hz	29 °C	15 %	0.52 %/°C
Piezo 3	500 Hz	27 °C	13 %	0.46 %/°C
Piezo 3	700 Hz	43 °C	21 %	0.48 %/°C
			Average	0.49 %/°C

8. Compensation

Section 7 showed that self heating is possible to measure without a temperature sensor using the current consumed. In this section, the emphasis will be on the compensation of the increase in the displacement amplitude induced by self heating using information on the current consumption of the actuator.

The compensation approach is to keep the peak to peak current constant when the actuator is driven by a reciprocating signal resulting in self heating.

Figure 10 presents the block diagram of the proposed control method; an actuator current i is measured, and converted into a peak to peak current I_{pp}. A controller adjusts the amplitude A in order to maintain the current I_{pp} at a set point current I_{sp}. The set point current equals to the peak to peak current at the beginning, $I_{sp} = I_{pp\ at\ t\ zero}$. In the block diagram f presents the frequency, v the voltage and d the displacement.

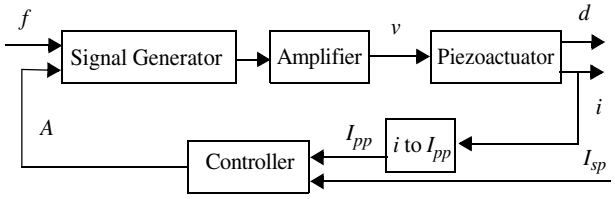

Figure 10: The block diagram of the proposed control method.

The devices utilized in the experiment are a current meter, a PC with data acquisition, a laser displacement sensor, a signal generator and a piezo amplifier. A manual control is utilized in these first experiments.

The proposed method is experimented with two actuators in the same conditions as in previous section; (triangular wave, Piezo 1: 100 Hz, 120 Hz, 180 Hz; Piezo 3: 500 Hz, 700 Hz). Each test was repeated five times. For a reference, the same experiments were done also without the compensation.

Table 2 presents the results; Error is the relative difference between the original displacement amplitude and the final displacement amplitude. It is noticeable that the difference in the displacement amplitudes might have been slightly greater than this during the process. The temperature increase is the average value in the tests; in the compensated case the temperature is typically couple of degrees less, and in the uncompensated couple of degrees more than the average.

Table 2: Average results from the experiments.

Stack no.	Freq.	Tempe-rature increase	Error without compen-sation	Error with compen-sation
Piezo 1	100 Hz	16 °C	3 %	0.7 %
Piezo 1	120 Hz	19 °C	4 %	0.7 %
Piezo 1	180 Hz	28 °C	6 %	3 %
Piezo 3	500 Hz	25 °C	4 %	1.1 %
Piezo 3	700 Hz	39 °C	9 %	3 %
		Average	5.2 %	1.7 %

As can be seen, the results are far better when the compensation is used; the differences between the displacement amplitudes in the beginning and at the end are in average three times smaller with compensation than without compensation.

Figure 11 presents typical results from the first tests (Piezo 1, 100 Hz): the displacement amplitude of the uncompensated case increases until a certain point, while the displacement amplitude of the compensated case remains quite constant. The difference in the origin of the compensated and uncompensated cases is probably due to some remaining heat in the uncompensated case after the previous measurement. The actuator was cooled down between measurements with an air fan and even though the surface of the actuator was at the room temperature, the temperature of the inner body of the actuator could have been slightly higher. This decreases the displacement error of the uncompensated case and by eliminating this remaining heat the results would appear to be even better than presented now.

In the experiments, where the compensated result differed significantly from the original and was as great as 3 %, (Piezo 1 180 Hz and Piezo 3 700 Hz), the compensation decreased the displacement amplitude and the final amplitude was smaller than in the beginning. It therefore seems that in some cases the proposed compensation method too effectively decreases the increased displacement amplitude due to self heating.

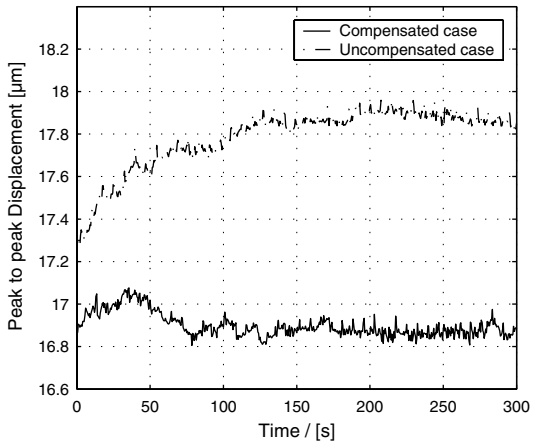

Figure 11: Typical results from the first test (Piezo 1, 100Hz), the uncompensated case with a dash-dot line and the compensated case with a continuous line.

9. Application Areas

The temperature measurement by measuring the peak to peak current could be used as a safety feature preventing overheating, or as a trigger to start an additional cooler. An interesting application could also be piezoelectric pumps, where it might be possible to detect the media inside the pump due to their different cooling capability.

The proposed compensation method can be utilized in applications, which use a periodic control signal, and where the overall performance can be increased by controlling the actuator amplitude more precisely. They include different piezoelectric pumps, liquid dispensers and motors, for example.

Piezoelectric stepper motors could benefit in open loop accuracy by using the compensation method. Then the step size would be more constant and dependency on the temperature would be decreased. Naturally load would remain as the main source of inaccuracy in piezo motors. In robotic applications where high accuracy is required, feedback sensors are naturally used, but a current measurement could give valuable information of the temperature of the motor.

Piezoelectric pumps can easily be thought to be used in applications where constant flow is required, but an implementation of a flow sensor would be impossible due to size / price requirements. Such application would benefit from the proposed compensation.

10. Conclusion

This paper presented issues concerning self heating of piezoelectric actuators. Besides the effects of the frequency and amplitude of the driving voltage, a load and the size of the actuator on the self heating, a novel method was presented for determining the state of self heating in a piezoelectric actuator without temperature measurement. Furthermore, a compensation method for the reduction of the self heating induced displacement variations was proposed. The displacement error of an actuator driven by a high-frequency reciprocating signal reduces in average down to one part in three when the proposed compensation is used.

The future work will include the application of the proposed control method to a practical device, such as a reciprocating piezoelectric pump or motor, and to develop the control system such that the peak-to-peak current can be utilized more efficiently in the control.

Materials and Methods

Three piezoelectric actuators were used in the experiments of the paper. The manufacturers, sizes and the materials of the actuators are presented in Table 3.

Table 3: Actuator properties.

Stack no.	Manuf.	Size mm^3	Mat.
Piezo 1	Noliac	5*5*18	S2
Piezo 2	Noliac	10*10*10	S2
Piezo 3	Marco	3*3*18	FPM231

S2 is a soft doped PZT material with a high strain performance and a high dielectric constant [15].

FPM 231 is a soft material with a high deformation, a low mechanical quality factor and a relatively high dielectric constant [16].

Thermistors are glued with thermally conductive glue on to the actuators to measure the actuator temperatures.

Other devices used in the experiments are a current meter, a PC with data acquisition, a laser displacement sensor, a signal generator and a piezo amplifier.

Acknowledgment

The authors would like to thank the GETA (Graduate school in Electronics, Telecommunication and Automation) and the Finnish Cultural Foundation.

References

[1] Ge, P. & Jouaneh M. 1996. *Tracking Control of a Piezoceramic Actuator.* IEEE Transactions on Control Systems Technology, Vol. 4, No. 3, May.

[2] Croft, D., Shedd, G. & Devasia, S. 2000. *Creep, Hysteresis, and Vibration Compensation for Piezoactuators: Atomic Force Microscopy Application*. Proceedings of the American Control Conference, Chicago, Illinois, June 2000.

[3] Choi, G. S., Kim, H.-S. & Choi, G. H. 1997. *A Study on Position Control of Piezoelectric Actuators*. Proceedings of the IEEE International Symposium on Industrial Electronics, Guimaraes, Portugal, July 7-11, 1997. Vol. 3.

[4] Newcomb, C. V. & Flinn, I. 1982. *Improving the Linearity of Piezoelectric Ceramic Actuators*. Electronics Letters, Vol. 18, No. 11, May.

[5] Ronkanen, P., Kallio, P. & Koivo, H. *Current Control of Piezoelectric Actuators with Power Loss Compensation*. IEEE/ RSJ International Conference on Intelligent Robots and Systems, IROS'02. Lausanne, Switzerland, October 2002.

[6] Comstock, R. H. 1981. *Charge Control of Piezoelectric Actuators to Reduce Hysteresis Effects*. U.S. Patent 4,263,527.

[7] Perez, R., Agnus, J., Breguet, J.-M., Chaillet, N., Bleuler, H. & Clavel, R. 2001. *Characterisation and Control of a 1DOF Monolithic Piezoactuator (MPA).* Proceedings of SPIE Volume 4568: Microrobotics and Microassembly III, Boston, USA, October 2001.

[8] Furutani, K., Urushibata, M. & Mohri, N. 1998. *Improvement of Control Method for Piezoelectric Actuator by Combining Induced Charge Feedback with Inverse Transfer Function Compensation*. Proceedings of the 1998 IEEE International Conference on Robotics & Automation, Leuven, Belgium, May 1998.

[9] Takahashi, S., Hirose, S., Uchino, K. & Oh, K.-Y. 1994. *Electro-Mechanical Characteristics of Lead-Zirconate-Titanate Ceramics Under Vibration-Level Change*. Proceedings of the Ninth IEEE International Symposium on Applications of Ferroelectrics, University Park, PA, USA, August 1994.

[10] Uchino, K. & Hirose, S. 2001. *Loss Mechanisms in Piezoelectrics: How to Measure Different Losses Separately.* IEEE Transactions on Ultrasonics, Ferroelectrics, and Frequency Control, Vol. 48, No. 1, January 2001.

[11] Yao, K., Uchino, K., Xu, Y, Dong, S. & Lim, L. S. *Compact Piezoelectric Stacked Actuators for High Power Applications*. IEEE Transactions on Ultrasonics, Ferroelectrics, and Frequency Control, Vol. 47, No. 4, July 2000.

[12] Lesieutre, G. A., Fang, L., Koopmann, G. H., Pai, S. P. & Yoshikawa, S. 1996. Proceedings of SPIE Volume: 2717, Smart Structures and Materials 1996: Smart Structures and Integrated Systems, May 1996.

[13] Yarlagadda, S., Chan, M. H. W. Lee, H. Lesieutre, G. A. & Jensen, D. W. 1995. *Low Temperature Thermal Conductivity, Heat Capacity, and Heat Generation of PZT.* Journal of Intelligent Material Systems and Structures, Vol. 6, November 1995.

[14] Zhou, Q., Corral, C., Esteban, P., Albut, A. & Koivo, H. *Environmental Influence on Microassembly.* IEEE/RSJ International Conference on Intelligent Robots and Systems, IROS'02. Lausanne, Switzerland, October 2002.

[15] Noliac A/S. *Piezoelectric Materials.* http://www.noliac.com/ index.asp?id=98. 3.3.2004.

[16] Marco Systemanalyse und Entwicklung GmbH. *Piezo Ceramic Components*. http://www.marco.de/E/D/pb/001.html. 3.3.2004.

Tampereen teknillinen yliopisto
PL 527
33101 Tampere

Tampere University of Technology
P.O. Box 527
FIN-33101 Tampere, Finland